Politecnico di Torino

Department of Environment, Land, and Infrastructure Engineering
Master of Science in Georesource and Geoenergy Engineering
A. y. 2024/2025
March 2025

Investigation of the main aspects affecting the sealing efficiency of cap rock for the safety assessment of underground gas storage via Machine Learning algorithms

Supervisors:
Professor Vera Rocca
Professor raoof Gholami

Candidate:
Maziar Ashrafi

Abstract

Underground gas storage plays a pivotal role in ensuring energy security, effective carbon management, and robust industrial applications. Our research takes a deep dive into the complex interplay between geological formations and fluid properties; particularly breakthrough and snap-off pressures that govern the long-term stability of gas containment. While previous studies have focused primarily on lithological factors, we discovered that relying solely on lithology can be misleading. Instead, our work emphasizes the role of mineralogical composition to better capture the nuances of cap rock behavior. Using advanced experimental methods like breakthrough pressure tests and mercury intrusion porosimetry, we evaluated how pore structure, interfacial tension (IFT), and contact angle influence fluid displacement dynamics in formations ranging from CO_2 and N_2 to CH_4 systems. By compiling a comprehensive dataset from global laboratory experiments and geological formations, we developed a model that correlates breakthrough and snap-off pressures with key cap rock parameters such as pressure, temperature, porosity, permeability, IFT, and wettability. A correlation matrix illuminated several critical trends: higher interfacial tension lowers the threshold for N_2 to force its way in ($r = -0.80$), higher temperatures raise the pressure required for CO_2 to breach the rock ($r = 0.47$), and more porous cap rock are more easily penetrated by CH_4 ($r = -0.51$). Mineralogy emerged as equally pivotal, with smectite content boosting CO_2 containment ($r = 0.46$), while smectite-illite mixtures ($r = -0.37$) had the opposite effect. These findings underscore how certain clays, pore structures, and thermal and pressure conditions can either strengthen or weaken a cap rock's sealing capacity.

Building on these detailed experiments, we employed state-of-the-art machine learning techniques—specifically K-Nearest Neighbors (KNN) and CatBoost—to analyze the nonlinear relationships inherent in subsurface storage systems. A focal point of our study was the renowned Opalinus Clay formation, recognized for its effectiveness as a cap rock, where our findings underscore the significant impact of mineralogical variations on pressure dynamics. For instance, our correlation analysis revealed that higher interfacial tension and lower porosity markedly enhance capillary sealing efficiency, while temperature and specific clay mineral contents (like smectite versus smectite-illite mixtures) influence breakthrough pressures in unexpected ways. By integrating geological expertise with data-driven modeling, our approach not only advances the understanding of subsurface fluid storage but also refines pressure estimation.

Table of contents

CHAPTER 1 (introduction)

Introduction

Underground gas storage plays a crucial role in energy security, carbon management, and industrial applications. Whether used for natural gas reserves, carbon dioxide (CO_2) sequestration, or hydrogen (H_2) storage, the efficiency and safety of gas containment depend on a complex interaction between geological and fluid properties. Cap rock serves as a natural barrier that prevents the escape of subsurface fluids, ensuring the safety of underground storage systems. Its integrity is shaped by factors such as permeability, capillary entry pressure, mechanical strength, and geochemical stability. The effectiveness of its seal, known as sealing efficiency, depends on pore structure, fluid properties, stress conditions, and the potential for fractures. To ensure its reliability, scientists assess sealing efficiency through lab experiments, field studies, and advanced simulations, using methods like breakthrough pressure analysis, geophysical monitoring, and fluid migration modeling to predict long-term performance and safety. Among the key parameters characterizing the cap rock and governing gas retention and movement are breakthrough (BT) pressure and snap-off pressure, which govern how gas displaces fluids within porous media. These pressures are directly linked to rock properties, fluid characteristics, and cap rock conditions. While lithology, the study of rock type and structure—has been widely studied in relation to these pressures, the role of mineralogy remains less understood. Mineral composition affects wettability, pore throat connectivity, and capillary forces, all of which influence gas mobility and retention. However, current predictive models often overlook these mineralogical dependencies, leading to gaps in accurately forecasting the sealing effectiveness of cap rock in different reservoirs.

This research aims to address this gap by developing a correlation model which could be used for prediction that establishes relations between BT pressure, snap-off pressure, and key cap rock parameters, including test pressure, temperature, porosity, permeability, interfacial tension (IFT), and contact angle. While lithological relationships have been well-defined, they could be misleading so in this approach we decided to move on with mineralogy. Also, no widely accepted model explicitly incorporates mineralogical influences. To build a more comprehensive and globally applicable model, this study utilizes data collected from multiple research papers and experimental studies conducted worldwide. These datasets encompass various geological formations, laboratory experiments, and in-field measurements, and gases allowing for a robust analysis of how different rock types and mineral compositions influence pressure behavior.

A key aspect of this research is the experimental procedures used to gather pressure-related data.. One Commonly used approach is the step-by-step test, where gas is injected into a rock sample at incremental pressure levels to observe its behavior under controlled conditions. This method helps assess gas flow initiation, pore throat blocking effects, and pressure buildup patterns, providing detailed data on gas migration tendencies. Breakthrough (BT) pressure, which is the pressure required for gas to pass through a fluid-saturated porous medium is another valuable outcome of this test. Residual capillary pressure refers to the pressure difference in porous materials caused by capillary forces when one fluid is displaced by another. Imbibition and drainage processes play a crucial role in this phenomenon, as imbibition allows a fluid to be absorbed into the pores, while drainage involves fluid displacement.

Beyond its theoretical contributions, this study has important practical applications. Predicting pressure behavior in subsurface formations is critical for optimizing gas storage operations, improving hydrocarbon recovery efficiency, and ensuring the long-term security of CO_2 and H_2 sequestration sites, However, these tests are time-consuming and expensive. The correlations that has been calculated can considerably help us find an initial screening of the sealing efficiency of cap rocks. A deeper understanding of how mineralogy, in conjunction with other cap rock properties, influences pressure dynamics can lead to improved decision-making in cap rock selection, gas injection strategies, and leakage risk assessments. The predictive model developed in this research will provide a valuable tool for industry professionals, offering practical insights that can be applied to real-world storage and extraction systems.

From a methodological perspective, this study represents a shift from traditional empirical correlations to advanced data-driven modeling. Machine learning techniques, particularly K-Nearest Neighbors (KNN) and CatBoost, are utilized to analyze complex, nonlinear relationships between multiple cap rock parameters. KNN is effective for identifying local patterns within datasets, while CatBoost is a powerful gradient boosting algorithm that handles numerical and categorical data efficiently, reduces overfitting, and improves predictive accuracy. By comparing these algorithms, this research aims to determine the most reliable approach for forecasting BT and snap-off pressures under different mineralogical conditions and according to different gas-brine systems. The inclusion of globally sourced data ensures that the model is adaptable to various cap rock types, increasing its applicability in different regions and storage projects.

One of the primary challenges in this study is the availability and quality of mineralogical data. The detailed mineralogical datasets are often more difficult to obtain. To address this issue, this research compiles data from various peer-reviewed publications, laboratory experiments, and field studies conducted across different geological settings. Feature selection and optimization techniques are applied to extract the most relevant mineralogical factors affecting pressure behavior, ensuring that the final predictive model is both comprehensive and capable of identifying key trends that may have been overlooked in previous studies.

Ultimately, this thesis seeks to bridge the knowledge gap between mineralogy and pressure dynamics in porous media. By developing a data-driven predictive model, this research contributes to a deeper understanding of subsurface gas storage and flow behavior. The findings will enhance gas storage efficiency, optimize reservoir performance, and improve the safety and reliability of carbon sequestration and hydrogen storage projects. By integrating geological knowledge with modern machine learning techniques, this study offers a novel approach to predicting BT and snap-off pressures, providing valuable insights for both academic research and industrial applications.

CHAPTER 2 (Description of Theory)

1.Drainage & Imbibition

Cap rock acts as a natural seal, trapping hydrocarbons or gases like CH_4 and CO_2 within underground reservoirs and preventing their escape. Its ability to hold these fluids depends on factors such as seal strength, thickness, and stability under pressure changes. Typically made of shales, mudstones, evaporites, and carbonates, cap rocks have extremely low permeability, making them effective barriers. Clay minerals like illite and smectite further enhance sealing, but over time, natural processes like mineral dissolution or fracturing can weaken their integrity.

Drainage and imbibition are key processes that control how fluids move through porous rocks. These mechanisms are driven by capillary forces, pressure differences, and surface interactions, playing a major role in oil recovery, groundwater movement, and environmental remediation. When fluids are injected or withdrawn from a reservoir, they alter the conditions in the cap rock. Drainage occurs when gas pushes water out of the pores, while imbibition happens when water re-saturates the rock after fluid withdrawal. If the pressure exceeds the cap rock's limit, fluids can break through, leading to leaks. Repeated stress cycles may also cause fractures, deformation, or chemical changes that weaken the seal over time. Understanding these processes is essential for maintaining secure storage and improving fluid management in various industrial and environmental applications.

Drainage refers to the process in which a non-wetting fluid (such as oil or gas) displaces a wetting fluid (such as water) from the pore spaces of a porous medium. For this displacement to occur, the non-wetting fluid must overcome capillary forces that naturally resist fluid movement. This process is typically initiated by applying external pressure to force the non-wetting fluid into the porous structure. One of the key factors governing drainage is capillary forces. The non-wetting fluid must exceed the capillary entry pressure to push out the wetting fluid. This relationship is described by the equation:

$$P_c = P_{non-wetting} - P_{wetting} \text{ (Eq.1)}$$

where smaller pores exhibit higher capillary entry pressures, making them more resistant to invasion.

At the pore scale, drainage begins in larger pores, as they have lower capillary entry pressures. The non-wetting fluid moves through these larger pathways first, leaving behind smaller pores still occupied by the wetting fluid. As drainage progresses, fluid connectivity and relative permeability shift— the wetting fluid becomes increasingly disconnected, reducing its permeability, while the non-wetting fluid spreads through the pore network, increasing its permeability. Moreover, Wettability also plays a crucial role in drainage efficiency. In strongly water-wet systems, the solid surfaces preferentially attract water, increasing resistance to drainage. Hydrophilic surfaces further enhance water retention, making it more difficult for the non-wetting fluid to displace the wetting phase.

Imbibition is the reverse of drainage, where a wetting fluid (such as water) displaces a non-wetting fluid (such as oil or gas) from the pore spaces of a porous medium. This process is often spontaneous, driven by capillary forces, but it can also be induced by applying external pressure to accelerate fluid movement. (fig.1)

Capillary forces play a crucial role in imbibition. In contrast to drainage, where the non-wetting fluid must overcome capillary resistance, imbibition occurs as negative capillary pressure pulls the wetting fluid into the pores. This relationship is expressed as:

$$P_c = \frac{-2\gamma}{r} \quad \text{(Eq.2)}$$

where γ represents interfacial tension and r is the pore radius. Smaller pores, which have higher surface energy, are filled first, making capillary-driven imbibition a naturally selective process.

Wettability significantly influences imbibition efficiency. In water-wet systems, the wetting fluid spreads easily along solid surfaces, facilitating the displacement of the non-wetting fluid. However, in hydrophobic or oil-wet systems, the porous medium prefers to retain the non-wetting fluid, making spontaneous imbibition more difficult and requiring external pressure for displacement.

Imbibition can be classified into two types: spontaneous imbibition, which occurs naturally when capillary forces are sufficient to drive the wetting fluid into the pores, and forced imbibition, which requires external pressure to overcome additional barriers, such as viscous resistance or pore constrictions. Even after imbibition, some residual non-wetting fluid often remains trapped within the pore network in the form of disconnected clusters or ganglia. These trapped pockets of non-wetting fluid result from capillary entrapment, making complete displacement challenging.

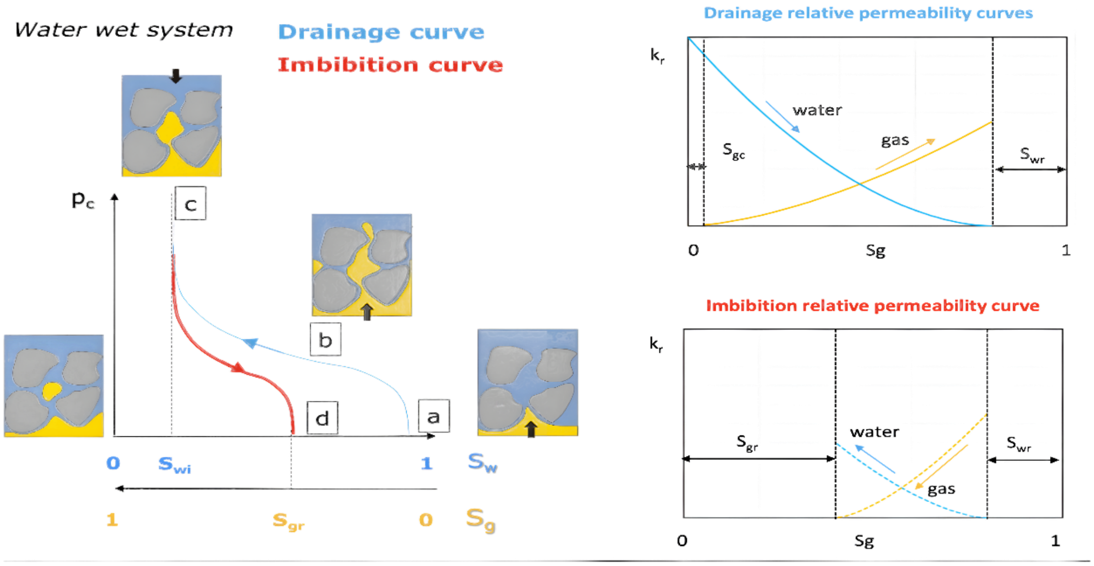

Fig.1 Description of drainage and imbibition with relative permeability

The efficiency and behavior of drainage and imbibition depend on several key factors, which play a crucial role in optimizing industrial and environmental systems. Understanding these parameters allows for better control over fluid movement in porous media.

1. One of the most important factors is wettability, which defines the preference of a solid surface for a specific fluid phase. In water-wet systems, water strongly adheres to the solid surface, favoring imbibition by allowing water to displace non-wetting fluids like oil or gas. Conversely, in oil-wet systems**,** the non-wetting phase adheres better to the surface, making drainage more efficient. Wettability can be altered by factors such as the chemical composition of the solid surface, the presence of surfactants, or the interaction with other fluids and contaminants. Adjusting wettability, such as through the use of surfactants, can significantly enhance fluid displacement efficiency.

2. Pore geometry also plays a major role in fluid movement. Pore size and shape determine capillary entry pressure, with smaller pores requiring higher capillary pressure for drainage and being preferentially filled during imbibition. A broad distribution of pore sizes can lead to complex fluid behavior, including partial trapping of displaced fluids. Connectivity is another crucial aspect. It is a highly interconnected pores allow for easier fluid mobility, while isolated or poorly connected pores increase the likelihood of fluid entrapment, reducing efficiency. Additionally, irregularly shaped pores or those with constrictions can create bottlenecks that impede fluid movement and increase resistance to flow.

3. Capillary pressure is the driving force behind both drainage and imbibition. Positive capillary pressure promotes drainage by pushing the non-wetting fluid through the porous medium, while negative capillary pressure encourages imbibition, allowing the wetting fluid to spread through the pore network. The magnitude of capillary pressure depends on pore size, interfacial tension, and contact angle, all of which influence how easily fluids displace one another.

4. Another critical parameter is interfacial tension (IFT**),** which represents the energy at the interface between immiscible fluids and directly affects capillary forces. Low IFTreduces the energy required for fluid movement, making both drainage and imbibition more efficient. Since IFT determines how fluids interact at phase boundaries, reducing it minimizes resistance to displacement, facilitating smoother fluid flow in porous systems.

5. Fluid properties such as viscosity, density, and compressibility further influence drainage and imbibition behavior. Higher viscosity slows fluid movement, affecting displacement efficiency and overall flow dynamics. Density differences introduce gravitational forces that can either assist or oppose fluid movement, depending on the orientation of the system. Additionally,

fluid compressibility affects how fluids respond to pressure changes, influencing both drainage and imbibition under varying conditions.

1.1 Pore Geometry and Pore Throats

Pore geometry and throat distribution play a crucial role in fluid movement through porous materials, directly influencing imbibition (where a wetting fluid enters pores) and drainage (where one fluid displaces another). These structural features determine fluid flow efficiency, affecting how well substances are trapped or displaced in reservoirs (Bear, 2013).

During drainage, the non-wetting fluid must overcome pressure from the smallest pore throats. In homogeneous rocks, this process is smooth, but in rocks with varying pore sizes, certain flow paths dominate, leading to irregular movement, capillary fingering, and snap-off, which can trap displaced fluids. Variations in contact angles further disrupt fluid flow (Lenormand et al., 1988).

In imbibition, the wetting fluid moves into the pore spaces, but its efficiency depends on pore size and connectivity. Poor connectivity or small pores can prevent full saturation, leaving pockets of non-wetting fluid behind (Blunt, 2017).

The balance between capillary and viscous forces, governed by the capillary number, also influences fluid behavior. At low capillary numbers, capillary forces dominate, making imbibition more effective, whereas higher viscous forces can cause flow instability. This balance is especially critical in fractured reservoirs to optimize fluid movement and CO_2 injection.
(Joekar-Niasar et al., 2008)

1.2 Pore-scale Displacement in drainage

Pore-scale displacement during drainage refers to how a non-wetting fluid displaces a wetting fluid within the tiny pores of a rock or soil. This process is controlled by capillary and viscous forces, as well as the pore network's structure. Different displacement patterns, including capillary fingering, viscous fingering, and stable displacement, occur depending on factors such as fluid properties and pore structure. Capillary fingering causes irregular fluid movement, leaving pockets of trapped fluid, while viscous fingering leads to inefficient displacement. Stable displacement, on the other hand, is efficient and desirable, but rarely achieved in heterogeneous geological formations .One way to predict the dominant displacement mechanism in each system is by calculating the capillary number, which expresses the balance between viscous and capillary forces. The capillary number is defined as:

$$Ca = \mu V / \gamma \quad \text{(Eq.3)}$$

where μ is the viscosity of the displacing fluid, V is its velocity, and γ is the interfacial tension between the two fluids. When the capillary number is very low ($Ca < 10^{-6}$), capillary forces dominate, leading to capillary fingering. When the capillary number is moderate ($10^{-6} < Ca < 10^{-3}$), both viscous and capillary forces play a role, creating mixed displacement patterns. At high capillary numbers ($Ca > 10^{-3}$), viscous forces dominate, and the non-wetting fluid moves more uniformly, often resulting in stable displacement or, in some cases, viscous fingering (Lenormand et al., 1988; Joekar-Niasar et al., 2008; Homsy, 1987).

Pore-scale displacement during drainage has important implications for real-world applications. In CO_2 storage, the way CO_2 moves through the rock determines how securely it will remain trapped in underground formations, making displacement mechanisms a critical factor in long-term storage security (Bachu, 2008)

1.3 The effect of fluid viscosity on drainage

The effect of fluid viscosity on drainage is critical in determining how efficiently a non-wetting fluid displaces a wetting fluid in a porous medium. Viscosity, which measures a fluid's internal resistance to flow, directly influences the stability of the displacement front, the rate of fluid movement, and the amount of residual wetting-phase saturation left behind. In drainage, the viscosity contrast between the two fluids plays a key role in determining whether displacement occurs smoothly or in an unstable manner.

The mobility ratio is used to quantify the impact of viscosity contrast on drainage and is defined as the ratio of the mobility of the displacing phase to that of the displaced phase. A mobility ratio greater than one, where the non-wetting fluid has a much lower viscosity than the wetting fluid, leads to unstable displacement and inefficient drainage. When the mobility ratio is less than one, meaning the non-wetting fluid has a similar or higher viscosity than the wetting fluid, the displacement front remains stable, resulting in more efficient drainage.

The capillary number, which represents the balance between viscous and capillary forces, also influences drainage efficiency. A low capillary number indicates that capillary forces dominate, leading to poor displacement and significant trapping of the wetting phase. As the capillary number increases, viscous forces begin to control the displacement process, improving drainage efficiency. However, if the viscosity contrast is too high, viscous fingering can still occur, reducing the overall effectiveness of fluid displacement.

1.4 Experimental methods for measuring drainage

Experimental methods for measuring drainage characteristics are essential for understanding how a non-wetting fluid displaces a wetting fluid in porous media. These methods provide critical data on parameters such as capillary pressure, relative permeability, and residual saturation. Different experimental techniques are used depending on the scale of observation, ranging from pore-scale imaging to core-scale flow experiments.

One of the most common techniques for measuring drainage characteristics is mercury intrusion porosimetry (MIP), which provides detailed information on pore size distribution and capillary entry pressures. In this method, mercury, a non-wetting fluid, is forced into a porous sample under increasing pressure. The relationship between applied pressure and mercury saturation allows for the determination of pore throat sizes based on the Washburn equation:

$$Pc=2\gamma\cos\theta/r \text{ (Eq.4)}$$

This technique is particularly useful for characterizing drainage in fine-grained materials, where high capillary entry pressures play a significant role in fluid movement.

Another widely used method is the core flooding experiment, in which a core sample is saturated with a wetting phase and then subjected to drainage by injecting a non-wetting fluid under controlled pressure and flow conditions. This setup allows for the measurement of relative permeability curves, which describe how the presence of one fluid affects the ability of another to flow through the porous medium. By monitoring fluid saturations and pressure differentials across the core, researchers can determine the efficiency of drainage and the extent of wetting-phase trapping.

Centrifuge drainage experiments offer an alternative approach to measuring capillary pressure and relative permeability. In this method, a core sample is spun at high speeds, generating a radial pressure gradient that forces the non-wetting fluid to displace the wetting phase. The resulting saturation profiles can be used to construct capillary pressure curves and estimate residual saturation levels. This technique is particularly useful for studying fluid retention in heterogeneous formations.

Micro-CT imaging and nuclear magnetic resonance (NMR) techniques provide non-destructive methods for visualizing drainage at the pore scale. Micro-CT imaging uses X-rays to capture high-resolution 3D images of fluid distribution within a rock sample during drainage, allowing researchers to observe pore-scale displacement patterns and trapping mechanisms. NMR, on the other hand, measures hydrogen nuclei responses in fluids to quantify fluid saturations and distribution within the porous medium. These advanced techniques are invaluable for validating theoretical models and improving the understanding of multiphase flow behavior.

The choice of experimental method depends on the specific application and the desired level of detail. For reservoir engineering, core flooding and centrifuge methods provide practical insights into drainage efficiency, while MIP and micro-CT imaging offer fundamental pore-scale information for refining fluid flow models.

2. Wettability and Contact angle

Wettability is classified into three main categories based on the contact angle (θ), which is measured between the solid surface and the tangent of the fluid-fluid interface:

Strongly water-wet ($\theta<90^\circ$): The rock surface prefers water, and water spreads easily along the pore walls. In this case, capillary pressure resists drainage because the wetting phase strongly adheres to the solid surface, requiring a high entry pressure for the non-wetting phase to invade the pores. Neutral-wet ($\theta\approx90^\circ$): The solid surface has no strong preference for either fluid, leading to more balanced displacement behavior. Strongly oil-wet ($\theta>90^\circ$) – The rock surface prefers the non-wetting phase (e.g., oil or gas), making drainage more favorable as the non-wetting phase spreads more easily. In these conditions, capillary barriers are weaker, and the non-wetting phase invades with less resistance.

2.1 Theoretical Models of Wettability

2.1.1 Young's Equation

Young's equation provides a fundamental description of equilibrium wettability, defining the relationship between surface tensions at the solid-liquid-vapor interface:

$$\cos\theta = \frac{\gamma_{SV}-\gamma_{SL}}{\gamma_{LV}} \text{ (Eq.5)}$$

where:

- γ_{SV} is the surface tension of the solid-vapor interface.
- $\gamma_{SL}$is the surface tension of the solid-liquid interface.
- γ_{LV} is the surface tension of the liquid-vapor interface.

This equation explains how wettability is influenced by the balance of interfacial tensions. A lower solid-liquid surface tension **(γ_{SL})** results in better wetting (low contact angle), whereas a higher solid-liquid surface tension increases hydrophobicity.

2.1.2 Wenzel Model

The Wenzel model expands on Young's equation by incorporating surface roughness, which amplifies the material's inherent wettability. The equation is:

$$\cos\theta^{*}= \mathrm{r}\cos\theta \text{ (Eq.6)}$$

where θ^* is the apparent contact angle, and r is the roughness ratio, defined as the ratio of the actual surface area to its projected area. If the surface is intrinsically hydrophilic, roughness enhances wetting (lowering the contact angle). Conversely, if the surface is hydrophobic, roughness increases water repellency, making the surface more resistant to wetting.

2.1.3 Cassie-Baxter Model

The Cassie-Baxter model describes surfaces that contain composite interfaces, where liquid partially rests on solid and air pockets instead of fully wetting the surface. The equation is:

$$\cos\theta^{*}= \mathrm{f}\cos\theta + (1\text{-f}) \text{ (Eq.7)}$$

where f represents the fraction of the solid in contact with the liquid. This model explains extreme superhydrophilicity, such as the behavior seen in lotus leaves, where water beads up and rolls off the surface due to trapped air pockets reducing liquid adhesion.

Both the Wenzel and Cassie-Baxter models demonstrate how surface texture and structure can be engineered to manipulate wettability, making them essential for designing self-cleaning materials, water-resistant coatings, and advanced biomedical surfaces.

Wettability is shaped by several factors, including the properties of the solid surface, the characteristics of the liquid, environmental conditions, and the methods used to measure it. On the surface side, high-energy materials like metals and glass tend to allow liquids to spread easily, whereas low-energy surfaces, such as Teflon or certain polymers, resist wetting—an effect that is amplified by surface roughness and modified by surface chemistry. The liquid's own properties, such as surface tension and viscosity, determine how readily it spreads; for example, high surface tension fluids like water form higher contact angles on non-polar surfaces, while low surface tension liquids spread more easily. Environmental conditions, temperature, humidity, and pressure—can further alter these interactions by affecting a liquid's surface tension and equilibrium state. Finally, techniques like contact angle measurements (using methods such as the Wilhelmy plate, sessile drop, and capillary rise) are essential for quantifying wettability.

2.2 Wettability and Contact angle in drainage

In drainage, in a water-wet system, the wetting fluid remains strongly adhered to the pore walls, and the non-wetting phase can only enter the pore space by overcoming a high capillary entry pressure, described by the Young-Laplace equation:

$$Pc=2\gamma\cos\theta/r \quad \text{(Eq.8)}$$

where Pc is capillary pressure, γ is the interfacial tension, θ is the contact angle, and r is the pore throat radius. A strongly water-wet medium with a low contact angle ($\theta<30^\circ$) will exhibit higher capillary pressure, making drainage less efficient because the non-wetting phase struggles to displace the wetting phase. Conversely, in oil-wet systems, the contact angle is higher ($\theta>90^\circ$), and capillary forces favor the displacement of water, resulting in lower entry pressures and more efficient drainage.

The wettability of a rock surface is also heterogeneous, meaning that different regions of the cap rock may exhibit varying degrees of water-wet and oil-wet behavior. This heterogeneity can cause localized trapping of the wetting phase, leading to inefficient displacement and higher residual wetting-phase saturation. In mixed-wet systems, where some pores are water-wet and others are oil-wet, drainage can be highly irregular, with preferential flow paths forming in oil-wet regions while water remains trapped in water-wet regions.

Wettability also influences relative permeability curves, which describe the ability of each fluid to flow through the porous medium as a function of saturation. In strongly water-wet formations, relative permeability to the non-wetting phase remains low until a high saturation of the non-wetting phase is reached, as capillary forces retain the wetting phase within the pore network. In contrast, in oil-wet formations, the non-wetting phase is more mobile even at lower saturations, allowing for more efficient drainage.

2.3 Wettability effects on the Imbibition process

In spontaneous imbibition, the degree of wettability determines whether the wetting phase can enter the pore network without external pressure. In strongly water-wet conditions, imbibition occurs naturally, driven by high capillary forces (Lenormand et al., 1988). In oil-wet systems, capillary resistance prevents spontaneous imbibition, requiring an applied pressure gradient to force the wetting phase into the medium (Joekar-Niasar et al., 2008). Wettability also affects the rate of imbibition, with water-wet formations exhibiting faster spontaneous imbibition rates compared to oil-wet systems (Blunt, 2017).

During forced imbibition, where an external force is applied, wettability determines the distribution of fluids within the pore network. In oil-wet formations, forced imbibition can lead to bypassing effects, where water moves preferentially through high-permeability zones without fully displacing the non-wetting phase from low-permeability regions (Morrow, 1976). In contrast, in water-wet formations, forced imbibition follows a more uniform front, leading to more efficient displacement of the non-wetting phase (Lenormand et al., 1988).

In capillary trapping, wettability affects how much of the non-wetting phase remains immobilized after imbibition. In strongly water-wet systems, capillary forces trap non-wetting phase droplets in small pores, leading to high residual saturation (Joekar-Niasar et al., 2008). In oil-wet systems, non-wetting phase connectivity is higher, resulting in lower residual trapping (Blunt, 2017).

The relative permeability of the wetting phase is also affected by wettability. In water-wet formations, relative permeability to water increases more quickly as saturation increases, while in oil-wet formations, water struggles to move efficiently, leading to reduced flow capacity (Morrow, 1976).

2.4 Contact Angle Hysteresis in Imbibition

Contact angle hysteresis is a key phenomenon influencing the imbibition process, as it affects the movement of the wetting phase into a porous medium and the efficiency of fluid displacement. hysteresis occurs when there is a difference between the advancing contact angle (θ_A) and the receding contact angle (θ_R), which describes how a fluid interacts with a solid surface under dynamic conditions. in imbibition, contact angle hysteresis directly impacts fluid retention, capillary trapping, and the rate of wetting-phase infiltration (joekar-niasar et al., 2008).

The advancing contact angle (θ_A) represents the angle formed when the wetting phase front moves forward, while the receding contact angle (θ_R) describes the angle at which the non-wetting phase retracts. The difference between these angles, expressed as $\Delta\theta = \theta_A - \theta_R$, defines the extent of hysteresis. Higher hysteresis means greater resistance to fluid movement, affecting how efficiently the wetting phase can imbibe into the porous structure (morrow, 1976).

> In mixed-wet and weakly water-wet formations, high contact angle hysteresis can slow down spontaneous imbibition.
>
> Contact angle hysteresis contributes to higher non-wetting phase trapping during imbibition. As the wetting phase advances, it may fail to completely displace the non-wetting phase due to the difference between advancing and receding angles. This results in capillary entrapment of the non-wetting phase in pore corners and constricted pore throats, increasing residual oil or gas saturation (joekar-niasar et al., 2008).

> Contact angle hysteresis can be affected by wettability alteration processes. in water-wet systems, imbibition is more efficient due to lower hysteresis values, whereas in oil-wet systems, high hysteresis inhibits imbibition, requiring external interventions such as surfactant or chemical treatments to modify wettability and reduce the hysteresis effect (blunt, 2017).

Due to hysteresis, capillary pressure does not immediately stabilize when imbibition begins. The system takes time to reach capillary equilibrium, meaning that wetting-phase displacement continues over an extended period (lenormand et al., 1988).

3. Interfacial Tension (IFT)

Interfacial Tension (IFT**)** is a fundamental physical property that defines the force per unit length acting at the interface between two immiscible phases, such as liquid-liquid, liquid-gas, or liquid-solid. It arises due to an imbalance in intermolecular forces experienced by molecules at the interface compared to those within the bulk phases. This property plays a crucial role in natural processes and industrial applications, including oil recovery, emulsification, and fluid transport in porous media.

IFT originates from the molecular interactions at phase boundaries. In the bulk of a liquid, molecules experience equal attractive forces in all directions, leading to a stable state. However, at the interface, molecules lack similar interactions on one side, creating an energy gradient. This imbalance results in interfacial tension, requiring additional energy to expand the surface area of the interface.

IFT is measured in dynes per centimeter (dyne/cm) in the CGS system or millinewtons per meter (mN/m) in the SI system and is mathematically represented as:

$$\gamma = \frac{F}{L} \quad \text{(Eq.9)}$$

where **γ** is interfacial tension, F is the force, and L is the length over which the force acts.

A closely related concept is surface tension, which specifically refers to the tension between a liquid and air, while interfacial tension applies to interactions between two immiscible liquids or a liquid and a solid. For example, the surface tension of water and air is relatively high (~72 mN/m at 25°C), whereas the interfacial tension between water and oil is lower, typically ranging between 20-50 mN**.**

Interfacial tension (IFT) is influenced by factors like fluid nature, temperature, surfactants, chemical composition, and pressure. Strongly polar substances like water exhibit high IFT when paired with non-polar substances like oil due to immiscibility and molecular differences. Increasing temperature reduces molecular cohesion at the interface, lowering IFT. Surfactants, such as soaps and detergents, lower IFT by disrupting cohesive forces between molecules, which is useful in emulsification and fluid mixing. Chemical additives can either increase or decrease IFT depending on their interactions with the fluids. Pressure affects IFT in gas-liquid systems by compressing the gas phase, but it has negligible effects in liquid-liquid systems unless the fluids are highly compressible.

3.1 Measurement Techniques

Accurate measurement of interfacial tension (IFT) is crucial for understanding fluid interactions and optimizing processes, with several techniques used for this purpose. Drop Shape Analysis involves analyzing the curvature of a droplet suspended in an immiscible liquid using the Young-Laplace equation. The Du Noüy Ring Method measures the force required to detach a platinum-iridium ring from the interface, while the Wilhelmy Plate Method calculates IFT by measuring the force acting on a partially immersed plate. The Spinning Drop Method, useful for very low IFTs, relies on the elongation of a droplet in a rotating tube, and the Pendant Drop Method analyzes the shape of a droplet formed at the end of a needle using high-resolution imaging. Each method has its own advantages and specific applications for different fluid interfaces.

4. Capillary Pressure in drainage & Imbibition

Capillary pressure (Pc) arises due to the difference in pressure across the interface of two immiscible fluids. It governs fluid distribution in porous media and is mathematically defined as:

$$P_c = P_{nw} - P_{w=}\ 2\frac{(\sigma_{nw-w})\cos\theta}{r} \quad \text{(Eq.10)}$$

Where:

- σ_{nw-w} represents interfacial tension between the non-wetting and wetting fluids.
- θ is the contact angle that defines wettability.
- r is the pore throat radius, controlling fluid entry thresholds.

Capillary pressure is a fundamental concept in fluid mechanics, particularly relevant in porous media, where it plays a significant role in the distribution and movement of fluids. This part provides a detailed exploration of capillary pressure, its principles, governing equations, factors influencing it, and practical applications.

Capillary pressure (ΔP_c) is defined as the pressure difference across the interface between two immiscible fluids in a porous medium. Mathematically:

$$\Delta P_c = P_{nw} - P_w \quad \text{(Eq.11)}$$

Where:

- P_{nw}: Pressure in the non-wetting phase.
- P_w: Pressure in the wetting phase.

This pressure difference arises due to interfacial tension and the curvature of the fluid-fluid interface, governed by the Young-Laplace equation:

$$\Delta P_c = 2\sigma r \quad \text{(Eq.12)}$$

Where:

- σ: Interfacial tension between the two fluids.
- r: Radius of curvature of the interface.

Capillary pressure reflects the tendency of a liquid to rise or be depressed in a narrow tube (capillary) due to surface tension and adhesive forces between the liquid and the solid.

In porous media, the geometry is far more intricate than that of a simple capillary tube. Pores vary in size, shape, and connectivity, resulting in significant variations in capillary pressure throughout the medium. The relationship between capillary pressure and the saturation of fluids within a porous medium is represented by the capillary pressure curve. This curve is essential for understanding how fluids are distributed, retained, and flow within reservoirs or soil. By analyzing the capillary pressure curve, researchers and engineers can gain valuable insights into fluid behavior, such as the wettability of the medium, fluid saturation levels, and the efficiency of fluid storage or extraction in geological formations. (fig.2)

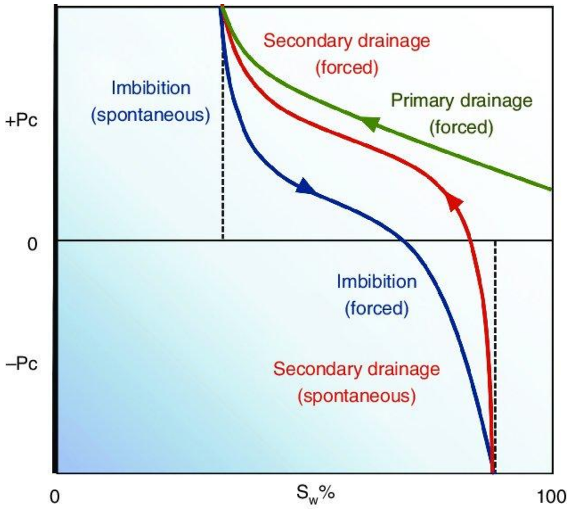

Fig.2 capillary pressure curve

Capillary pressure is measured using various techniques depending on the fluid and application. Mercury Injection Capillary Pressure (MICP) injects mercury into a sample to record pressure-saturation data. The Porous Plate Method displaces one fluid with another through a porous plate, while the Centrifuge Method creates a pressure gradient by spinning the sample. Direct Observation techniques use imaging to analyze fluid interfaces, and Pressure Chamber Techniques control water content under pressure, commonly used for soils.

4.1 Dynamic Capillary Pressure

Dynamic capillary pressure refers to the time-dependent changes in capillary pressure that occur during processes like drainage and imbibition under transient conditions. Unlike static capillary pressure, which assumes equilibrium, dynamic capillary pressure considers factors such as flow rate, fluid viscosity, and the system's response time. This phenomenon becomes particularly significant in certain conditions, such as high-flow rate systems, where the non-equilibrium behavior of fluids can lead to discrepancies between measured and predicted capillary pressures. Additionally, in unsteady-state conditions, such as during fluid injection or withdrawal in porous media, dynamic effects can cause variations in interface curvature and contact angle, altering the expected capillary behavior. Understanding dynamic capillary pressure is crucial as it helps predict real-world fluid movement more accurately in subsurface environments. Mathematical models incorporating dynamic capillary pressure often include a rate-dependent term:

$$P_c(t) = P_c(static) + f(\text{rate, viscosity, saturation}) \quad \text{(Eq.13)}$$

5. Permeability and Hydraulic Conductivity and critical/residual saturation

Permeability is a fundamental property of porous media that describes a rock's ability to transmit fluids. It is influenced by pore structure, grain size, cementation, and the presence of fractures (Bear, 2013). In cap rocks, low permeability is crucial to minimize fluid migration and ensure their effectiveness as barriers, with rocks like shales, mudstones, and evaporites typically exhibiting permeability values in the nano- to micro-darcy range, effectively restricting fluid flow and preventing leakage (Blunt, 2017). This low permeability also plays an essential role in hydraulic sealing by maintaining pressure integrity within storage formations (Bachu, 2008).

Permeability anisotropy is another significant factor, where permeability varies based on the orientation of fluid flow relative to rock fabric. This anisotropy is caused by sedimentary layering, diagenetic changes, and structural deformation, creating preferential flow paths within the rock matrix. In fractured formations, fractures can act as high-permeability conduits, enhancing fluid flow along specific directions while leaving the bulk rock relatively impermeable (Joekar-Niasar et al., 2008) .

Hydraulic conductivity is closely related to permeability but incorporates the effects of fluid properties such as density and viscosity. It describes the ease with which a fluid moves through a porous medium under a given hydraulic gradient and is defined as:

$$K = \frac{k\rho g}{\mu} \quad \text{(Eq.14)}$$

where k is permeability, ρ is fluid density, g is gravitational acceleration, and μ is fluid viscosity. While permeability is an intrinsic rock property, hydraulic conductivity depends on both rock and fluid characteristics, making it important. (Bear, 2013).

Low hydraulic conductivity is crucial for effective sealing in cap rocks, as it prevents fluid migration. Even with very low permeability, subtle pressure differences over time can cause fluid movement, threatening the integrity of the cap rock. This is especially important in CO_2 risk assessment, where maintaining low permeability and hydraulic conductivity is essential to prevent leaks. Some cap rocks, like clays, have self-sealing properties, swelling when exposed to fluids, which further reduces permeability and improves containment.

5.1 Permeability alteration in drainage

Permeability alterations due to drainage refer to the changes in a porous medium's ability to transmit fluids when a non-wetting fluid displaces a wetting fluid. During drainage, the displacement process modifies the distribution of fluids within the pore network, affecting the connectivity and flow paths available for subsequent fluid movement. The permeability of a porous medium is initially defined by its structure, but as drainage occurs, the interaction between fluids and the rock matrix modifies how easily fluids can move through it.

In single-phase flow, absolute permeability (k) determines the ease with which a fluid flows through the porous medium, following Darcy's Law. However, in two-phase systems, permeability is affected by the presence of both fluids, leading to the concept of relative permeability. Relative permeability (k_r) quantifies how much of the absolute permeability is available to each phase, considering that some portion of the pore space is occupied by the other phase. During drainage, the relative permeability of the wetting phase (k_{rw}) decreases as the non-wetting phase (k_{rnw}) begins to dominate the pore system. This transition reduces the capacity of the porous medium to conduct the wetting phase, often leading to an increase in capillary end effects and fluid trapping (Bear, 2013).

One of the most significant changes in permeability during drainage is caused by the reduction in the connectivity of the wetting phase. As the non-wetting fluid invades, the wetting phase becomes isolated in disconnected pores or thin films along the pore walls. This process, known as snap-off, creates isolated pockets of the wetting fluid, reducing its ability to flow. This effect is particularly pronounced in water-wet rocks, where water adheres to the pore walls, leaving disconnected clusters of fluid behind, thereby decreasing the effective permeability of the wetting phase (Lenormand et al., 1988). The reduction in relative permeability can lead to higher irreducible water saturation, where a fraction of the wetting phase remains trapped even at high non-wetting phase saturation levels.

The permeability of the non-wetting phase also evolves during drainage, as it depends on the extent of its saturation and the pore structure. In highly heterogeneous porous media, the displacement of the wetting phase by the non-wetting phase can be non-uniform, with some regions retaining more wetting fluid than others. This heterogeneity results in preferential flow paths, where the non-wetting phase moves through the most permeable regions, leaving lower-permeability zones partially saturated with the wetting fluid. (Joekar-Niasar et al., 2008).

Permeability alterations due to drainage are influenced by wettability, pore structure, and capillary pressure. The structure of the porous medium also plays a crucial role—materials with narrow pore throats and high tortuosity exhibit greater permeability reduction during drainage due to increased capillary retention (Morrow, 1976). high capillary pressures increasing the likelihood of trapping and permeability reduction.

5.2 Relative permeability in imbibition

Relative permeability curves for imbibition differ from those observed in drainage due to hysteresis effects. As the wetting phase saturation increases, the mobility of the non-wetting phase declines non-linearly. In water-wet reservoirs, water preferentially coats the pore walls, creating thin wetting films that enhance connectivity for the wetting phase. However, the advancing wetting phase can also trap the non-wetting phase in disconnected ganglia, reducing its effective permeability (joekar-niasar et al., 2008).

Relative permeability relationships are commonly modeled using empirical correlations such as the brooks-corey and van genuchten models, which describe how permeability changes with saturation (lenormand et al., 1988).

5.3 Residual saturation and trapping mechanisms in drainage

Residual saturation and trapping mechanisms in drainage refer to the portion of the wetting phase that remains trapped in the porous medium even after a non-wetting fluid displaces it.

Residual saturation is typically categorized into residual wetting-phase saturation and residual non-wetting-phase saturation. Residual wetting-phase saturation (S_{rw}) refers to the portion of the wetting phase that remains in the pores after drainage, while residual non-wetting-phase saturation (S_{rnw}) refers to the portion of the non-wetting phase that remains after imbibition. During drainage, capillary forces create disconnected clusters or films of the wetting phase within the pore network, preventing complete displacement by the non-wetting phase. This trapping occurs because small pore throats require a high capillary pressure to overcome the entry resistance, leading to snap-off and entrapment of the wetting phase in isolated pores (Lenormand et al., 1988).

The magnitude of residual saturation depends on several factors, including wettability, pore structure, and capillary pressure. In strongly water-wet systems, the wetting phase preferentially coats the pore walls, and drainage occurs by the displacement of water from the larger pore centers while thin films of water remain attached to the solid surface. In contrast, in oil-wet systems, oil tends to adhere to the rock surfaces, making water displacement more effective and reducing residual oil saturation (Morrow, 1976). Pore geometry also plays a crucial role, as irregularly shaped and poorly connected pores increase the likelihood of trapping the wetting phase.

Capillary pressure, governs the amount of residual saturation in drainage. The relationship between capillary pressure and saturation is represented by capillary pressure curves, which exhibit hysteresis due to trapping effects. As drainage progresses, the wetting-phase saturation decreases, but some of it remains immobilized when the capillary pressure drops, leading to an irreducible wetting-phase saturation (Joekar-Niasar et al., 2008). This hysteresis is a key factor in understanding two-phase flow behavior in porous media.

6. Comparison between capillary driven and viscous driven flow

6.1 Darcy's Law and two-phase flow in drainage

Darcy's Law and two-phase flow in drainage describe how a non-wetting fluid displaces a wetting fluid in a porous medium under the influence of pressure gradients and permeability constraints. Darcy's Law, originally formulated for single-phase flow, states that the flow rate of a fluid through a porous medium is proportional to the pressure gradient and the permeability of the medium while being inversely proportional to the fluid's viscosity. The equation is expressed as:

$$Q = -\frac{kA}{\mu}\frac{dP}{dx} \quad \text{(Eq.15)}$$

where Q is the volumetric flow rate, k is the absolute permeability, A is the cross-sectional area, μ is the dynamic viscosity of the fluid, and $\frac{dP}{dx}$ is the pressure gradient. However, in drainage, where two immiscible fluids coexist, the standard form of Darcy's Law is no longer sufficient because the fluids interact and compete for space within the pore network, affecting permeability.

To account for these interactions, Darcy's Law is modified for two-phase flow by introducing relative permeability, which quantifies the reduction in permeability due to the presence of a second fluid. The modified equation for a specific phase iii (wetting or non-wetting) is:

$$Q_i = -\frac{k_{ri}kA}{\mu_i}\frac{dP_i}{dx} \quad \text{(Eq.16)}$$

where k_{ri} is the relative permeability of phase i, which depends on the saturation of that phase in the pore system. The sum of the relative permeabilities of the wetting and non-wetting phases is always less than one, meaning that fluid interactions hinder each other's movement. This reduction in effective permeability impacts the efficiency of drainage.

During drainage, the non-wetting phase invades the pore network, displacing the wetting phase. The efficiency of this displacement depends on the balance between viscous forces, capillary forces, and gravity. In systems where capillary forces dominate, the displacement is irregular, forming capillary fingering patterns. In contrast, when viscous forces dominate, the displacement front can become unstable, leading to viscous fingering.

In drainage, permeability is reduced for both phases because the pore space is shared, leading to residual wetting-phase saturation even after significant drainage. The trapping of the wetting phase occurs due to capillary forces, especially in fine-grained materials where pore-throat sizes restrict non-wetting fluid entry.

6.2 Gravity-driven and capillary-driven mechanisms

It describes two competing forces that control how a non-wetting fluid displaces a wetting fluid in a porous medium, and this applies to both drainage and imbibition processes. The dominance of either mechanism depends on the interplay between gravitational forces, capillary forces, and the characteristics of the porous medium, including pore structure, permeability, and fluid properties (Dullien, 1992; Bear, 2013).

In gravity-driven drainage, fluid movement is primarily influenced by the density difference between the wetting and non-wetting phases. The non-wetting fluid, typically a lower-density phase such as gas or oil, rises due to buoyancy forces, while the denser wetting phase, often water, drains downward under the influence of gravity. The efficiency of gravity-driven drainage depends on the density contrast between the fluids, the permeability of the rock, and the thickness of the geological formation. A higher density difference enhances buoyancy effects, promoting vertical segregation of the fluids. However, in heterogeneous formations with varying permeability, gravity-driven flow can be disrupted by capillary retention, leading to uneven fluid distribution (Lake, 1989).

In capillary-driven drainage, the displacement of a wetting fluid by a non-wetting fluid occurs due to capillary pressure differences across the pore network. This process is common in tight formations or fine-grained rocks where small pore throats generate strong capillary forces that oppose the invasion of the non-wetting phase. Capillary-driven drainage often results in snap-off effects and the formation of disconnected fluid clusters, which can significantly impact storage capacity and flow behavior in porous media (Lenormand et al., 1988; Blunt, 2017).

Conversely, imbibition refers to the reverse process, where a wetting fluid displaces a non-wetting fluid. In capillary-driven imbibition, the wetting fluid spontaneously fills the pores due to capillary pressure. The ability of the wetting phase to invade the porous medium depends on wettability, pore connectivity, and interfacial tension between the fluids (Morrow, 1976; Al-Yaseri et al., 2015). In gravity-driven imbibition, the wetting phase moves downward due to its higher density, while the non-wetting fluid is displaced upwards, typically occurring in large-scale migration of CO_2 or hydrocarbon leaks. The interaction between capillary and gravity-driven imbibition can create complex saturation distributions, influencing containment and migration behavior in subsurface storage applications (Hirasaki et al., 1990; Pentland et al., 2011).

The Bond number (Bo) is commonly used to determine whether gravity or capillary forces dominate in each system. It is defined as:

$$B_o = \Delta\rho . g . k/\gamma \quad \text{(Eq.17)}$$

where $\Delta\rho$ is the density difference between the fluids, g is gravitational acceleration, k is the permeability of the medium, and γ is the interfacial tension. A high Bond number (Bo>1) indicates that gravity forces dominate, leading to gravity-driven drainage, while a low Bond number (Bo<1) suggests that capillary forces are stronger, resulting in capillary-driven drainage. In most subsurface environments, capillary forces tend to dominate at the pore scale, whereas gravity becomes more significant at larger scales, such as in thick reservoirs or during large-scale fluid migration.

6.3 Viscous and Inertial Effects on Fluid Displacement

In both drainage and imbibition, fluid motion is governed by the balance of capillary, viscous, and inertial forces. At low capillary numbers ($Ca=\mu V/\gamma$), capillary forces dominate, leading to slow, controlled displacement where fluid movement follows equilibrium capillary pressure curves. However, at higher capillary numbers, viscous forces become more significant, altering flow patterns and reducing the influence of capillarity.

Inertia also plays a role when fluid velocities are high, particularly in fractured formations or high-permeability channels, where momentum effects can lead to flow instability, fingering, and bypassing of certain regions. These inertial effects can modify saturation distributions and impact the efficiency of fluid displacement, especially when a phase transition occurs between drainage and imbibition (Blunt, 2017).

7. Geochemical Interactions and Rock fluid interactions

Prolonged exposure to reactive fluids, such as CO_2 and brine, can cause significant geochemical changes in cap rocks, impacting their mineralogy, porosity, and permeability, which may reduce their sealing efficiency. One concern is mineral dissolution, where CO_2-rich brines dissolve certain minerals, potentially creating fractures or increasing pore sizes, thereby increasing permeability and weakening the seal. Conversely, CO_2-brine reactions can lead to mineral precipitation, such as carbonates, which may block pore spaces and improve sealing. However, the stress from mineral buildup can also cause fractures, weakening the cap rock. Additionally, CO_2 can trigger clay mineral swelling, which can seal fractures and enhance the rock's sealing capacity, but excessive swelling may lead to stress, increasing the risk of failure.

To mitigate these risks, strategies such as geochemical modeling, inhibitor injection, and continuous monitoring can be employed. Geochemical modeling helps predict changes in the rock’s properties, allowing operators to plan mitigation strategies. Inhibitor injections reduce harmful reactions like mineral dissolution; while monitoring and surveillance of fluid composition and rock properties can provide early warnings of potential degradation, enabling timely interventions to preserve cap rock integrity.

7.1 Adhesion and Cohesion

Cap rock sealing efficiency is vital for keeping hydrocarbons and CO_2 contained within subsurface reservoirs. This efficiency hinges on two key forces: cohesion and adhesion. Cohesion, the internal forces such as electrostatic interactions and van der Waals forces that hold rock particles together, ensures the rock maintains its structure and resists fracturing, which in turn helps preserve low permeability. In contrast, adhesion is the attraction between the rock surface and the fluids, affecting how well a protective water film forms on water-wet cap rocks and increasing the capillary entry pressure that stops non-wetting fluids from seeping through. Together, strong cohesion and adhesion create a robust barrier by boosting capillary entry pressure, thereby preventing fluid migration even under high-pressure conditions, such as those encountered during CO_2 injection or in hydrocarbon reservoirs. This combined effect is especially significant in clay-rich shales, where the inherent strength and bonding of clay minerals contribute to long-term sealing integrity.

8. Cap rock properties

8.1 Definitions and Components

A cap rock is a layer of impermeable rock that sits above a reservoir, acting as a natural barrier to stop fluids from moving upward into other formations. Its main role is to seal the reservoir and keep fluids contained. The effectiveness of this seal, known as sealing efficiency, depends on three main factors: capillary, hydraulic, and mechanical sealing. Capillary sealing efficiency is about the rock's ability to resist fluid movement through its pores. This resistance is based on capillary entry pressure, which is the minimum pressure needed for fluid to penetrate the rock. Hydraulic sealing efficiency relies on the rock’s very low permeability, which prevents fluids from flowing through it. Lastly, mechanical sealing efficiency refers to the cap rock’s strength and ability to handle stress without cracking, ensuring it stays intact under operational and natural geological conditions.

The importance of a strong and effective cap rock cannot be overstated. In hydrocarbon storage, a reliable cap rock is crucial to keep oil and gas from escaping to the surface or nearby formations. It maintains the pressure inside the reservoir and resists the upward push of hydrocarbons. It needs to hold up against the buoyant forces of CO_2 and any pressure changes from injection processes. Similarly, for natural gas storage in places like depleted reservoirs or salt caverns, the integrity of the cap rock is key to stopping gas from migrating into surrounding formations. Overall, the sealing efficiency of a cap rock is critical for ensuring safe, effective, and environmentally friendly storage in these applications.

8.2 Mechanical Strength of Cap Rocks

The mechanical strength of cap rocks is crucial for preventing fluid migration from underlying reservoirs in subsurface fluid storage applications. These rocks must withstand stress and remain intact to maintain their sealing function, ensuring long-term containment integrity (Bear, 2013). The in-situ stress regime, including tectonic forces, overburden pressure, pore fluid pressure, and differential stress, influences the mechanical stability of cap rocks. Shales, mudstones, and evaporites typically have low permeability and high capillary entry pressure, effectively preventing leakage, but increased stress from fluid injection—such as during CO_2 storage—can compromise their stability, potentially leading to fractures, fault reactivation, or shear failure (Bachu, 2008).

Natural fractures and faults within cap rocks also affect their sealing ability. While low-permeability cap rocks may resist leakage, pre-existing fractures can act as conduits for fluid migration if they are reactivated by stress changes. Geomechanical models are used to predict stress distribution, fault behavior, and fracture reactivation potential, incorporating rock strength, in-situ stress, and fluid pressure data to evaluate cap rock stability under various conditions (Blunt, 2017).

In CO_2 risk assessing, maintaining cap rock integrity is critical for secure storage. The injection of CO_2 increases pore pressure, reducing effective stress and potentially triggering fractures. Controlled injection strategies and monitoring techniques, such as microseismic analysis and borehole stress measurements, help manage these risks by tracking stress evolution and providing early warnings of potential failure (Joekar-Niasar et al., 2008).

Cap rock mechanical properties are also influenced by mineral composition and porosity. Clay-rich rocks like shales tend to deform ductilely under stress, while more brittle rocks, like carbonates, are prone to sudden fracturing. Some clay-rich formations, like Opalinus Clay, can self-seal over time by allowing fractures to heal through clay swelling and compaction (Bachu, 2008). Understanding the mechanical strength of cap rocks is also essential for groundwater protection and waste isolation, as unstable cap rocks can lead to contamination. Hydromechanical coupling models, which integrate fluid flow and stress interactions, are used to predict cap rock behavior in response to natural anthropogenic pressures (Bear, 2013). By combining stress analysis, fracture mechanics, and fluid pressure monitoring, the mechanical sealing efficiency of cap rocks can be optimized for long-term storage security in geological applications.

9.Sealing Efficiency of Cap Rocks in Subsurface Storage Systems

A) Definition of the parameters

The sealing efficiency of a cap rock is paramount in ensuring the secure and sustainable operation of subsurface storage systems, encompassing a wide range of applications, including hydrocarbon reservoirs, carbon capture and storage (CCS) sites, and natural gas storage facilities. A cap rock, typically composed of impermeable formations like shale, salt, or anhydrite, acts as a crucial barrier, preventing the upward migration of stored fluids, such as oil, gas, CO_2, and other substances.

9.1 Cap rock sealing efficiency

The sealing capacity of cap rocks is primarily controlled by pore throat size, interfacial tension (γ), and contact angle (θ). Fine-grained rocks like shale have smaller pore throats, leading to higher capillary entry pressures and better sealing efficiency. Higher interfacial tension between hydrocarbons and water strengthens the resistance to migration, while the contact angle defines the wettability of the rock. Water-wet rocks (higher θ) improve the ability of the cap rock to retain fluids by favoring water retention over hydrocarbon penetration.

Beyond capillary entry pressure, the effectiveness of a cap rock is influenced by threshold displacement pressure and snap-off pressure. Snap-off enhances long-term trapping by fragmenting the non-wetting phase into disconnected pockets, improving storage security in CO_2 sequestration and hydrocarbon retention.

9.2 Residual Pressure, Re-Imbibition, and Long-Term Seal Efficiency

Following fluid displacement events, residual saturation of the non-wetting phase remains within the cap rock, exerting a pressure that affects further fluid migration. During re-imbibition, the wetting phase re-enters the pore space, leading to pressure drops that further enhance the capillary trapping of hydrocarbons or CO_2. The magnitude of snap-off pressures and residual saturation depends on the rock's wettability and pore connectivity. High residual CO_2 saturation in sequestration projects reduces the risk of long-term leakage.

9.3 Buoyant Force and Displacement

9.3.1 Buoyant Force and Its Role in Hydrocarbon Migration

Buoyant force is the upward force exerted by a denser fluid, such as water, on a less dense fluid, like oil or gas. This force is created due to the density difference between the two fluids and is a key driver of hydrocarbon migration in sedimentary basins. Since hydrocarbons are lighter than water, they naturally rise through porous reservoir rocks, seeking to escape until they encounter an impermeable barrier, known as a cap rock, which prevents further movement and leads to hydrocarbon accumulation.

The magnitude of the buoyant force (Fb) can be calculated using the equation:

$$F_b = (\rho_{water} - \rho_{hc}) \times g \times V_{hc} \quad \text{(Eq.18)}$$

where:

- F_b = Buoyant force
- ρ_{water}= Density of water
- ρ_{hc} = Density of hydrocarbons
- g = Acceleration due to gravity
- V_{hc}= Volume of hydrocarbons

The greater the density difference between water and hydrocarbons, the stronger the buoyant force, which drives hydrocarbon migration. However, buoyant force alone does not dictate hydrocarbon movement, other geological factors, such as capillary pressure and displacement forces, counteract this movement and influence how hydrocarbons accumulate.

9.3.2 Displacement and Its Impact on Hydrocarbon Accumulation

Displacement is the process by which water is pushed aside as hydrocarbons migrate upward through the reservoir rock, generating a counteracting hydraulic resistance. For hydrocarbons to accumulate effectively, the buoyant force must overcome this resistance; otherwise, they may become trapped at lower depths. Moreover, displacement pressure can lead to capillary trapping, particularly in water-wet reservoirs where rock surfaces retain water, resulting in residual hydrocarbon saturation that hinders the formation of larger accumulations.

9.3.3 The interaction Between Buoyancy, Displacement, and Cap Rock Sealing

The balance between buoyant force, displacement pressure, and cap rock sealing determines whether migrating hydrocarbons remain trapped or break through their barrier. In essence, a high-quality cap rock must have enough capillary entry pressure to counteract the upward push of hydrocarbons. If the buoyant force is too strong, it can overcome this resistance, allowing hydrocarbons to breach the seal and potentially seep to the surface or enter non-productive formations. These same principles apply to CO_2 sequestration and gas storage, where buoyant forces drive injected gases toward the cap rock while displacing native fluids and affecting overall pressure. Ensuring that the cap rock's sealing capacity exceeds the buoyant forces at play is therefore critical to preventing leakage in long-term storage projects.

9.3.4 Buoyant and Displacement Forces in Hydrocarbon and Gas Storage

Buoyant forces arise due to density differences between fluids and play a significant role in fluid migration. In hydrocarbon reservoirs and CO_2 storage, buoyancy determines the maximum height of a hydrocarbon or CO_2 column that can be retained beneath the cap rock. If the buoyant force exceeds the combined capillary entry and displacement pressures, leakage may occur.

The critical hydrocarbon column height is a key factor in assessing storage integrity and is given by:

$$h_{critical} = \frac{2\gamma \cos\theta}{(\rho_{water} - \rho_{hc}) \times g} \quad \text{(Eq.19)}$$

where:

- $h_{critical}$ = Maximum hydrocarbon column height that can be supported
- γ = Interfacial tension between hydrocarbons and water
- θ = Contact angle between the fluids and rock
- ρ_{water} = Density of water
- ρ_{hc} = Density of hydrocarbons
- g = Acceleration due to gravity

This equation provides a theoretical limit on how much hydrocarbon can be stored beneath a cap rock before breaching occurs. If the hydrocarbon column exceeds this critical height, the risk of leakage increases, making it a crucial parameter in hydrocarbon exploration and storage assessments.

9.4 Effectiveness of cap rock

The effectiveness of a cap rock in sealing hydrocarbons depends on multiple factors that influence buoyant force, displacement, and fluid migration. These factors range from fluid properties and cap rock characteristics to reservoir geometry and external geological forces. Understanding these influences is essential for assessing reservoir integrity, predicting hydrocarbon accumulation, and ensuring long-term containment in geological storage projects.

9.4.1 Fluid Properties

The density of hydrocarbons and the interfacial tension between hydrocarbons and water are key factors affecting buoyancy and capillary forces in a cap rock. Lower-density hydrocarbons like natural gas experience stronger buoyant forces compared to heavier ones such as crude oil, making them more prone to upward migration and thus requiring higher capillary entry pressures to be effectively contained. At the same time, a higher interfacial tension creates greater resistance to fluid movement, enhancing the cap rock's ability to prevent hydrocarbons from penetrating through it.

9.4.2 Cap Rock Properties

Smaller pore throats increase the capillary entry pressure, making it harder for hydrocarbons to migrate—fine-grained formations like shale are especially effective in this regard. Additionally, water-wet cap rocks enhance sealing efficiency by resisting hydrocarbon entry; higher contact angles between hydrocarbons and rock surfaces boost this capillary resistance. Finally, low permeability is essential for maintaining an effective seal, as ultra-low permeability formations such as shale and evaporites act as robust, long-term barriers against fluid leakage.

9.4.3 Reservoir and Trap Geometry

The total hydrocarbon volume that can be stored depends on the available space and the water displaced by the hydrocarbons—larger reservoirs offer more storage capacity, while smaller ones may become over-pressurized, increasing leakage risks. Additionally, the geometry of the geological trap, whether it’s an anticline, fault block, or stratigraphic trap, significantly influences hydrocarbon migration and retention. Effective traps provide natural containment and rely on continuous seals and fault sealing properties to prevent hydrocarbons from escaping laterally, ensuring better overall reservoir performance.

9.5 Evaluation and Monitoring of Cap Rock Sealing Efficiency

9.5.1. Laboratory Analysis

Laboratory tests play a crucial role in understanding the physical properties of cap rock, ensuring it can effectively seal and contain fluids over time. Mercury Injection Capillary Pressure (MICP) is a widely used technique that simulates capillary entry pressure by injecting mercury into rock samples, helping to determine pore throat size distribution and capillary pressures. Core permeability tests provide further insight by measuring how easily fluids can pass through the rock under controlled pressure conditions, giving a direct assessment of its ability to resist fluid migration (Gu et al., 2024). To get a clearer picture of storage potential, porosimetry techniques like helium pycnometry and nitrogen adsorption are used to measure porosity and pore size distribution. Geomechanical tests, such as uniaxial and triaxial compression tests, help evaluate the rock's mechanical strength and how it reacts under stress, ensuring it can withstand pressure changes without fracturing. Fluid-rock interaction experiments are also valuable, as they simulate chemical reactions between injected fluids and cap rock minerals to identify any changes in permeability or mechanical stability over time. Another important method is the snap-off test, which looks at how non-wetting fluids move and become trapped within pore networks, helping to assess the risk of leakage and the effectiveness of natural capillary barriers—we will explore this test in more detail later.

9.5.2. Field Assessment

Field techniques complement laboratory analyses by examining cap rock properties on a larger scale. Seismic surveys provide detailed information on the thickness, continuity, and structural integrity of the cap rock, identifying any potential weaknesses or discontinuities. Additionally, well logging techniques analyze lithology, porosity, and fluid distribution within the reservoir and cap rock, offering valuable data on the geological conditions influencing storage integrity.

9.5.3. Monitoring Systems

Monitoring during and after injection operations is critical to ensure the cap rock remains intact. Pressure and gas migration sensors are installed to detect potential breaches in real time, providing continuous data on the integrity of the cap rock seal. Advanced techniques enhance these monitoring efforts. Geochemical tracers, such as stable isotopes or noble gases, are used to detect potential leaks from the storage reservoir. Micro seismic monitoring detects seismic activity induced by injection operations, providing insights into potential fracturing or stress-related damage to the cap rock. Remote sensing techniques, like satellite-based interferometric synthetic aperture radar (InSAR), monitor subtle surface deformations that may indicate subsurface fluid migration or pressure changes. These tools collectively ensure comprehensive monitoring and early detection of any risks to the cap rock's sealing efficiency.

B) Lab Tests (Experimental Methodology)

1. Mercury Injection Porosimetry (MIP)

Mercury Injection Porosimetry (MIP) is a valuable technique used to analyze the pore structure of materials like rocks and soils. It works by injecting mercury, a non-wetting fluid, into the pore spaces under increasing pressure. This process helps measure pore throat sizes, pore size distribution, and capillary entry pressure. The technique provides crucial insights into properties such as porosity and fluid flow behavior, making it essential for evaluating cap rock integrity.

Principles of Mercury Injection Porosimetry

MIP is based on the physics of capillary pressure, where mercury, being a non-wetting fluid, does not spontaneously infiltrate porous materials and thus requires external pressure to overcome surface tension forces and enter the pores. The fundamental relationship governing this process is described by the Washburn equation:

$$r = \frac{2\gamma \cos\theta}{P} \quad \text{(Eq.20)}$$

where r represents the pore throat radius, γ is the surface tension of mercury (0.485 N/m), θ is the contact angle of mercury with the pore wall (typically ~140°), and P is the applied pressure. This equation highlights that smaller pores require higher pressures for mercury intrusion, establishing a direct link between applied pressure and pore size distribution.

Parameters estimated by MIP

MIP offers a wealth of quantitative data on pore structure, enabling the evaluation of reservoir quality, cap rock efficiency, and fluid transport mechanisms. The most critical parameters estimated include pore size distribution, which determines the frequency of different pore sizes within a material. Larger pores are accessed at lower pressures, whereas smaller pores require significantly higher pressures for mercury intrusion. Another essential parameter is the pore throat radius, which represents the narrowest pathways within the pore network and plays a crucial role in influencing capillary entry pressure and fluid flow properties. The threshold pressure, which is the minimum pressure required to overcome capillary forces and initiate mercury penetration into the smallest pore throats, provides insights into the sealing efficiency of cap rocks. Additionally, MIP enables porosity estimation, which is determined from the total mercury intrusion volume, providing a measure of the void space within the sample. Other important parameters include bulk and skeletal density(fig.3), with bulk density accounting for both solid and pore space, while skeletal density is calculated by excluding the pore space. Pore connectivity, capillary entry pressure, and total pore volume further contribute to understanding the material's capacity for fluid retention and transport.

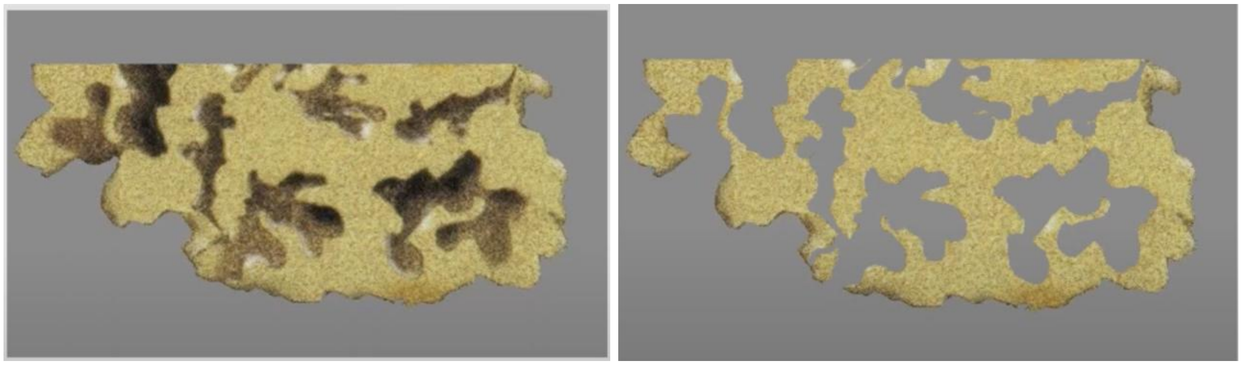

Fig.3 a)bulk density and b)skeletal density

Experimental Procedure of MIP

The MIP experimental workflow follows a systematic approach to ensure precise and reproducible results. It begins with sample preparation, where the material, whether a rock core, soil sample, or synthetic porous medium—is selected based on the study objective. The sample is thoroughly dried to eliminate any residual moisture that might interfere with mercury intrusion, and its weight and dimensions are recorded to facilitate calculations of bulk density and porosity. The next step involves loading the sample into a sealed chamber connected to a mercury reservoir. (fig.4,5) The experiment progresses in two stages: the low-pressure stage, where mercury is introduced at pressures ranging from 0.01 MPa to 0.2 MPa to infiltrate macropores, and the high-pressure stage, where pressure is increased up to 400 MPa to access nanopores and finer pore throats. Throughout the process, the volume of intruded mercury is continuously measured, allowing for the generation of pore size distribution curves, capillary pressure estimates, and connectivity assessments.

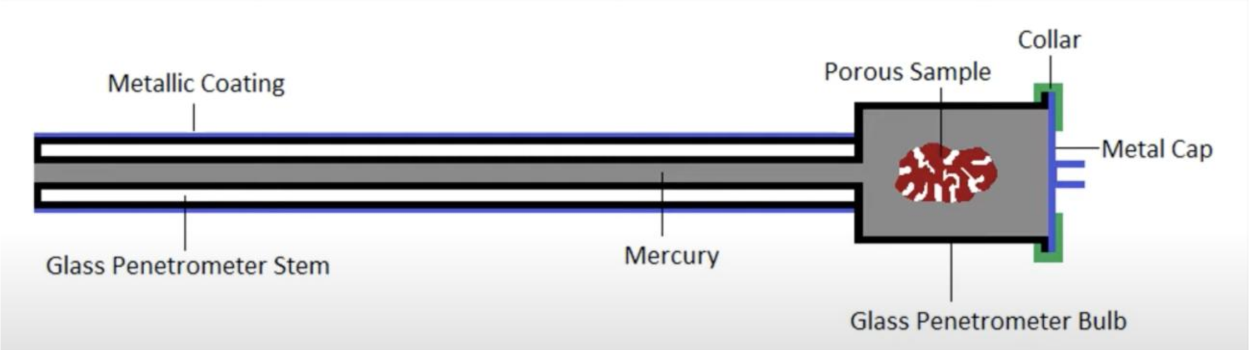

Fig. 4

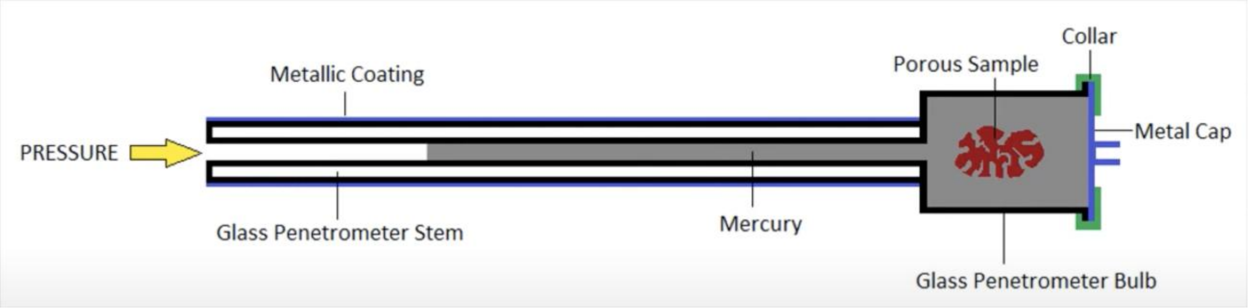

Fig.5

Test Outputs

MIP data are presented through numerical and graphical outputs that provide insights into pore structure and material properties. Key results include pore size distribution curves, which show the volume and frequency of pores at different pressure levels. The threshold pressure indicates the pressure required to access the smallest pore throats, while the capillary pressure curve helps estimate capillary entry pressure in cap rocks. Additionally, MIP offers data on bulk and skeletal densities, distinguishing total porosity from effective porosity. These parameters are crucial for evaluating reservoir and cap rock integrity, supporting decisions in hydrocarbon extraction and geological storage projects.

Advantages of Mercury Injection Porosimetry

One of its most significant benefits is its ability to provide precise, quantitative data on pore size distribution, porosity, and capillary pressure. Its broad pressure range allows for the measurement of macropores (~10 µm) down to nanopores (~3 nm), covering a wide spectrum of geological and synthetic materials. Additionally, MIP is a fast and repeatable technique, offering high reproducibility and efficiency, making it ideal for industrial and academic applications. The technique is also versatile, being applicable across multiple disciplines, including geoscience, materials science, and engineering, where it aids in studying rocks, soils, ceramics, and engineered porous materials.

Limitations of Mercury Injection Porosimetry

Despite its many advantages, MIP also has some limitations. One notable drawback is the assumption that pores are cylindrical, which may not accurately reflect the complex geometry of natural rock pore systems. Furthermore, the high pressures used in MIP can potentially compress or damage fragile samples, altering their pore structure and affecting results. Another limitation is the toxicity of mercury, which requires strict safety protocols for handling and disposal. Additionally, while MIP provides pore connectivity estimates, it does not directly measure permeability, necessitating complementary methods for a more comprehensive fluid flow analysis.

2. Step-by-Step (Breakthrough Pressure) Test

The breakthrough pressure test is a critical method for evaluating the sealing efficiency of cap rocks in geological formations. The primary objective of the test is to determine the minimum gas pressure required to overcome the capillary forces within the water-saturated rock, allowing continuous gas flow through the sample. This breakthrough pressure is a crucial parameter in assessing a cap rock's ability to retain fluids over long periods under various subsurface conditions. The procedure involves several systematic steps to ensure accuracy and reliability.

Procedure of the Test

1. Sample Preparation

The process begins with meticulous sample preparation, where the rock sample is thoroughly cleaned and fully saturated with water or brine to replicate in-situ reservoir conditions. This step is vital in ensuring that the rock's natural fluid saturation state is accurately represented, as any deviation could impact the measurement of breakthrough pressure. The prepared sample is then placed into a specially designed core holder, which is capable of withstanding high pressures to simulate the natural stress conditions of the subsurface environment.

2. Confining Pressure Application

Once the sample is securely positioned, confining pressure is applied around it to replicate the stress conditions the cap rock experiences underground. This confining pressure simulates overburden pressure and any lateral stresses acting on the rock formation, ensuring that the test conditions closely resemble the real geological setting.

3. Gas Injection

After establishing the appropriate confining pressure, the next step is the controlled injection of a selected gas, such as nitrogen, methane, or carbon dioxide, into the upstream end of the core holder. The gas pressure gradually increased in small, controlled increments to monitor the rock's response and determine the precise point at which breakthrough occurs.

4. Monitoring and Data Acquisition

Throughout the test, precise monitoring and data acquisition play a crucial role. The gas pressure and any observable flow through the downstream end of the core holder are continuously recorded using sensitive pressure transducers and flow meters.

5. Breakthrough Pressure Determination

The breakthrough pressure is identified as the point at which a stable and continuous gas flow is detected at the downstream end, indicating that the gas has successfully displaced the wetting fluid within the rock and overcome the capillary forces holding it in place.

Advantages of the Breakthrough Pressure Test

One of the significant advantages of this method is its ability to directly simulate in-situ conditions, including confining pressure and fluid saturation, making it a highly realistic approach to evaluating cap rock integrity. It provides a direct and reliable measurement of the pressure required to breach the cap rock, which is essential for assessing sealing efficiency in both hydrocarbon and CO_2 storage applications. Furthermore, the versatility of the method allows for testing different gas types, making it possible to evaluate the cap rock's resistance to various subsurface fluids.

Limitations of the Test

However, the test is not without limitations. One of the primary drawbacks is the time-consuming nature of the procedure, as the gradual pressure increments, and stabilization requirements extend the duration of the test. Additionally, the method necessitates precise control and monitoring equipment, such as high-pressure gas injection systems and sensitive measuring instruments, which can add to operational complexity and cost. Another consideration is the potential for sample disturbance during preparation, confining pressure application, and gas injection, which may introduce variability in the test results.

3. Residual Capillary Pressure Test

The Residual Capillary Pressure Test is a key experimental method used to evaluate the sealing efficiency of cap rocks after a fluid displacement event. When non-wetting fluids like gas or hydrocarbons invade the pore network of a cap rock, some portion remains trapped due to capillary forces, creating a residual saturation. During re-imbibition, the wetting phase (usually water or brine) re-enters the pore space, displacing the trapped non-wetting fluid. The pressure required to expel this residual fluid is known as residual capillary pressure. This test provides valuable insights into the ability of cap rocks to maintain their sealing capacity over time, influencing fluid retention, capillary trapping efficiency, and the potential for leakage. It is crucial for applications in underground gas storage, where ensuring effective long-term containment is essential for storage security.

Experimental Procedure for the Residual Capillary Pressure Test

1. Breakthrough Stage

The test begins with a breakthrough pressure measurement, where gas is injected into a fully water-saturated rock sample under controlled conditions. The breakthrough pressure is determined as the minimum gas pressure required to overcome capillary forces and initiate continuous gas flow through the rock. This stage simulates the initial invasion of non-wetting fluids into the cap rock and serves as a baseline for evaluating resealing behavior.

2. Re-imbibition Stage

Once breakthrough occurs, gas injection is stopped**,** and the system is allowed to stabilize. The wetting fluid (water or brine) is then introduced, displacing the trapped gas phase. Re-imbibition can be carried out using two different approaches:

- Pressure Reduction: Gradually lowering the gas pressure allows the wetting fluid to naturally re-enter the pore network due to capillary forces.
- Direct Injection: Actively injecting the wetting fluid into the system forces the non-wetting phase out of the pores, accelerating the process.

Throughout this stage, pressure differences between the gas and wetting fluid phases are continuously monitored to track fluid displacement behavior in real time.

3. Measuring Residual Capillary Pressure

Once equilibrium is reached, residual capillary pressure is recorded**,** representing the pressure required to expel the remaining trapped non-wetting fluid from the pore network. The magnitude of this pressure provides essential data on the resealing potential of the cap rock and its ability to maintain long-term containment of hydrocarbons or injected gases.

Key Factors Influencing Test Results

Capillary pressure exhibits hysteresis, meaning the pressure required to displace the non-wetting fluid during re-imbibition is typically lower than the pressure required to initially invade the pore space. This is due to fluid retention, changes in interfacial tension, and modifications in pore connectivity after displacement. Recognizing this hysteresis effect is crucial when interpreting residual capillary pressure data. Changes in rock wettability can significantly influence residual saturation and capillary pressure behavior. Several factors may contribute to wettability alterations, including organic adsorption, where organic compounds modify rock surfaces, changing their preference for wetting or non-wetting fluids, and mineral precipitation, where geochemical reactions between injected fluids and cap rock minerals can form precipitates that alter pore throat size, fluid interactions, and capillary entry pressures. These alterations affect the efficiency of re-imbibition and the long-term containment capacity of the cap rock.

The pore structure and connectivity of the cap rock strongly influence residual saturation and fluid migration behavior. Several factors play a role, including pore throat size distribution, where smaller pore throats increase residual saturation by preventing complete displacement of the non-wetting phase, pore shape, where irregularly shaped pores create isolated zones where fluids can remain trapped indefinitely, and dead-end pores, which trap fluids permanently, increasing retention and reducing overall fluid mobility. Understanding these characteristics helps in predicting fluid migration risks and improving sealing efficiency in storage applications.

CHAPTER 3 (Problem statement, workflow, ML)

1.Problem statement

The effectiveness of underground gas storage—whether for carbon capture and storage (CCS), hydrocarbon reservoirs, or underground gas storage (UGS) facilities—relies on the ability of cap rocks to prevent fluid migration over geological time scales. A cap rock functions as a seal, restricting the upward movement of gases such as CO_2, methane, or hydrogen. However, the integrity of these geological barriers is dictated by critical pressures, including breakthrough pressure (Pb), threshold displacement pressure (Pd), snap-off pressure, and residual capillary pressure. These pressures define the point at which a gas phase can breach the cap rock, migrate through its pore network, and ultimately escape into overlying formations or the atmosphere.

The accurate prediction of these pressures is fundamental for assessing sealing efficiency and ensuring long-term containment. However, due to the complexity of subsurface geology, current methods for estimating critical pressures face significant limitations in accuracy, scalability, and applicability. This presents a major challenge for industries involved in geological storage, energy transition, and subsurface engineering, where understanding cap rock integrity is crucial for risk assessment and operational decision-making.

1.1 Challenges in Predicting Critical Pressures

Traditional laboratory-based methods, such as mercury injection porosimetry (MIP), high-pressure gas breakthrough experiments, and core flooding tests are widely used to determine cap rock sealing efficiency. While these methods provide valuable insights, they suffer from several key limitations:

1. High Cost and Time-Intensity: Experimental procedures require physical rock samples, complex instrumentation, and extended testing periods, making them expensive and impractical for large-scale reservoir assessments.
2. Limited Spatial Representation: Laboratory tests are conducted on small core samples, which may not be fully representative of the geological heterogeneity found in field-scale formations**.** Variability in mineralogy, pore structure, and stress conditions can lead to uncertain extrapolations of cap rock behavior.
3. Simplified Assumptions in Empirical Models: Traditional regression-based models used to predict breakthrough pressures often assume linear relationships between geological properties and sealing capacity. However, cap rock behavior is inherently nonlinear**,** influenced by multiple interacting factors**,** such a**s** wettability, pore throat connectivity, and in-situ stress conditions**.**
4. Lack of Integration with Geological and Reservoir Data: Current methodologies rarely incorporate large-scale petrophysical, geophysical, and well log data, which are critical for understanding subsurface variability. As a result, existing models may overlook essential parameters that influence capillary sealing mechanisms**.**

Given these challenges, there is a clear need for an alternative approach that can enhance the accuracy, efficiency, and scalability of critical pressure predictions for cap rock integrity.

1.2 Problem Definition and Research Gap

Despite advancements in cap rock characterization, there is currently no widely adopted, data-driven framework capable of predicting critical pressures with high accuracy across diverse lithologies and cap rock conditions**.** The challenge lies in the complex interplay of mineral composition, pore geometry, fluid properties, and stress conditions, which collectively dictate sealing efficiency**.** Existing models fail to capture these multidimensional dependencies**,** leading to uncertain estimates of cap rock stability.

Research Gap: The lack of an integrated, machine-learning-based predictive model that utilizes large-scale geological datasets, experimental measurements, and petrophysical properties to accurately estimate breakthrough and displacement pressure**s** remains a significant limitation in subsurface engineering. This gap presents a barrier to cost-effective site selection, risk assessment, and long-term monitoring strategies in CCS, gas storage.

Proposed Solution: Machine Learning for Predictive Modeling of Critical Pressures

To address these limitations, this study proposes the development of a machine learning (ML)-driven framework for predicting critical pressures in cap rock formations. By leveraging large datasets from experimental tests, well logs, and geophysical surveys, ML models can be trained to recognize hidden patterns and nonlinear relationships between geological parameters and sealing efficiency. This approach offers several key advantages:

1. Data-Driven Insights**:** Machine learning can analyze high-dimensional data, capturing complex multivariate dependencies that traditional models overlook.
2. Scalability and Efficiency**:** Unlike costly and time-consuming lab experiments, ML models can rapidly generate predictions for multiple formations, improving decision-making at regional and field scales.
3. Integration with Real-World Data**:** ML frameworks can incorporate diverse data sources, including core measurements, seismic surveys, and petrophysical logs**,** leading to a more holistic understanding of cap rock behavior**.**
4. Nonlinear Relationship Modeling**:** ML techniques such as random forests, neural networks, and support vector machines (SVMs) can identify nonlinear interactions between pore throat distributions, interfacial tension, wettability, and permeability, providing more accurate predictions.

By developing and validating an ML-based predictive model, this research aims to bridge the gap between experimental studies and large-scale geological assessments, offering a practical, scalable, and scientifically robust solution for assessing cap rock integrity in subsurface storage projects.

1.3 Research Objectives and Expected Impact

The primary objective of this study is to develop a machine learning model capable of accurately finding the best correlation for breakthrough pressure, displacement pressure, and other critical sealing parameters based on geological, petrophysical, and fluid properties. Specifically, the research seeks to:

1. Analyze and integrate large-scale datasets from cap rock experiments, reservoir models, and well logs to identify key controlling parameters for sealing efficiency.
2. Train and optimize ML algorithms to predict critical pressures based on rock mineralogy, pore structure, wettability, and stress conditions.
3. Validate the predictive models against experimental results and field data, ensuring reliability and applicability across different lithologies and storage conditions.
4. Develop a decision-support tool for geoscientists and engineers, enabling rapid and accurate assessments of cap rock integrity for CCS, hydrocarbon storage, and underground gas containment.

By addressing these objectives, this research aims to revolutionize the way cap rock integrity is assessed, providing a cost-effective, scalable, and high-precision alternative to conventional experimental approaches. The expected impact includes Improved risk assessment for subsurface gas storage projects, reducing the likelihood of leakage and environmental contamination. Enhanced site selection processes, allowing operators to identify the most suitable geological formations for long-term CO_2 sequestration and gas storage. Integration of advanced geoscience and AI, bridging the gap between data-driven analytics and traditional geomechanical modeling.

By leveraging the power of machine learning, this study seeks to transform the future of subsurface engineering, ensuring safer, more efficient, and scientifically informed decisions in geological storage and reservoir management.

2. WORKFLOW

In my research, I have conducted an extensive analysis of over 40 academic and industrial papers alongside experimental data from laboratory studies. This broad approach has enabled me to examine a wide range of factors that influence geological and fluid interactions. Key parameters include pressure, temperature, porosity, permeability, mineral composition, rock type, interfacial tension, contact angle, breakthrough and snap-off pressures, and the characteristics of different fluid types.

The study covers diverse geological and environmental settings worldwide, offering a well-rounded perspective on how these factors interact under varying conditions. By integrating multiple sources, I have identified patterns, correlations, and variations that shape fluid behavior in porous media. For instance, the relationship between pressure and temperature dictates phase transitions and fluid mobility, while porosity and permeability play a crucial role in determining how fluids move through rock formations.

Mineralogy and lithology influence surface interactions, such as wettability, interfacial tension, and contact angle. Breakthrough and snap-off pressures provide valuable insights into capillary forces and fluid trapping mechanisms, which are essential for understanding how fluids migrate and are stored within reservoirs.

The research considers various fluid types, including CO_2, CH_4, N_2, and Hg, each of which behaves differently under specific geological and environmental conditions. CO_2 is particularly relevant in carbon capture and storage (CCS) due to its phase behavior and solubility. Methane, as a key component of natural gas, requires careful evaluation of its flow dynamics in reservoirs. Nitrogen is frequently used in gas injection processes, while mercury is considered due to its interactions with certain rock formations. In addition to analyzing these properties, the research incorporates detailed experimental methodologies, including core flooding, capillary pressure measurements, wettability assessments, step-by-step test and residual test. These tests simulate subsurface conditions at various depths, pressures, and temperatures, ranging from shallow reservoirs to ultra-deep, high-pressure, high-temperature (HPHT) environments. Such extreme conditions significantly impact fluid-rock interactions, phase behavior, and transport mechanisms.

To further enhance the predictive capabilities of this research, I implemented machine learning techniques to develop models capable of estimating key cap rock properties based on mineralogical compositions and other geochemical parameters. Using CatBoosta gradient boosting algorithm and k-nearest neighbors (KNN) algorithm optimized for structured datasets, I trained a model that effectively predicts critical pressures based on other geological factors, and their correlation with mineralogies.

Given the extensive dataset available, I focused my mineralogical analysis on minerals that consistently appeared in high percentages across all formations. This selection ensured that the predictive models remained robust and generalizable. The study specifically investigates formations that dominate global subsurface geology: Carbonate, Siliciclastic, and Evaporite formations. These formations are highly significant in reservoir studies due to their distinct properties: Carbonate formations often exhibit complex porosity structures, strong interactions with fluids, and significant variations in wettability. Siliciclastic formations provide a crucial reference for permeability and capillary behavior in clastic rock systems. Evaporite formations influence subsurface sealing potential, especially in carbon sequestration applications.

The workflow for building these predictive models followed a structured approach:

1. Data Collection & Preprocessing: The dataset was compiled from multiple sources, including laboratory experiments and literature reviews. The data underwent cleaning, normalization, and feature engineering to ensure consistency and remove outliers.
2. Feature Selection & Engineering: Key parameters such as mineralogy, porosity, permeability, and pressure-temperature relationships were carefully selected to train the models. Dimensionality reduction techniques were applied to optimize computational efficiency.
3. Model Training & Optimization: The CatBoost model was trained using hyperparameter tuning to improve prediction accuracy, leveraging its ability to handle categorical and

numerical data efficiently. The KNN approach was utilized for classification tasks, ensuring robust generalization across different rock formations.

4. Validation & Testing: The models were validated using cross-validation techniques and tested against unseen data to assess their predictive performance and reliability in estimating geological parameters.
5. Interpretation & Deployment**:** The results were analyzed to identify key influencing factors in cap rock behavior.

Now, by turning our attention to the dataset and its visual representations, we can explore trends related to gas behavior in cap rock. Examining how wettability, depth, interfacial tension, permeability, porosity, pressure, and temperature interact will help us understand underground storage and mobility, shedding light on long-term containment efficiency and the implications for sustainable resource management.

3.Machine Learning

Machine learning involves a variety of tasks, and different libraries specialize in handling them efficiently. Data handling and preprocessing is a critical first step, and libraries like Pandas and NumPy are indispensable. Pandas work with tabular data in the form of "DataFrames" and performs tasks such as data cleaning, filtering, merging, and aggregation. For example, it can read a CSV file and calculate summary statistics or handle missing data through imputation. NumPy provides support for n-dimensional arrays and matrix operations, serving as the backbone for many other libraries like Scikit-learn and TensorFlow. An example of its use is performing element-wise operations on arrays or generating random data for simulations.

Understanding data and results is essential in machine learning, and data visualization libraries like Matplotlib and Seaborn help achieve this. Matplotlib, while low-level, is highly customizable for creating a variety of plots, such as a line plot of a dataset or a scatter plot for analyzing data relationships. Seaborn, built on Matplotlib, provides better default aesthetics and additional features, such as creating a correlation heatmap for visualizing relationships between variables or a boxplot for examining data distributions.

For implementing machine learning algorithms, libraries like Scikit-learn, XGBoost, and LightGBM are widely used. Scikit-learn offers a broad range of algorithms, including linear regression, k-means clustering, and decision trees, and can be used to train a linear regression model or evaluate it using cross-validation. XGBoost is optimized for gradient boosting, making it ideal for tabular datasets and competitions, as demonstrated by using it for classification tasks or handling missing values effectively. LightGBM, on the other hand, is faster than XGBoost on large datasets, especially those with many categorical features, as shown by fitting a LightGBM model and leveraging its categorical feature support.

3.1 Machine Learning Algorithms

3.1.1 Linear Regression

Linear regression is a fundamental algorithm for regression tasks. (James et al. 2013) It assumes a linear relationship between the input features and the target variable. Libraries like Scikit-learn provide efficient implementations, and an example of its use is predicting house prices based on features like size, location, and age. Regularized versions, such as Ridge and Lasso regression, are used to prevent overfitting.

Mathematical Background: Linear regression models the relationship between a dependent variable y and one or more independent variables X using the equation:

$$y = \beta_0 + \beta_1 x_1 + \beta_2 x_2 + \cdots + \beta_n x_n + \epsilon \quad \text{(Eq.21)}$$

Here:

- β0 is the intercept.
- β1, β2,…,βn are the coefficients.
- ϵ is the error term. The coefficients are estimated by minimizing the Mean Squared Error (MSE):

$$MSE = \frac{1}{n}\sum_{i=1}^{n}(y_i - \hat{y}_i)^2 \quad \text{(Eq.22)}$$

3.1.2 Logistic Regression

Logistic regression is used for binary classification tasks and predicts the probability of an instance belonging to a class. It works by applying a logistic (sigmoid) function to a linear combination of features. (Hastie et al. 2009) For example, it can classify whether an email is spam or not. Scikit-learn provides tools to train and evaluate logistic regression models.

Mathematical Background

Logistic regression predicts probabilities using the sigmoid function:

$$\sigma(z) = \frac{1}{1+e^{-z}} \quad \text{(Eq.23)}$$

$$z = \beta_0 + \beta_1 x_1 + \beta_2 x_2 + \cdots + \beta_n x_n \quad \text{(Eq.24)}$$

The decision boundary is determined by thresholding the probability at 0.5. The model optimizes the log-loss function

$$\text{Log-Loss}= -\frac{1}{n}\sum_{i=1}^{n}[y_i \log(\hat{y}_i) + (1 - y_i)\log(1 - \hat{y}_i)] \quad \text{(Eq.25)}$$

3.1.3 Decision Trees

Decision trees are versatile algorithms used for classification and regression. They split the dataset into subsets based on feature values, creating a tree-like structure. (Murphy ,2012) An example use case is classifying customer behavior based on demographic features. Decision trees are easy to interpret and implemented in libraries like Scikit-learn.

Mathematical Background

A decision tree splits data at each node to minimize a metric like Gini Impurity or Information Gain. For classification:

$$\text{Gini Impurity} = 1 - \sum_{i=1}^{k} {p_i}^2 \quad \text{(Eq.26)}$$

$$\text{Information Gain} = \text{H(parent)} - \sum_i \frac{|child_i|}{|parent|} \text{H} \; (child_i) \quad \text{(Eq.27)}$$

Where H is the entropy:

$$H = - \sum_{i=1}^{k} p_i \log_2(p_i) \quad \text{(Eq.28)}$$

3.1.4 Random Forest

Random forests are ensembles of decision trees that improve prediction accuracy by averaging predictions for regression or taking a majority vote for classification. (Breiman ,2001) An example is predicting loan defaults based on customer data. Scikit-learn provides a robust implementation of random forests.

Mathematical Background

Random forests create multiple decision trees using random subsets of data and features. The final prediction is:

for classification :

$$\hat{y} = mode(y_{tree1}, y_{tree2}, \dots, y_{treeN}) \quad \text{(Eq.29)}$$

for regression:

$$\hat{y} = \frac{1}{N} \sum_{i=1}^{N} y_{tree_i} \quad \text{(Eq.30)}$$

3.1.5 K-Nearest Neighbors (k-NN)

k-NN is a non-parametric algorithm that predicts labels based on the closest data points. (Hastie et al.,2009) It works well for small datasets and is used in tasks like image classification or handwriting recognition. Scikit-learn includes a simple implementation of k-NN.

Mathematical Background:
k-NN calculates distances (e.g., Euclidean distance) between a query point q and all points in the dataset:

$$d(p, q) = \sqrt{\sum_{i=1}^{n} (p_i - q_i)^2}$$

(Eq.31)

The algorithm selects the k nearest neighbors and assigns the majority class (classification) or the average value (regression).

3.1.6 Support Vector Machines (SVM)

SVMs classify data by finding the optimal hyperplane that separates classes. (Shalev-Shwartz & Ben-David, 2014) They are effective for both linear and non-linear classification using kernels. An example is classifying sentiment in text data. SVMs are available in Scikit-learn.

Mathematical Background
SVMs maximize the margin M between data points and the hyperplane:

$$M = \frac{2}{\|w\|} \quad \text{(Eq.32)}$$

Where w is the weight vector. The optimization problem solved is:

$$\min \frac{1}{2} \|w\|^2$$

subject to y_i(w·x_i +b) ≥ 1, where y_i is the class label.

4. K-Nearest Neighbors (k-NN)

k-Nearest Neighbors (k-NN) is a non-parametric, instance-based learning algorithm widely used for classification and regression tasks. Unlike parametric methods, k-NN does not assume an explicit form for the decision boundary or a predefined model for the data. Instead, it retains the entire training dataset and makes predictions by analyzing the proximity of a query point to its neighbors within the feature space. The algorithm is conceptually straightforward, relying on local relationships within the dataset to derive predictions. (fig.6)

4.1 Mechanism of Operation

The k-NN algorithm functions through a series of steps to predict either categorical labels (classification) or continuous values (regression):

1. Identify the query point q for which a prediction is required.
2. Compute the distance between q and each data point pi in the training set using a chosen distance metric.
3. Sort all training points by their distance to q and select the k-nearest points as the neighbors.
4. Aggregate the outputs of the neighbors to derive the prediction.

4.2 Distance Metrics

The selection of an appropriate distance metric is critical for determining the proximity of neighbors in k-NN. Common metrics include:

- **Euclidean Distance:** Measures the straight-line distance between two points in an m-dimensional space.

$$d_{Euclidean}(p,q) = \sqrt{\sum_{i=1}^{m}(p_i - q_i)^2}$$

(Eq.33)

- **Manhattan Distance:** Computes the sum of absolute differences between feature values.

$$d_{Manhattan}(p,q) = \sum_{i=1}^{m}|p_i - q_i|$$

(Eq.34)

- **Minkowski Distance:** A generalized distance metric parameterized by r, where r=1 corresponds to Manhattan distance and r=2 to Euclidean distance.

$$d_{Minkowski}(p,q) = \left(\sum_{i=1}^{m}|p_i - q_i|^r\right)^{1/r}$$

(Eq.35)

- **Cosine Distance:** Evaluates the angular similarity between two high-dimensional vectors.

$$Cosine\ Distance = 1 - \frac{\sum_{i=1}^{m} p_i q_i}{\|p\|.\|q\|}$$

(Eq.36)

- **Hamming Distance:** Counts the number of mismatches between corresponding feature values, typically used for categorical data.

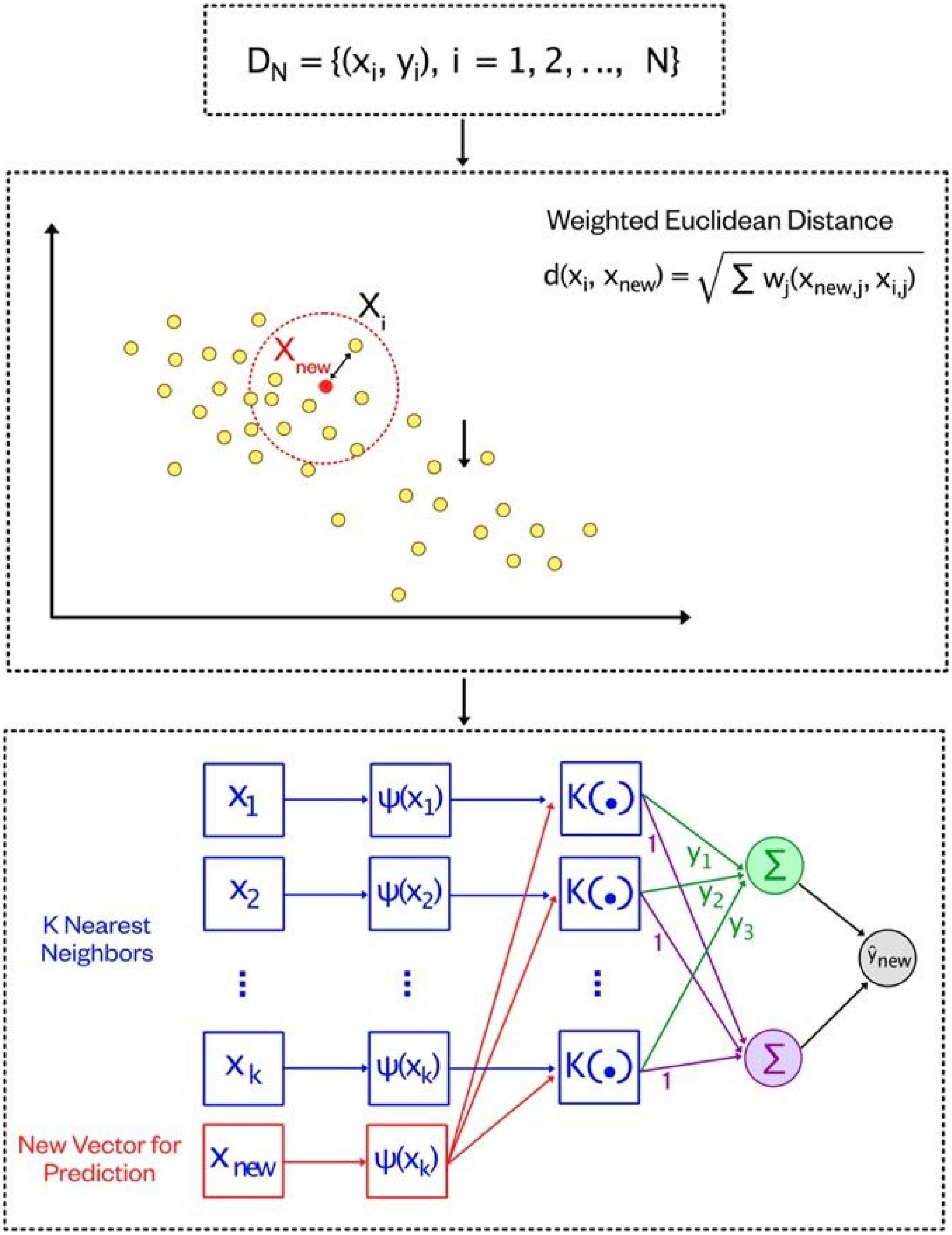

Fig.6 illustration of KNN algorithm

4.3 Prediction Mechanism

- **Classification:**
  For classification tasks, the algorithm predicts the class label of q based on a majority vote among the k-nearest neighbors. The most frequent label is assigned to q:

  $$\hat{y} = mode(\{y_1, y_2, \dots, k\}) \quad \text{(Eq.37)}$$

- **Regression:**
  For regression tasks, the predicted value for q is the average of the outputs of the k-nearest neighbors. In weighted k-NN, closer neighbors contribute more heavily to the prediction:

  $$\hat{y} = \frac{1}{k}\sum_{i=1}^{k} y_i$$

  (Eq.38)

  $$\hat{y} = \frac{\sum_{i=1}^{k} w_i y_i}{\sum_{i=1}^{k} w_i} \quad \text{(Eq.39)}$$

  $$w_i = \frac{1}{d(p_i, q) + \epsilon} \quad \text{(Eq.40)}$$

where ϵ is a small constant to prevent division by zero.

4.4 Challenges in k-NN

Although k-NN is straightforward, it is not without challenges:

4.4.1 Curse of Dimensionality

In high-dimensional spaces, distances between points tend to converge, making it difficult to distinguish between nearest neighbors. Dimensionality reduction techniques, such as Principal Component Analysis (PCA), or feature selection methods can mitigate this issue.

4.4.2 Feature Scaling

Features with larger ranges disproportionately influence distance computations. To ensure equitable contributions from all features, scaling techniques such as min-max normalization or standardization are employed:

- **Min-Max Scaling:**

  $$x' = \frac{x - \min(x)}{\max(x) - \min(x)} \quad \text{(Eq.41)}$$

- **Standardization:**

$$x' = \frac{x - \mu}{\sigma}$$

(Eq.42)

4.4.3 Selection of k

The choice of k directly impacts on the algorithm's performance. A smaller k makes predictions sensitive to noise (overfitting), while a larger k may over smooth the predictions (underfitting). Cross-validation is a standard technique for identifying the optimal k.

4.4.4 Computational Complexity

The algorithm requires computing distances for every query point against all training points, leading to a computational complexity of O(n·m), where n is the number of training points and m is the number of features. Optimizations such as kd-trees, ball trees, and Approximate Nearest Neighbors (ANN) can improve efficiency.

5. Gradient Boosting:

Gradient Boosting algorithms, such as XGBoost and LightGBM, build models sequentially to minimize errors. They are powerful for structured data, as shown in predicting sales using historical data. These algorithms are highly customizable and efficient (Chen & Guestrin, 2016; Ke et al., 2017).

5.1 CatBoost Regressor Features

CatBoost Regressor is a highly efficient and user-friendly machine learning algorithm with several notable features. One of its standout capabilities is its native support for categorical data. Unlike traditional algorithms that require preprocessing techniques like one-hot encoding or label encoding, CatBoost automatically transforms categorical variables into numeric representations based on statistics, significantly reducing manual effort and improving workflow efficiency.

The algorithm implements efficient gradient boosting techniques, such as ordered boosting, which helps reduce overfitting by preventing data leakage during training. Additionally, it uses oblivious decision trees, a type of symmetric tree structure that ensures faster and more predictable training while enhancing model interpretability and robustness (Dorogush et al., 2018, Prokhorenkova et al., 2018)

CatBoost is particularly robust against overfitting, even when working with small datasets. This is achieved through advanced regularization techniques, making the algorithm reliable in a variety of scenarios. It also supports GPU acceleration, allowing for faster training on large datasets, which is essential for time-sensitive tasks. Furthermore, CatBoost requires minimal hyperparameter tuning to deliver competitive performance, making it accessible for users with varying levels of expertise in machine learning. (Hancock & Khoshgoftaar, 2020)

5.2 Key Parameters of CatBoost Regressor

CatBoost Regressor includes several key parameters that influence model performance and efficiency. Iterations determine the number of trees, where higher values improve accuracy but may cause overfitting. Learning rate controls each tree's contribution, with smaller values ensuring stable but slower training. Depth sets tree complexity, capturing intricate patterns while balancing overfitting risks. The loss function, such as RMSE or MAE, guides optimization. Categorical features (cat_features) allow automatic handling of categorical data. Verbose adjusts logging frequency for training monitoring, while random seed ensures reproducibility. Task type specifies whether training runs on CPU or GPU, optimizing resource use. These features make CatBoost Regressor a powerful and adaptable tool for regression tasks. (Chen & Guestrin, 2016).

5.3 Mathematical Concepts Behind CatBoost Regressor

CatBoost Regressor is a gradient boosting framework that uses decision trees as its base model. Its mathematical foundation is built on gradient boosting, ordered boosting, and oblivious decision trees. Below are the core mathematical concepts behind CatBoost. (Dorogush et al., 2018).

5.3.1 Gradient Boosting

Gradient Boosting is an iterative method that combines weak learners, such as decision trees, to create a strong learner. (Friedman, 2001) At each iteration:

- **Initial Prediction**: The algorithm starts with an initial prediction, often the mean value of the target variable for regression tasks.
-

$$F_0(x) = mean\ (y) \text{ (Eq.43)}$$

- **Minimizing the Loss Function**: At each step, the model minimizes a predefined loss function L(y,F(x)), where y is the true value, and F(x) is the model's prediction.
-
- **Computing the Negative Gradient**: The gradient represents the direction of the steepest descent of the loss function. For each data point ii, the residual r_i is computed as:

$$r_i = -\frac{\partial L(y_i, F(x_i))}{\partial F(x_i)}$$

(Eq.44)

- **Fitting a Weak Learner**: A new decision tree h(x) is trained to approximate the residuals r_i.

$$h(x) = \arg\min_{h} \sum_{i=1}^{n} (g_i - h(x_i))^2$$
(Eq.45)

- **Updating the Model**: The predictions are updated by adding a fraction of the tree's prediction:

$$F_m(x) = F_{m-1}(x) + \nu . h_m(x) \quad \text{(Eq.46)}$$

Here, ν is the learning rate, which controls how much each tree contributes to the final prediction.

5.3.2 Ordered Boosting (CatBoost Innovation)

CatBoost addresses data leakage in traditional gradient boosting with Ordered Boosting, which ensures unbiased estimates when handling categorical features. It begins by randomly permuting the dataset to break dependencies, then computes residuals and makes splits using only earlier rows in the permutation, preventing future data from influencing the current model (Prokhorenkova et al., 2018). This approach effectively eliminates data leakage and enhances model accuracy. Mathematically, ordered boosting can be expressed as:

$$\mathcal{Y}_i = \mathcal{F}\big(\, x_i \mid history(x_{<i})\big) \quad \text{(Eq.47)}$$

5.3.3 Oblivious Decision Trees

CatBoost employs Oblivious Decision Trees, where all nodes at the same depth share the same splitting criterion. This symmetric structure enhances efficiency by reducing computational complexity, requires fewer parameters, and prevents overfitting through inherent regularization. Additionally, it improves interpretability, as each split uniformly impacts all paths, making model decisions easier to analyze.

Example: In a depth-2 oblivious tree:

- Level 1: Split on Feature A>5.
- Level 2: Split on Feature B<10.

This results in four symmetric leaf nodes:

1. Feature A≤5 and Feature B<10
2. Feature A≤5 and Feature B≥10
3. Feature A>5 and Feature B<10
4. Feature A>5 and Feature B≥10

5.4 Handling Categorical Features

CatBoost handles categorical features using target-based statistics, avoiding the need for one-hot encoding. Instead, it replaces categorical values with conditional statistics derived from the target variable.
The mathematical representation for a categorical feature C:

$$Encoding\ (C) = \frac{\sum_{i=1}^{n} y_i.\, 1(C_i = c)}{\sum_{i=1}^{n} 1(C_i = c) + prior}$$

(Eq.48)

- Where:
- y_i: Target value.
- 1: Indicator function.
- prior: Smoothing terms to avoid overfitting.

CatBoost uses ordered statistics to compute these encodings, ensuring no data leakage.

5.5 Loss Function

The choice of loss function depends on the task. For regression tasks, commonly used loss functions include:

- **Root Mean Squared Error (RMSE)**:

$$L\big(y, F(x)\big) = \sqrt{\frac{1}{n}\sum_{i=1}^{n}(y_i - F(x_i))^2}$$

(Eq.49)

- **Mean Absolute Error (MAE)**:

$$L\big(y, F(x)\big) = \frac{1}{n}\sum_{i=1}^{n}|y_i - F(x_i)|$$

(Eq.50)

CatBoost also supports custom loss functions for specific tasks.

5.6 Regularization Techniques

Cat Boosting employs several regularization techniques to prevent overfitting. L2 Regularization adds a penalty proportional to the square of model weights, preventing excessive complexity. Limiting tree depth controls the model's capacity and avoids overfitting. Early Stopping halts training when validation performance stops improving. Shrinkage (learning rate) reduces the impact of each tree, ensuring gradual learning and improving generalization. Corresponding Formula is :

$$F_m(x) = F_{m-1}(x) + \nu . h_m(x) \quad \text{(Eq.51)}$$

Smaller ν values lead to slower but more stable learning.

These techniques, combined with CatBoost's innovations, make it a powerful framework for regression tasks, particularly in handling categorical data and mitigating overfitting risks.

CHAPTER 4 (Dataset and technical Approach)

1.Data Collection and classification

I have thoroughly examined many academic and industrial papers, along with analyzing experimental data obtained from laboratory studies. This comprehensive approach has allowed me to explore a wide array of critical parameters that influence various processes and phenomena. These parameters include, but are not limited to, pressure, temperature, porosity, permeability, mineralogy, lithology, interfacial tension (IFT), contact angle, breakthrough pressure, snap-off pressure, and the characteristics of different fluid types.

The scope of the study spans diverse geological and environmental conditions from all around the world, offering a robust understanding of the complexities involved. By integrating insights from multiple sources, I have been able to identify trends, correlations, and variations in these parameters under different conditions.

Mineralogy and lithology provide a detailed understanding of rock compositions, which influence wettability and other surface interactions, such as contact angles and interfacial tension. Breakthrough pressure and snap-off pressure offer insights into the capillary forces and fluid displacement mechanisms, which are essential for understanding fluid migration and trapping within porous media.

The study also accounts for a diverse range of fluid types, including CO_2, CH_4 (methane), N_2 (nitrogen), and Hg (mercury). Each of these fluids exhibits unique properties that significantly impact their behavior under varying environmental and geological conditions. For example, CO_2 plays a pivotal role in carbon capture and storage (CCS) projects due to its phase behavior and solubility. Methane, as a primary component of natural gas, requires careful analysis of its flow dynamics and interactions in reservoirs. Nitrogen is commonly used in applications like gas flooding.

In addition to these parameters, the research also incorporates detailed insights into the testing conditions and methodologies. Experiments are conducted under varying depths, simulating subsurface conditions ranging from shallow reservoirs to ultra-deep formations. The tests are carried out across a broad spectrum of pressures and temperatures to capture the influence of extreme conditions, such as those encountered in high-pressure, high-temperature (HPHT) reservoirs. These conditions play a critical role in determining the fluid-rock interactions, phase behaviors, and transport properties.

The type of tests employed include core flooding, capillary pressure measurements, wettability evaluations, and advanced imaging techniques such as micro-CT scanning to assess pore-scale phenomena. By analyzing these experimental conditions and data, a comprehensive understanding of the physical and chemical mechanisms at play is achieved.

1.1 CO2 DATASET

Let's now take a closer look at the dataset and its corresponding figures to uncover key insights into CO_2 behavior in geological formations. By examining these visual representations, we can identify distribution in wettability, depth distribution, interfacial tension, permeability, porosity, pressure, and temperature, factors that collectively influence CO_2 storage and mobility. This analysis will provide a deeper understanding of how different gases interact with cap rock conditions and what it means for long-term containment and efficiency.

Carbon dioxide (CO_2) plays a crucial role in storability and storage. Understanding how CO_2 behaves under different geological and physical conditions is essential for optimizing its storage, mobility, and long-term stability. The following figures provide a detailed analysis of key parameters influencing CO_2 interactions, including contact angle, depth, interfacial tension (IFT), permeability, porosity, critical pressures (breakthrough and snap-off), and temperature. Each of these factors affects how CO_2 moves through porous formations, how much can be stored, and whether it will remain trapped over time.

1.1.1 Pressure

Pressure is a key factor in CO_2 sequestration, influencing phase behavior, density, and storage efficiency. Maintaining CO_2 in a supercritical state enhances storage capacity and reduces leakage risks. Higher pressures indicate greater depths, which improve containment by increasing rock compaction. However, excessive pressure can lead to reservoir fracturing, increasing leakage potential. Understanding pressure distribution helps assess storage feasibility and long-term stability. (Fig.7)

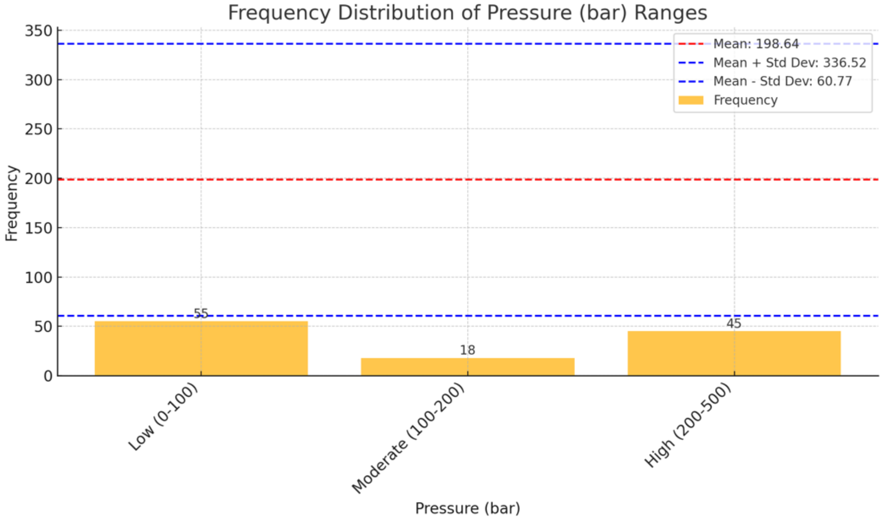

fig.7. Pressure distribution (Frequency vs Pressure)

The figure categorizes pressure into Low (0-100 bar, 55 occurrences), Moderate (100-200 bar, 18 occurrences), and High (200-500 bar, 45 occurrences). The mean pressure is 198.64 bar, with standard deviation boundaries at 60.77 bar (lower) and 336.52 bar (upper). The bimodal distribution suggests that cap rocks tend to operate either at very low or high pressures, with fewer cases in the moderate range. The low-pressure range (0-100 bar) dominates, likely representing shallow cap rocks. Conversely, the high-pressure range (200-500 bar) corresponds to deep cap rocks, where lithostatic pressure keeps CO_2 dense and stable.

The mean pressure of 198.64 bar suggests most CO_2 reservoirs operate above the critical pressure of 73.8 bar, ensuring supercritical conditions for efficient storage. The wide standard deviation (±137.88 bar) highlights variability, with values ranging from 60.77 to 336.52 bar.

1.1.2 Temperature

Temperature significantly affects CO_2 sequestration by altering its phase behavior, density, and solubility in reservoir fluids. At higher temperatures, CO_2 becomes less dense and more mobile, which can impact trapping efficiency and long-term stability. Conversely, lower temperatures can enhance CO_2 solubility in brine, promoting dissolution trapping, which is a key mechanism in CO_2 sequestration projects. Understanding the temperature distribution within CO_2 reservoirs is essential for assessing storage conditions, injectivity, and the effectiveness of trapping mechanisms. (fig.8)

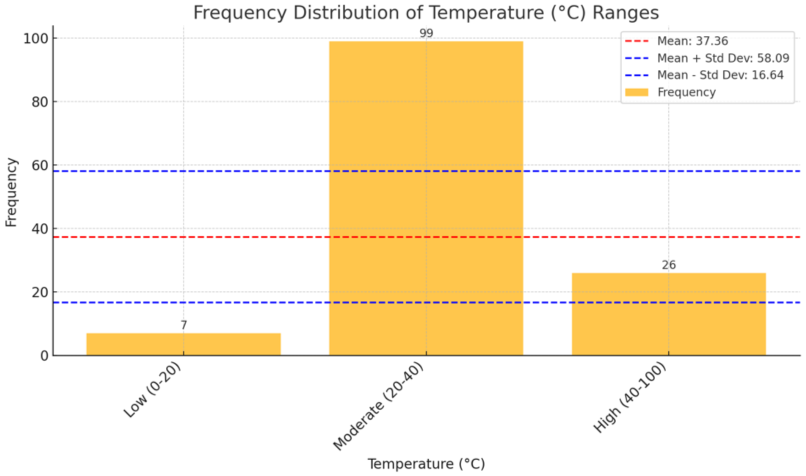

Fig.8 Temperature distribution

The figure categorizes temperature into three main ranges: low (0-20°C), moderate (20-40°C), and high (40-100°C). The moderate temperature range (20-40°C) has the highest frequency with 99 occurrences, indicating that most CO_2 storage sites operate within this temperature range. The high-temperature range (40-100°C) is the second most frequent, with 26 occurrences, while the low-temperature range (0-20°C) is the least common, with only 7 occurrences. The mean temperature is 37.36°C, marked with a red dashed line, while the standard deviation boundaries are at 16.64°C (lower blue dashed line) and 58.09°C (upper blue dashed line).

The dominance of the moderate temperature range (20-40°C) suggests that most Cap rocks maintain relatively stable thermal conditions, which is beneficial for long-term storage and minimal phase transitions. The presence of some high-temperature cap rocks(40-100°C) indicates that deep, high-pressure formations are also utilized for CO_2 storage, as temperature tends to increase with depth. However, the low frequency of cap rocks in the 0-20°C range suggests that CO_2 storage in colder environments is less common, likely due to reduced injectivity and potential phase instability. The mean temperature of 37.36°C aligns with optimal conditions for CO_2 storage, ensuring that CO_2 remains in a supercritical state while maintaining sufficient density for efficient containment. The wide standard deviation range (16.64°C to 58.09°C) indicates variability in cap rock conditions, highlighting the need for site-specific thermal management strategies to prevent unwanted phase changes that could affect storage integrity.

1.1.3 Depth

Depth is a crucial factor in CO_2 sequestration as it directly influences pressure, temperature, and phase behavior. At greater depths, CO_2 remains in a supercritical state, increasing its density and reducing buoyancy-driven migration. Deep formations also provide natural geological sealing, minimizing the risk of CO_2 leakage. However, excessive depth can pose challenges related to injection pressure, reservoir accessibility, and monitoring difficulties. Understanding the depth distribution of CO_2 storage sites helps in optimizing storage conditions and ensuring long-term containment. (Fig.9)

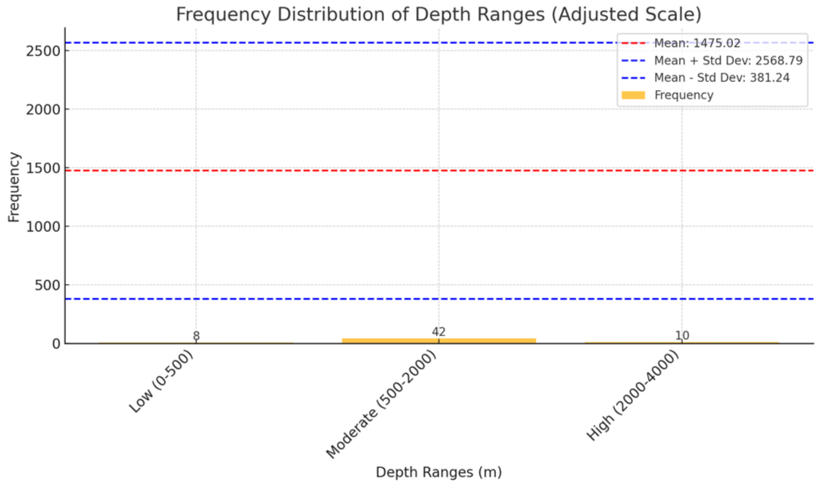

Fig.9 Depth distribution

The figure categorizes depth into three main ranges: low (0-500 m), moderate (500-2000 m), and high (2000-4000 m). The moderate depth range (500-2000 m) has the highest frequency with 42 occurrences, indicating that most CO_2 sequestration projects take place within this depth interval. The high-depth range (2000-4000 m) follows with 10 occurrences, suggesting that deep formations are also utilized, though less frequently. The low-depth range (0-500 m) is the least common, with only 8 occurrences, likely due to the increased risk of leakage and phase instability at shallow depths. The mean depth is 1475.02 m, marked by a red dashed line, while the standard deviation boundaries are at 381.24 m (lower blue dashed line) and 2568.79 m (upper blue dashed line). This suggests that most cap rocks fall between approximately 500 and 2500 meters, with a few extending beyond 3000 meters.

The dominance of moderate depths (500-2000 m) suggests that most CO_2 storage projects are designed to balance injection feasibility with long-term stability. At these depths, CO_2 can be maintained in a supercritical state without requiring excessive injection pressures, making it an optimal storage range. The presence of deep storage sites (2000-4000 m) indicates that some projects prioritize enhanced containment by utilizing deep geological formations with strong caprocks. However, the low occurrence of shallow storage sites (0-500 m) highlights the risks associated with CO_2 sequestration at low depths, such as increased mobility and leakage potential. The wide standard deviation range (381.24 m to 2568.79 m) suggests significant variability in cap rock depths, reinforcing the need for site-specific assessments to determine optimal injection and monitoring strategies. This distribution indicates that most CO_2 sequestration sites are in geologically stable, deep formations, ensuring effective containment and minimizing environmental risks.

1.1.4 Porosity

Porosity is a fundamental property that determines the capacity of a cap rock to secure CO_2. It represents the fraction of a rock's volume that consists of pore spaces, which can be filled with CO_2 when injected into a geological formation. Understanding the distribution of porosity in storage formations helps in selecting appropriate reservoirs for CO_2 injection and assessing their efficiency in retaining CO_2 over extended periods. (Fig.10)

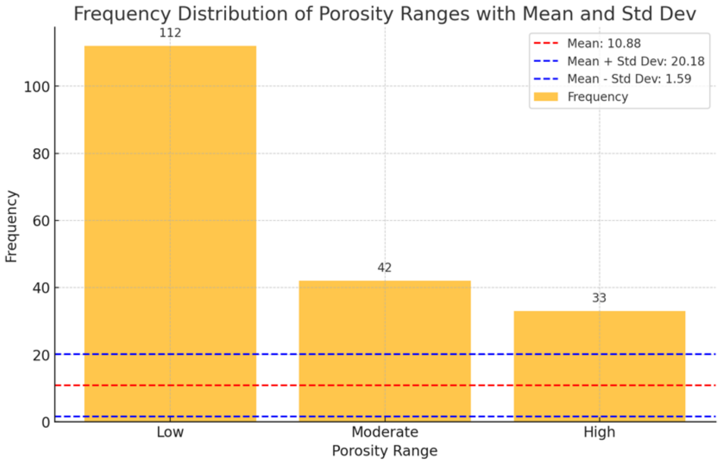

Fig.10 Porosity distribution

The figure categorizes porosity into three main ranges: low (1-15), moderate (15-22), and high (above 22). The low-porosity category has the highest frequency with 112 occurrences, indicating that we are dealing with cap rocks. The moderate-porosity range has 42 occurrences, while the high-porosity range has 33 occurrences. The mean porosity is 10.88, marked by a red dashed line, while the standard deviation boundaries are at 1.59 (lower blue dashed line) and 20.18 (upper blue dashed line). This suggests that the majority of cap rocks have porosity values falling between these limits, with fewer cases exhibiting extremely high or low porosity levels.

The dominance of the low-porosity category suggests that many CO_2 storage projects are conducted in formations where pore space is limited, emphasizing the role of residual trapping in securing CO_2 over long periods. Moderate-porosity formations, which have a lower frequency, may provide a balance between storage capacity and containment efficiency. The relatively small number of high-porosity formations suggests that while these reservoirs may offer greater storage capacity, they might also present challenges related to increased permeability, which could lead to CO_2 migration risks. The wide standard deviation range (1.59 to 20.18) highlights significant variability in cap rock porosity, reinforcing the need for site-specific assessments to determine the most suitable injection strategies.

1.1.5 Permeability

Permeability is a critical property that determines how easily CO_2 can move through a rock formation. It directly influences CO_2 injection efficiency, migration behavior, and long-term containment. Higher permeability allows for greater injectivity and ease of CO_2 movement, while lower permeability can restrict flow but enhance capillary trapping, helping to immobilize CO_2 in the subsurface. Understanding the permeability distribution within storage reservoirs is essential for optimizing injection strategies and ensuring long-term storage security. (Fig.11)

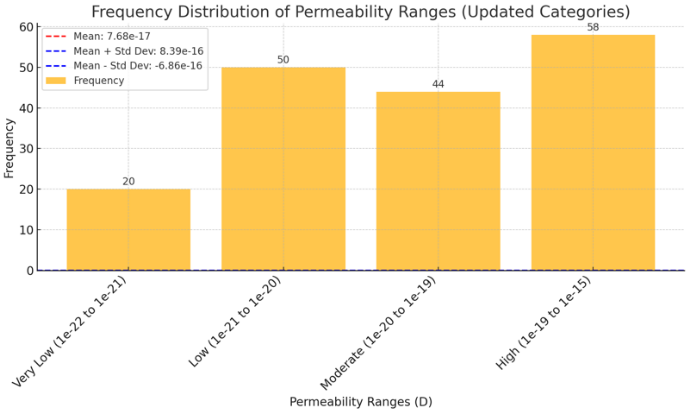

Fig.11 Permeability distribution

The figure categorizes permeability into four main ranges: very low ($1 \times e^{-22}$ to $1 \times e^{-21}$D), low ($1 \times e^{-21}$to $1 \times e^{-20}$ D), moderate ($1 \times e^{-20}$to $1 \times e^{-19}$D), and high ($1 \times e^{-19}$to $1 \times e^{-15}$D). The high-permeability category has the highest frequency, with 58 occurrences, followed by the low-permeability category with 50 occurrences and the moderate-permeability category with 44 occurrences. The very low-permeability category is the least common, with only 20 occurrences. The mean permeability is $7.68 \times e^{-17}$D, marked by a red dashed line, while the standard deviation boundaries extend from -$8.86 \times e^{-16}$ (lower blue dashed line) to $8.39 \times e^{-16}$D (upper blue dashed line). This suggests that most cap rocks have permeability values within this broad range, with significant variability among different storage formations.

The dominance of the high-permeability category suggests that many CO_2 storage projects take place in formations that allow easy injection and migration of CO_2. The relatively low occurrence of very low-permeability cap rocks suggests that extremely tight formations, where CO_2 injection may be difficult, are less commonly used for storage. The wide standard deviation range highlights substantial variation in cap rock permeability, emphasizing the need for site-specific assessments to determine the most appropriate injection rates and containment strategies.

1.1.6 Interfacial Tension

Interfacial tension (IFT) plays a crucial role in determining capillary pressure (Pc) and, consequently, the sealing efficiency of a cap rock. A higher IFT increases capillary entry pressure, enhancing the sealing efficiency by preventing CO_2 from penetrating low permeability caprocks, thereby supporting structural and residual trapping. Conversely, a lower IFT reduces capillary entry pressure, promoting CO_2 dissolution into injected fluids and enhancing solubility trapping, which can influence long-term containment strategies. Understanding the spatial and temporal variations of IFT within storage reservoirs is essential for predicting CO_2 migration, injection efficiency, and the overall effectiveness of caprock seals in preventing leakage. (Fig.12)

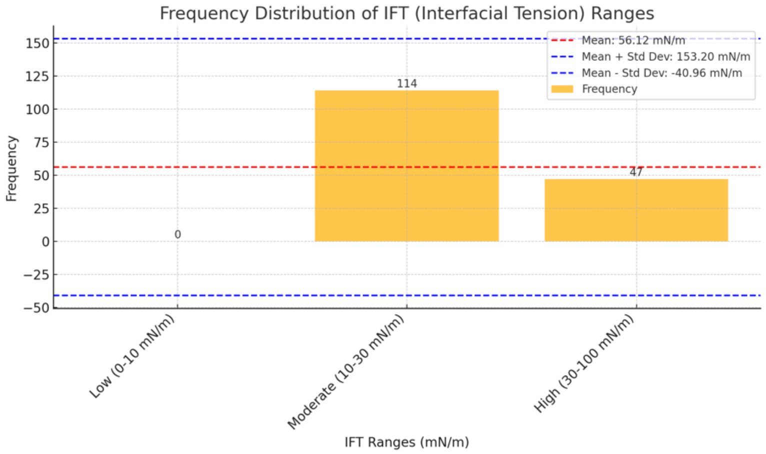

Fig.12 IFT distribution

The figure categorizes IFT into three main ranges: low (0-10 mN/m), moderate (10-30 mN/m), and high (30-100 mN/m). The moderate IFT range is the most frequent, with 114 occurrences, followed by the high IFT range with 47 occurrences. The low IFT category has zero occurrences, indicating that fully miscible conditions, where CO_2 and injected fluids mix entirely, are not observed in the dataset. The mean IFT value is 56.12 mN/m, marked by a red dashed line, while the standard deviation boundaries extend from -40.96 mN/m (lower blue dashed line) to 153.20 mN/m (upper blue dashed line). The lack of low IFT values suggests that CO_2 in these reservoirs typically does not dissolve completely into formation fluids but remains as a distinct phase.

The dominance of the moderate IFT category suggests that CO_2 in most cap rocks exhibits partial miscibility, meaning it interacts with injected fluids without fully dissolving. The presence of a significant number of high IFT occurrences indicates that in some cases, CO_2 remains in a separate phase, requiring structural trapping to ensure containment. The absence of low IFT values reinforces that these cap rocks do not exhibit fully miscible behavior, meaning CO_2 does not completely integrate with formation fluids but rather forms bubbles or discrete accumulations. The wide standard deviation range highlights variability in IFT values across different reservoirs, emphasizing the need for site-specific assessments to optimize CO_2 injection strategies.

1.1.7 Contact Angle

The contact angle is a critical parameter that determines the wettability of a surface, influencing how CO_2 interacts with cap rock and formation fluids. It directly affects the capillary trapping mechanism, which plays a major role in CO_2 sequestration. A lower contact angle indicates strong adhesion between CO_2 and the rock surface, leading to better capillary trapping, while a higher contact angle suggests that CO_2 forms droplets and remains more mobile. Understanding the distribution of contact angles in storage formations helps predict CO_2 retention efficiency and potential leakage risks. (Fig.13)

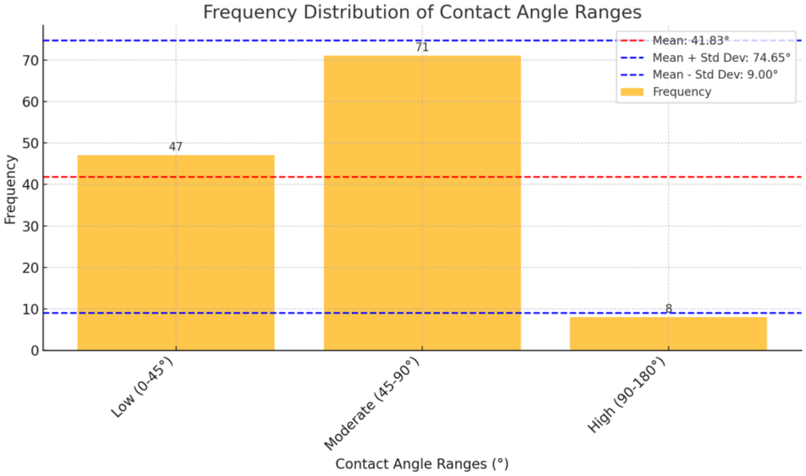

Fig.13 Contact angle distribution

The figure categorizes contact angles into three main ranges: low (0-45°), moderate (45-90°), and high (90-180°). The moderate contact angle range has the highest frequency, with 71 occurrences, followed by the low contact angle range with 47 occurrences. The high contact angle range is the least common, with only 8 occurrences. The mean contact angle is 41.83°, marked by a red dashed line, while the standard deviation boundaries extend from 9.00° (lower blue dashed line) to 74.65° (upper blue dashed line). The predominance of low and moderate contact angles suggests that CO_2 in these cap rocks tends to have water-wet wettability, which facilitates both mobility and trapping mechanisms.

The dominance of the moderate contact angle category suggests that CO_2 in most cap rocks exhibits balanced adhesion and mobility, meaning it neither spreads completely nor remains entirely non-wetting. The presence of a significant number of low contact angles indicates that strong capillary trapping is a key factor in CO_2 sequestration within these formations, preventing excessive migration. The limited number of high contact angle occurrences suggests that CO_2 rarely behaves as a completely non-wetting fluid, reinforcing the idea that most storage sites support some degree of capillary trapping. The wide standard deviation range highlights variability in wettability conditions across different cap rocks, emphasizing the need for site-specific evaluations to optimize CO_2 retention. This distribution suggests that most CO_2 sequestration sites rely on a combination of structural trapping and capillary forces to ensure effective long-term containment.

1.1.8 Breakthrough Pressure

Breakthrough pressure is the minimum pressure required for a gas to penetrate and continuously flow through a porous medium, displacing the resident fluid.

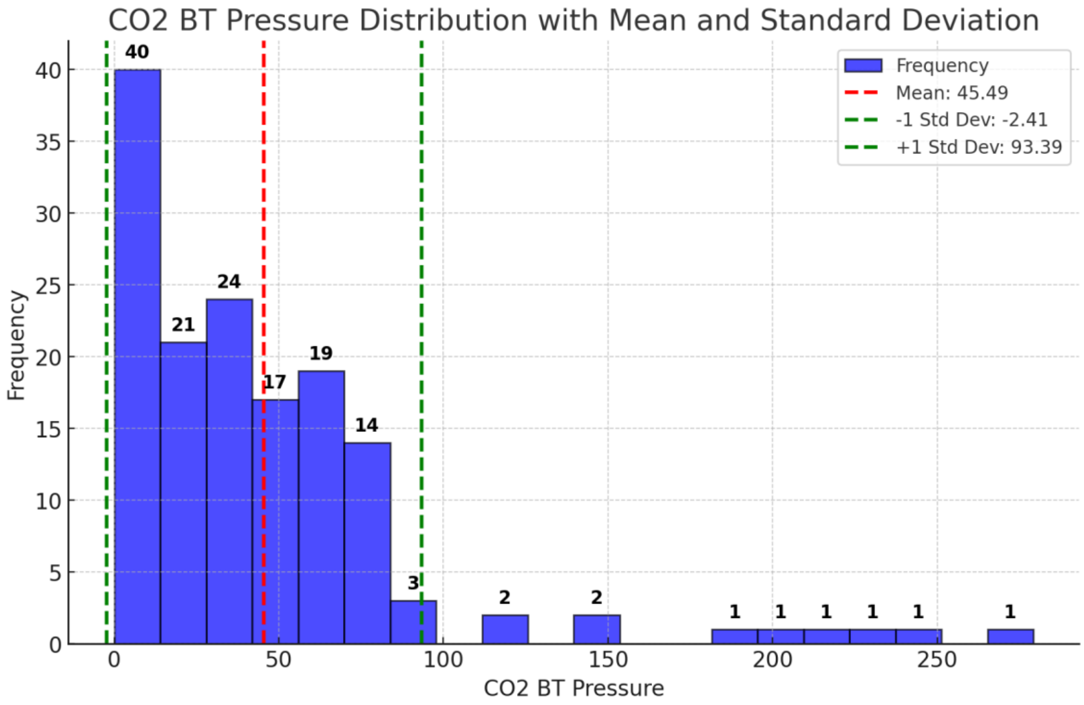

Fig.14 illustrations of BT pressure (bar)

The CO_2 breakthrough pressure distribution is strongly right-skewed, similar to its snap-off counterpart. This suggests that while CO_2 breakthrough usually occurs at moderate pressures, some cases require significantly higher forces to push CO_2 through the porous network.

1.1.9 Snap-off Pressure

Snap-off pressure refers to the pressure at which a continuous gas phase within a porous medium breaks apart due to capillary forces, causing gas bubbles to become disconnected and trapped.

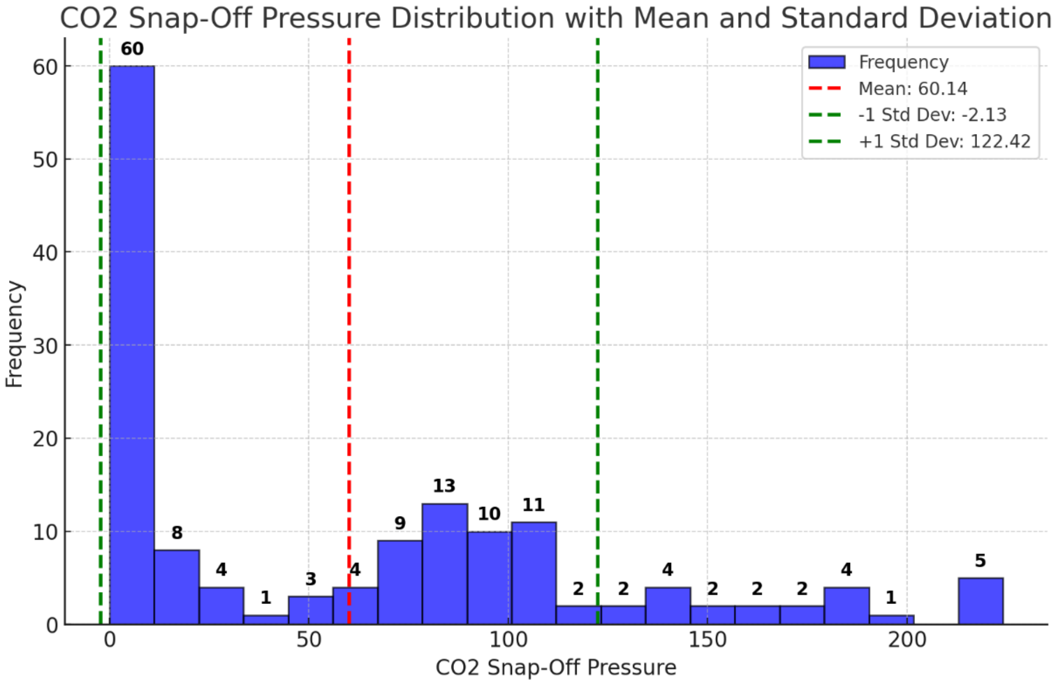

Fig.15 illustrations of Snap-off pressure (bar)

The CO_2 snap-off pressure distribution is right-skewed with multiple peaks, indicating that CO_2 experiences significant variability when snapping off. The high standard deviation confirms the wide range of conditions affecting CO_2 mobility, possibly due to variations in pore size, wettability, or capillary forces.

1.2 N2 Dataset

Sealing efficiency in N_2 storage is largely controlled by interfacial tension (IFT), capillary pressure (Pc), and rock-fluid interactions. A higher IFT increases capillary entry pressure, reducing the likelihood of N_2 leakage and enhancing the sealing capacity of caprocks. Conversely, lower IFT promotes N_2 penetration into porous media, increasing the risk of migration. Additionally, breakthrough and snap-off pressures dictate whether N_2 can escape through fractures or pore networks, directly affecting containment integrity. Understanding these factors is essential for optimizing injection strategies, ensuring long-term retention, and minimizing the risks of gas leakage from storage sites. The interaction of N_2 with cap rock and fluids is influenced by several key parameters, including contact angle, depth, interfacial tension (IFT), permeability, critical pressures (breakthrough and snap-off), porosity, pressure, and temperature. These factors determine how efficiently N_2 can be injected, stored, and retained within geological formations.

1.2.1 Pressure

Fig.16 shows the distribution of pressure for the analyzed dataset.

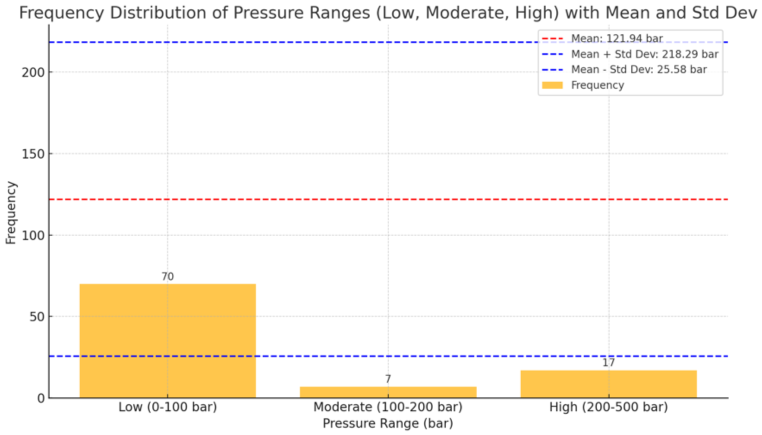

Fig.16 Pressure distribution for N2

The figure categorizes pressure into three main ranges: low (0-100 bar), moderate (100-200 bar), and high (200-500 bar). The low-pressure range has the highest frequency, with 70 occurrences, followed by the high-pressure range with 17 occurrences. The moderate-pressure range is the least common, with only 7 occurrences. The mean pressure is 121.94 bar, marked by a red dashed line, while the standard deviation boundaries extend from 25.58 bar (lower blue dashed line) to 218.29 bar (upper blue dashed line). The predominance of low-pressure conditions suggests that many N_2 storage sites are in shallower or depleted reservoirs where pressure has been reduced due to prior fluid extraction.

The dominance of low-pressure conditions (0-100 bar) indicates that a significant number of N_2 storage projects are conducted in formations where pressure management is essential to prevent excessive gas expansion and potential escape. The relatively lower number of moderate-pressure sites (100-200 bar) suggests that few reservoirs operate under conditions where pressure balances between retention and mobility. The presence of some high-pressure storage sites (200-500 bar) suggests that deep-cap rocks with strong sealing mechanisms are also utilized, providing enhanced containment but requiring careful monitoring to prevent over-pressurization.

1.2.2 Temperature

Fig.17 shows the distribution of temperature for the analyzed dataset.

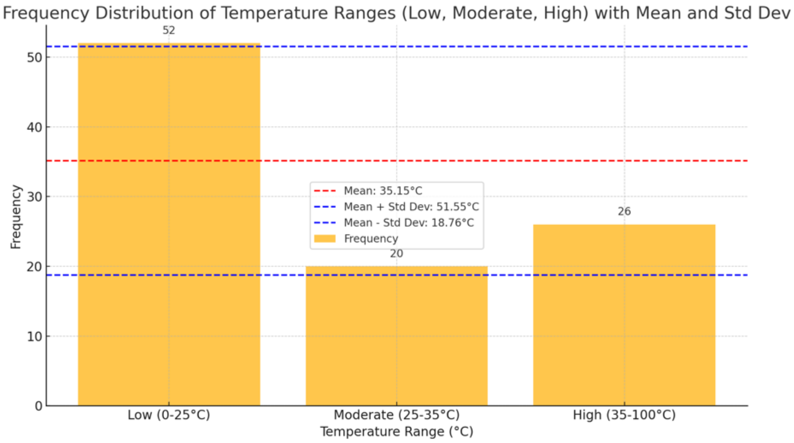

Fig. 17 Temperature distribution For N2

The figure categorizes temperature into three main ranges: low (0-25°C), moderate (25-35°C), and high (35-100°C). The low-temperature range has the highest frequency, with 52 occurrences, followed by the high-temperature range with 26 occurrences. The moderate-temperature range is the least common, with only 20 occurrences. The mean temperature is 35.15°C, marked by a red dashed line, while the standard deviation boundaries extend from 18.76°C (lower blue dashed line) to 51.55°C (upper blue dashed line). The prevalence of low-temperature conditions suggests that many N_2 storage sites are in relatively shallow formations or regions with lower geothermal gradients.

1.2.3 Porosity

Fig.18 completely shows the distribution in porosity for the database.

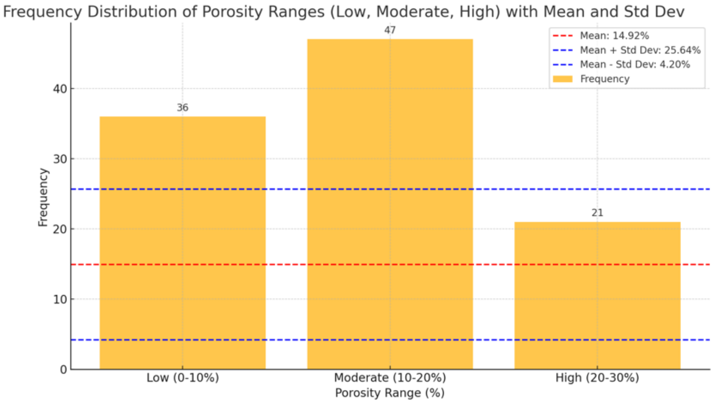

Fig .18 Porosity distribution for N2

The figure categorizes porosity into three main ranges: low (0-10%), moderate (10-20%), and high (20-30%). The moderate porosity range has the highest frequency, with 47 occurrences, followed by the low porosity range with 36 occurrences. The high porosity range is the least common, with only 21 occurrences. The mean porosity is 14.92%, marked by a red dashed line, while the standard deviation boundaries extend from 4.20% (lower blue dashed line) to 25.64% (upper blue dashed line). The dominance of the moderate porosity category suggests that most N_2 cap rocks have a balance between sufficient pore space for storage and structural integrity to prevent excessive migration.

The predominance of moderate porosity values (10-20%) indicates that many N_2 cap rocks provide an optimal balance between gas capacity and retention. The presence of a significant number of low porosity formations suggests that some reservoirs rely on structural and residual trapping rather than bulk volume for effective storage. The wide standard deviation range highlights variability in porosity across different formations, emphasizing the need for site-specific evaluations to optimize N_2 injection and retention strategies.

1.2.4 Permeability

Fig.19 shows the distribution of permeability for the analyzed dataset.

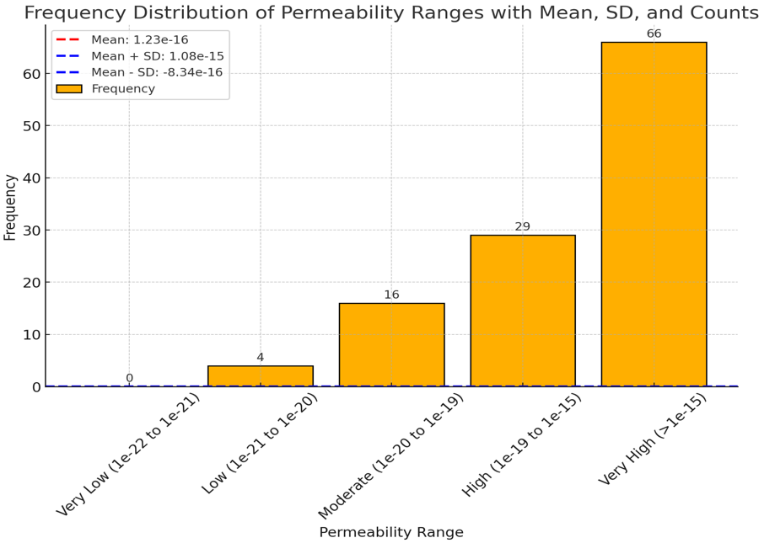

Fig.19 Permeability distribution for N2

The figure categorizes permeability into five main ranges: very low ($1 \times e^{-22}$ to $1 \times e^{-21}$D), low ($1 \times e^{-21}$to $1 \times e^{-20}$ D), moderate ($1 \times e^{-20}$to $1 \times e^{-19}$D), and high ($1 \times e^{-19}$to $1 \times e^{-15}$D). and very high (>$1 \times e^{-15}$D). The very high permeability range has the highest frequency, with 66 occurrences, followed by the high permeability range with 29 occurrences. The moderate permeability range has 16 occurrences, while the low permeability range has only 4 occurrences. There are no recorded instances in the very low permeability category. The mean permeability is $1.23 \times e^{-16}$D, marked by a red dashed line, while the standard deviation boundaries extend from -$8.34 \times e^{-16}$ D (lower blue dashed line) to $1.08 \times e^{-15}$ D (upper blue dashed line). The dominance of high and very high permeability values suggests that most N_2 storage sites are in formations where gas can flow relatively easily.

The moderate permeability category ($1 \times e^{-20}$to $1 \times e^{-19}$ D) appears less frequent, suggesting that fewer storage projects take place in formations where gas movement is more restricted. The very low permeability category is entirely absent, indicating that extremely tight formations are not utilized for N_2 storage, likely due to impractical injection rates. The wide standard deviation range highlights substantial variability in cap rock permeability, reinforcing the importance of site-specific assessments to determine optimal injection rates and containment strategies.

1.2.5 Interfacial Tension

Interfacial tension (IFT) is a crucial parameter influencing capillary pressure (Pc) and, consequently, the sealing efficiency of nitrogen (N_2) storage formations. Higher IFT values lead to an increase in capillary entry pressure, improving the sealing efficiency by preventing N_2 from breaching low permeability caprocks and enhancing structural and residual trapping. In contrast, lower IFT values reduce capillary entry pressure, facilitating N_2 dissolution into formation fluids and promoting solubility trapping, but potentially increasing the risk of migration due to reduced Pc. Understanding the spatial distribution of IFT is critical for predicting N_2 mobility, optimizing injection strategies, and ensuring the long-term integrity of the caprock seal in subsurface storage sites. (Fig.20)

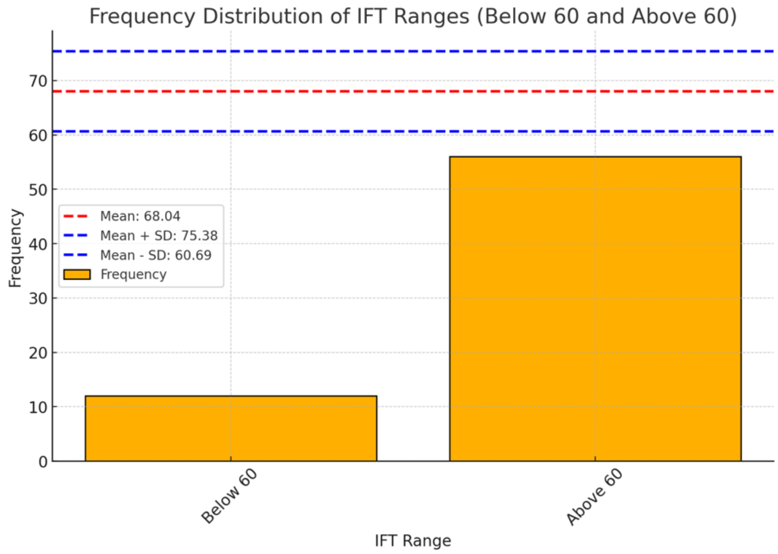

Fig.20 IFT distribution For N2

The data reveal that most N_2 storage sites exhibit high interfacial tension (IFT) values (>60 mN/m), with a mean of 68.04 mN/m and a narrow standard deviation range (60.69–75.38 mN/m). With 50 occurrences in the high IFT range compared to only 12 in the low IFT range (<60 mN/m), the findings indicate that N_2 primarily remains as a non-miscible phase, making structural and capillary trapping the dominant retention mechanisms. The limited occurrence of low IFT values suggests that solubility trapping is uncommon, meaning N_2 does not readily dissolve into injected fluids.

1.2.6 Contact Angle

The contact angle plays a key role in determining how well nitrogen (N_2) stays trapped in a storage formation. It affects how the gas interacts with surfaces and fluids, ultimately influencing how much can be securely stored. When the contact angle is low, N_2 sticks better to the surfaces, improving capillary trapping and boosting storage capacity. But if the contact angle is high, the gas tends to form droplets and move more freely, increasing the risk of leakage. Understanding these interactions helps in predicting how much N_2 a formation can hold and in designing better injection strategies to keep it stored safely for the long term. (Fig.21)

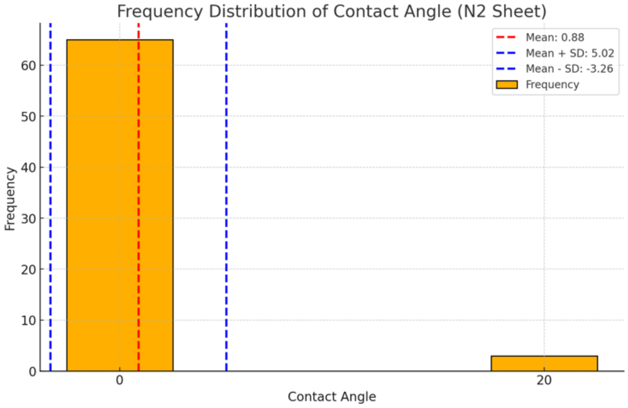

Fig. 21 Contact angle distribution

The figure shows that many contact angles are concentrated around 0°, with an exact frequency of 65 occurrences. Only 2 occurrences are observed at higher contact angles (>20°), making them relatively rare. The mean contact angle is 0.88°, marked by a red dashed line, while the standard deviation boundaries extend from -3.26° (lower blue dashed line) to 5.02° (upper blue dashed line). The dataset is heavily skewed toward low contact angles, indicating that N_2 in these reservoirs tends to exhibit strong wetting behavior, which promotes capillary trapping.

The dominance of 65 occurrences at near-zero contact angles indicates a strong water wet system which is extremely favorable for storage security. The presence of only 2 high contact angle occurrences indicates that in rare cases, N_2 may exhibit non-wetting behavior, which could reduce trapping efficiency and increase the risk of gas migration. The narrow standard deviation range highlights that most contact angles remain within a small and predictable range, reinforcing the idea that wettability conditions are generally consistent across different storage formations. This distribution suggests that most N_2 sequestration sites operate under conditions where strong capillary trapping enhances gas retention, reducing the likelihood of escape and improving overall storage security.

1.2.7 Breakthrough Pressure

Snap-off pressure for N_2 is the point at which nitrogen gas segments become disconnected in porous media due to capillary instabilities, leading to the trapping of gas bubbles.

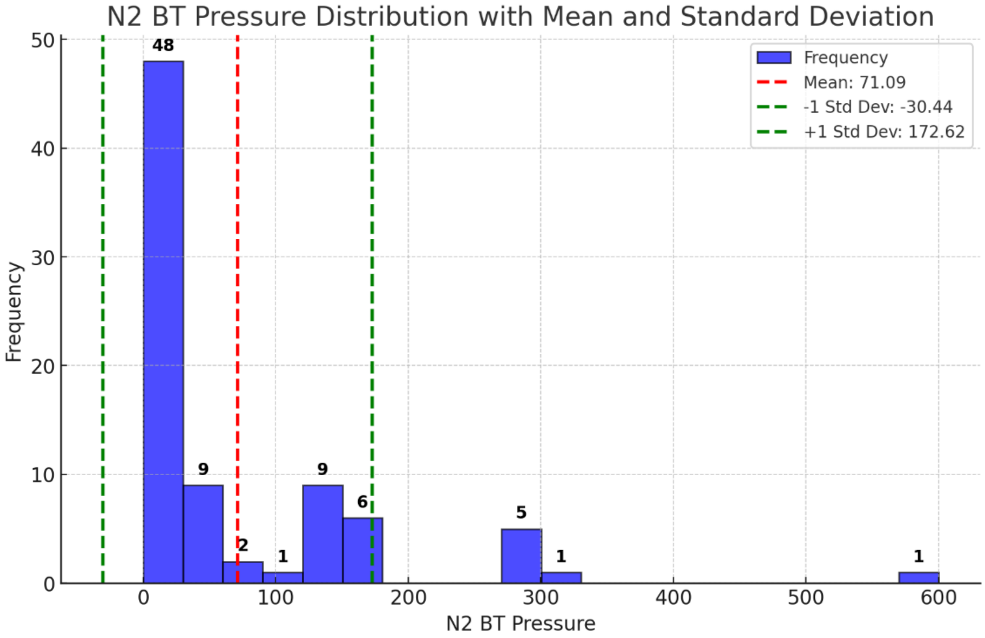

Fig.22 illustrations of BT pressure (bar)

The nitrogen snap-off pressure distribution appears more uniform and well-spread, indicating that N_2 undergoes a relatively predictable and consistent snap-off process.

1.2.8 Snap-off Pressure

The breakthrough pressure for N_2 is the pressure at which nitrogen overcomes capillary resistance and establishes continuous flow through a porous medium.

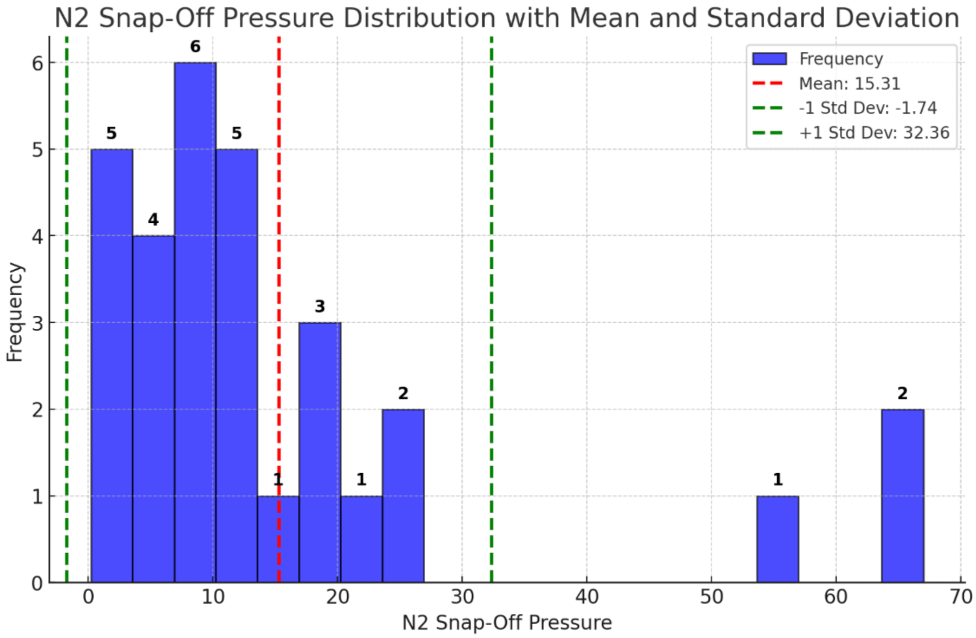

Fig. 23 illustrations of Snap-off pressure (bar)

1.3 CH4 Dataset

Methane (CH_4) is the main component of natural gas and plays a major role in underground storage, and carbon capture efforts. To safely and efficiently store CH_4 in geological formations, it's crucial to understand how it behaves under different conditions. Several factors influence CH_4 storage, including contact angle, depth, interfacial tension (IFT), permeability, critical pressures (breakthrough and snap-off), porosity, pressure, and temperature. These parameters determine how CH_4 interacts with cap rocks and fluids, how easily it moves through the formation, and how well it can be contained over time.

1.3.1 Pressure

Fig.24 shows the distribution of pressure for the analyzed dataset.

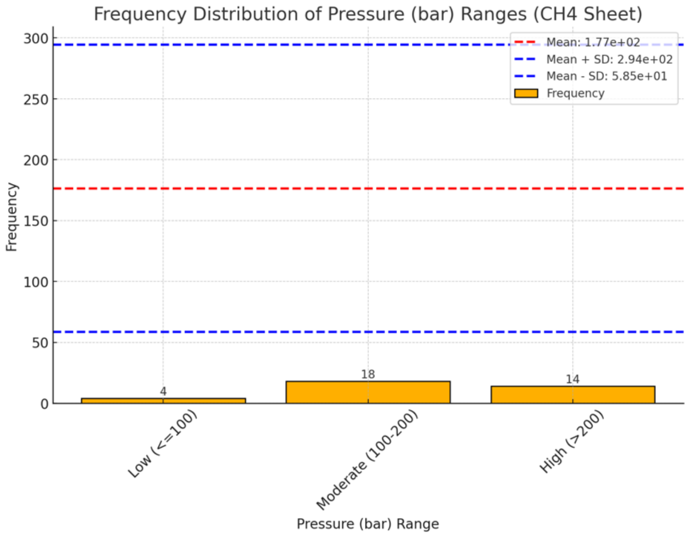

Fig.24 pressure distribution for CH4

The data indicate that CH_4 storage predominantly occurs in moderate (100–200 bar) and high-pressure (>200 bar) reservoirs, which offer both enhanced storage capacity and improved containment security. Moderate-pressure sites, the most common, provide a balance between capacity and safe injection dynamics, minimizing leakage risks. High-pressure reservoirs, though fewer, enable greater storage potential but require strict pressure management to prevent fracturing and ensure long-term stability. The rarity of low-pressure sites (≤100 bars) suggests that shallow or depleted formations are less favorable due to increased gas expansion and potential escape risks. The wide pressure variation (58.5–294 bar) underscores the need for site-specific strategies to maintain safe containment while optimizing storage efficiency.

1.3.2 Temperature

Fig.25 shows the distribution of temperature for the analyzed dataset.

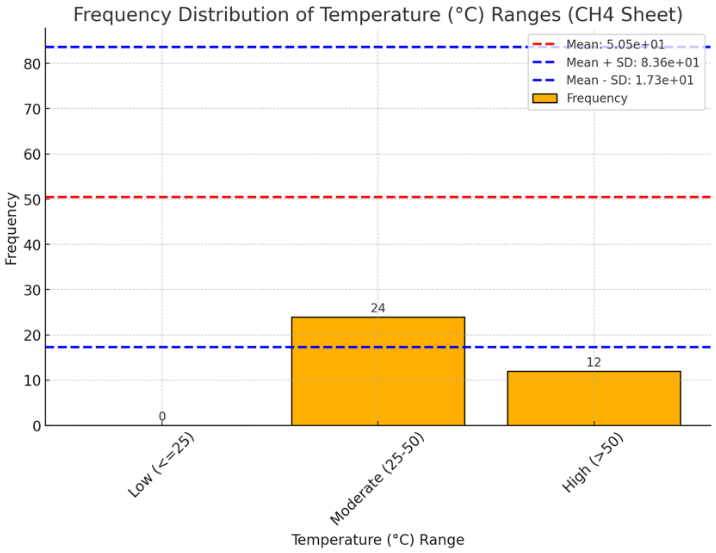

Fig.25 temperature distribution for CH4

CH_4 storage predominantly occurs in moderate (25–50°C) and high-temperature (>50°C) reservoirs, with no occurrences in low-temperature (≤25°C) formations. Moderate-temperature sites are the most common, providing an optimal balance between gas density and mobility, enhancing both storage capacity and containment security. High-temperature reservoirs, found in deeper formations, offer increased storage potential but require additional sealing measures due to elevated gas mobility.

1.3.3 Depth

Fig.26 shows distribution of this dataset.

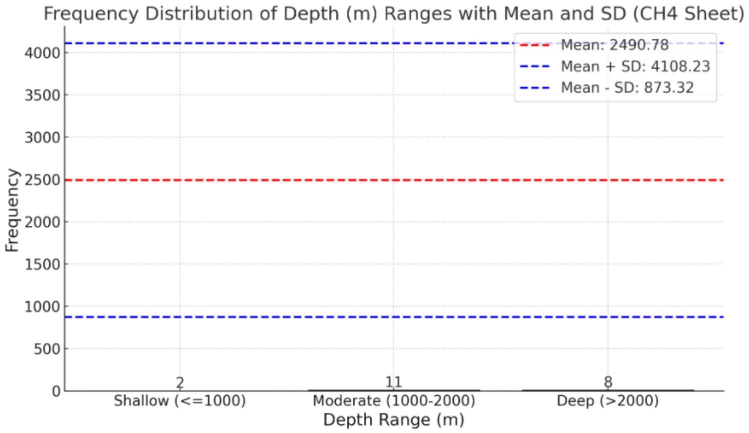

Fig.26 Depth distribution for CH4

The chart divides storage depths into three categories: shallow (≤1000 m), moderate (1000-2000 m), and deep (>2000 m). The most common storage sites fall in the moderate depth range, with 11 occurrences, followed by deep formations with 8 occurrences. Shallow sites are rare, with only 2 recorded cases. The average depth across all sites is about 2490.78 meters, as shown by the red dashed line. The spread of values is quite wide, with depths ranging from as low as 873.32 meters (lower blue dashed line) to as high as 4108.23 meters (upper blue dashed line). This pattern suggests that CH_4 storage typically happens at moderate to deep depths, where pressure is high enough to keep the gas stable but still within a practical drilling range.

The preference for moderate-depth storage (1000-2000 m) suggests that many projects aim for a balance between cost and efficiency—deep enough to ensure stability but not so deep that drilling and maintenance become too expensive. Some sites extend beyond 2000 meters into deep formations, benefiting from even higher pressure but requiring more advanced engineering solutions. Shallow storage (≤1000 m) is much less common, likely because lower pressure at these depths makes gas retention more difficult and increases the risk of leakage.

The variation in depth across different sites highlights that CH_4 storage isn't one-size-fits-all. While deeper formations generally offer better containment, they also bring technical challenges. Choosing the right depth means weighing the benefits of higher pressure against the realities of drilling costs, monitoring requirements, and long-term stability. This distribution suggests that most CH_4 storage projects focus on depths where pressure supports containment while keeping operations feasible.

1.3.4 Porosity

In Fig.27, it can clearly be seen that how porosity is distributed.

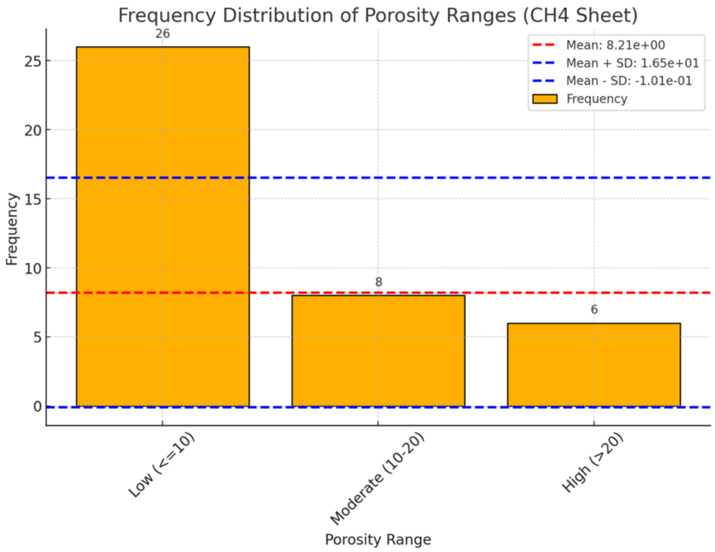

Fig.27 Porosity distribution for CH4

The figure classifies porosity into three main categories: low (≤10%), moderate (10-20%), and high (>20%). The low porosity range has the highest frequency, with 26 occurrences, followed by the moderate porosity range with 8 occurrences, and the high porosity range with 6 occurrences.

The mean porosity is 8.21%, marked by a red dashed line, while the standard deviation boundaries extend from -1.01% (lower blue dashed line) to 16.5% (upper blue dashed line). The concentration of values in the low porosity range indicates that most CH_4 storage reservoirs are characterized by relatively limited pore space, potentially requiring additional considerations for injection.

CH_4 storage primarily occurs in low-porosity (≤10%) and moderate-porosity (10–20%) formations, where containment stability is enhanced but may require higher pressures or trapping mechanisms to improve efficiency. High-porosity reservoirs (>20%) are less common, likely due to increased permeability and potential leakage risks. The wide variability in porosity across storage sites highlights the importance of factors like capillary forces and permeability in gas retention.

1.3.5 Permeability

his permeability distribution provides insight into how CH_4 storage formations are classified based on their ability to allow gas flow. The majority of formations fall into the very low permeability range ($\leq 1\times10^{-20}$ D), with 18 occurrences, highlighting that most CH_4 storage sites have extremely limited flow potential, often requiring additional pressure management. The moderate permeability range (1×10^{-18} to 1×10^{-15} D) appears 9 times, indicating a smaller but significant portion of formations with better flow characteristics, though capillary trapping remains a key factor. The low permeability range (1×10^{-20} to 1×10^{-18} D) is relatively rare, with only 3 instances, suggesting that intermediate formations are uncommon. Finally, the high permeability range (1×10^{-15} to 1×10^{-14} D) is the least frequent, with just 2 occurrences, showing that formations capable of higher gas flow are the rarest in this dataset. (Fig.28)

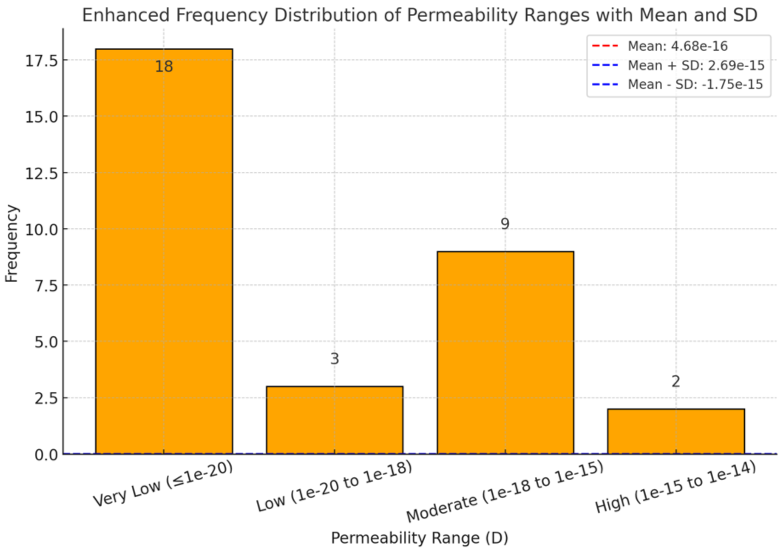

Fig. 28 Permeability distribution for CH4

The mean permeability is $4.68 \times e^{-16}$ D, reflecting an overall trend toward low permeability $2.22 \times e^{-15}$2.22e-15 D, highlighting significant variability in permeability values. This suggests that different CH_4 storage sites exhibit a wide range of geological conditions, making it necessary to assess site-specific parameters such as capillary trapping efficiency and fracture connectivity. The relatively high frequency of very low permeability formations implies that many CH_4 storage projects take place in tight reservoirs, where gas movement is restricted, necessitating enhanced recovery techniques or alternative injection strategies to optimize storage efficiency.

1.3.6 Breakthrough Pressure

Methane breakthrough pressure is the pressure at which CH_4 begins to flow continuously through a porous medium after surpassing capillary barriers. Compared to CH_4 and other gases, CO_2 exhibits a significantly wider breakthrough pressure range, with values up to an order of magnitude higher. This indicates that CO_2 storage sites require much greater pressures to initiate migration, highlighting the stronger capillary sealing efficiency in CO_2 sequestration.

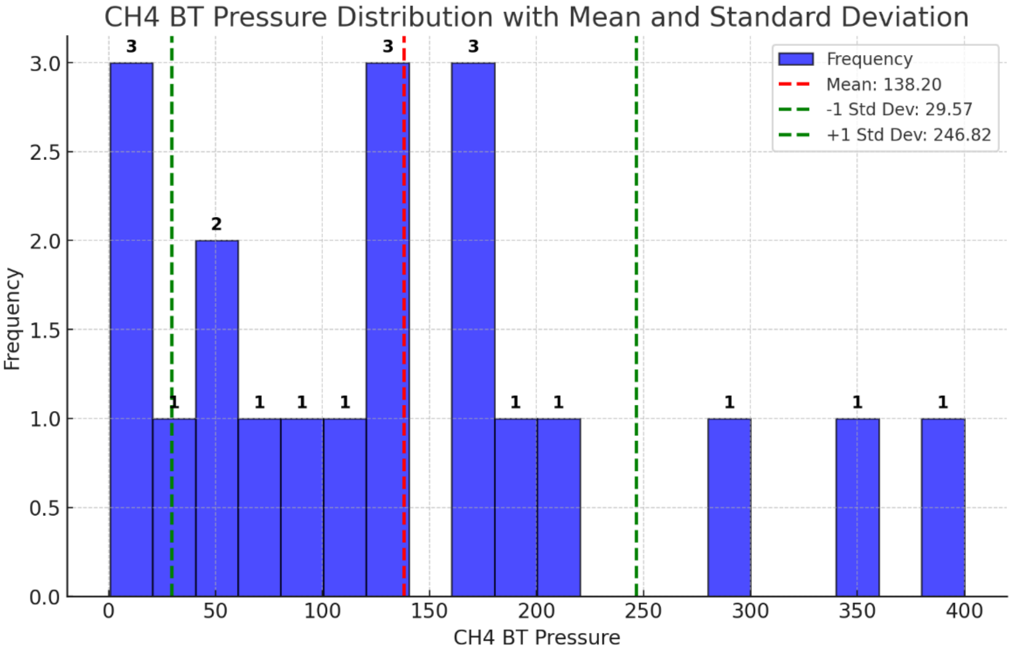

Fig.29 illustrations of BT pressure (bar)

The CH_4 breakthrough pressure chart shares similarities with its snap-off pressure chart, displaying a multi-modal distribution with several peaks. This suggests that methane does not break through at a single predictable pressure but exhibits different flow behaviors depending on pore structure and adsorption effects.

1.3.7 Snap-off Pressure

Snap-off pressure for CH_4 is the pressure at which methane bubbles break apart within a porous medium, disrupting continuous gas flow and trapping some portions of methane in isolated pores.

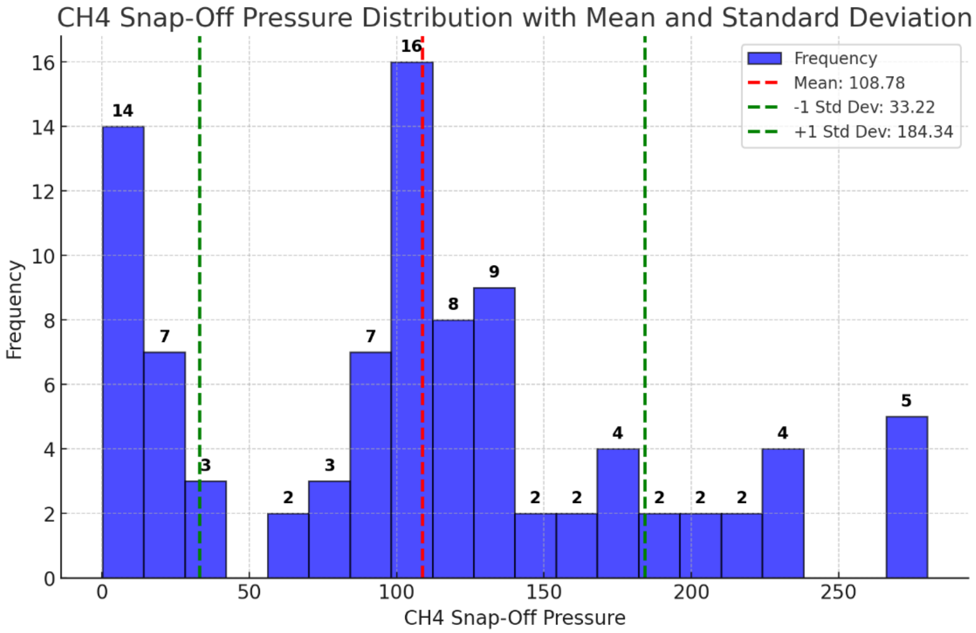

Fig.30 illustrations of Snap-off pressure (bar)

The CH_4 snap-off pressure distribution is multi-modal, meaning that methane snap-off occurs at various pressure levels depending on the surrounding conditions.

1.4 LITHOLOGY AND MINERALOGY

The geological makeup of underground formations plays an important role in how effectively gases like natural gas, carbon dioxide (CO_2), and Nitrogen (N_2) can be stored. The type of rock, its composition, and how it interacts with gas all influence the ability to safely and efficiently store these gases over long periods.

Lithology, which refers to the physical characteristics of rocks including their grain size, composition, and how tightly packed, directly affects their ability to store gas. (Fig.31)

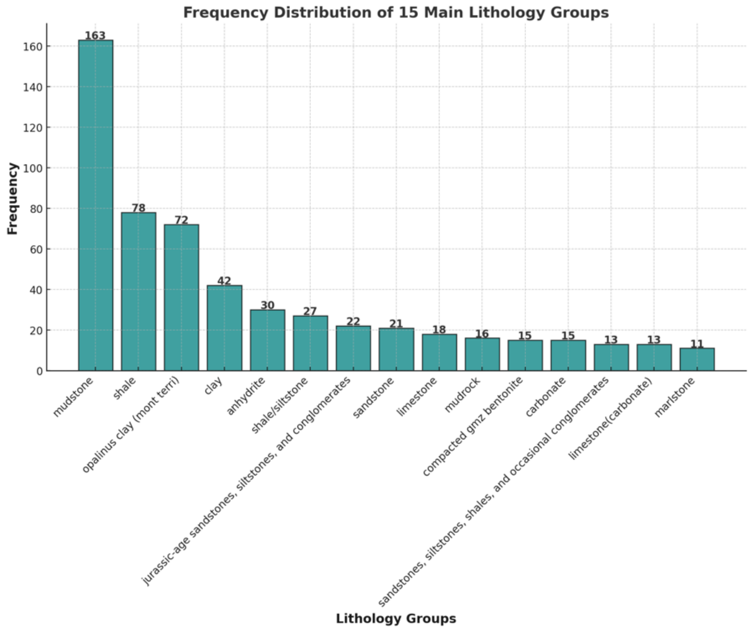

Fig.31 lithology distribution

Mineralogy, or the specific mineral content of rocks, is equally important. Some minerals, like clays (kaolinite, illite, smectite), can swell when exposed to certain fluids, clogging pore spaces and making gas flow more difficult. Other minerals, such as silica or calcite, act as cementing agents that determine the rock's strength and stability under pressure. Additionally, a rock's wettability affects storage efficiency. If a rock surface is more water-attracting (hydrophilic), it may hold onto water instead of gas, reducing the available storage space. Here is a detailed distribution of minerals in our rocks: (Fig.32)

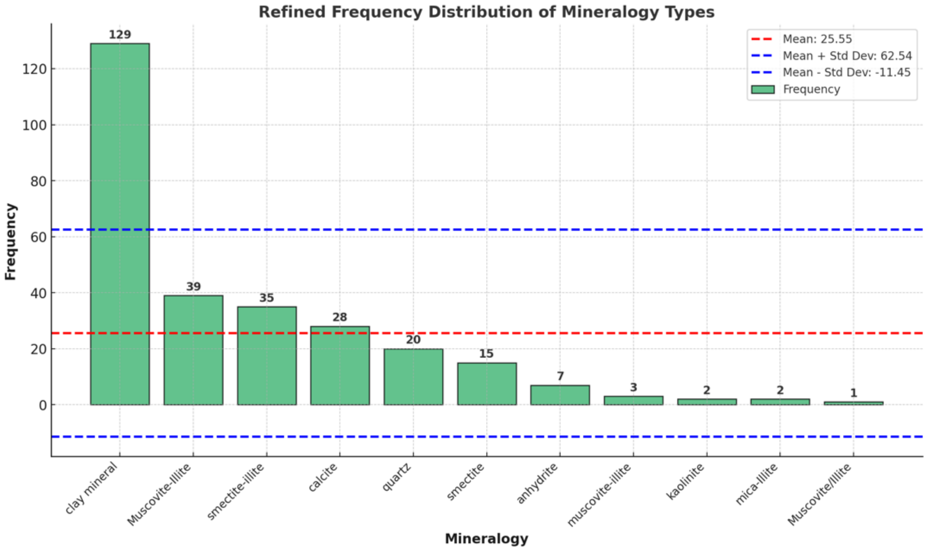

Fig.32 Mineralogy distribution

1.5 Opalinus Clay

Opalinus Clay is a fine-grained, low-permeability sedimentary rock that has garnered significant attention for its potential applications in underground gas storage, nuclear waste disposal, and geological sequestration. Predominantly found in Switzerland and other parts of Europe, this Jurassic-age formation, approximately 174 million years old, comprises mainly clay minerals, quartz, carbonates, and feldspars (EJP-EURAD, 2024).

In this work, the threshold pressure data on Opalinus clay according to different gases were analyzed to gather some insights on the effects of gases on sealing efficiency of the formation, given a well-defined mineralogical contest.

The composition of Opalinus Clay includes approximately 60–80% clay minerals, such as illite, kaolinite, and smectite. These minerals contribute to their extremely low permeability, making it an effective seal for gases and fluids. The remaining constituents include quartz, carbonates (mainly calcite and dolomite), and feldspars, which influence its mechanical behavior. Due to its high clay content, Opalinus Clay exhibits self-sealing properties; when fractures occur, they tend to close over time due to swelling and compaction, enhancing its containment capabilities. The mineralogy of Opalinus Clay significantly affects its geomechanical properties. It has a low porosity, typically ranging from 10% to 15%, with permeability in the range of 10^{-21} to 10^{-19} m^2. These characteristics make it an excellent natural barrier for preventing fluid and gas migration. However, its mechanical behavior varies depending on water saturation, stress conditions, and deformation history. Under undisturbed conditions, Opalinus Clay behaves as a viscoelastic material, but when subjected to excavation or stress changes, it can develop microfractures that temporarily enhance permeability before self-sealing mechanisms restore its integrity (EJP-EURAD, 2024).

Opalinus Clay has been extensively studied for its potential as a caprock in geological storage systems, including carbon dioxide (CO_2) and methane (CH_4) sequestration. Its ultra-low permeability and high retention capacity make it an ideal candidate for trapping gases and preventing their escape into overlying formations. Studies on gas diffusion, capillary entry pressure, and breakthrough pressure have provided valuable insights into how gases interact with this formation. One of the challenges associated with Opalinus Clay in gas storage applications is its sensitivity to gas entry pressure. Research has shown that when gas is injected into water-saturated Opalinus Clay, breakthrough occurs only at high pressures due to the strong capillary forces within its fine pore network. Once breakthrough happens, permeability can temporarily increase, but due to the self-sealing nature of the clay, fractures tend to close over time, restoring containment properties. This makes it an effective long-term seal but requires careful management of injection pressures to prevent excessive fracturing. Another important factor in gas storage within Opalinus Clay is the gas diffusion mechanism. Unlike more permeable reservoir rocks where gas migrates through connected pore spaces, Opalinus Clay primarily allows gas movement through diffusion. This means that gas molecules slowly migrate through the nano-scale pores over extended periods rather than flowing freely. As a result, the diffusion coefficient for gases in Opalinus Clay is much lower than in typical reservoir formations, contributing to its effectiveness as a long-term containment medium (NERC, 2011).

One of the most unique properties of Opalinus Clay is its ability to self-seal. When exposed to stress or excavation, the formation may develop fractures, which could potentially increase permeability and gas migration. However, due to the high clay content, particularly the presence of swelling clays like smectite—the material can reabsorb water, causing the fractures to close over time. (EJP-EURAD, 2024).

Additionally, Opalinus Clay is highly anisotropic, meaning that its mechanical and transport properties vary depending on the direction of measurement. This anisotropy is due to its layered sedimentary structure, which causes permeability and diffusion coefficients to differ along horizontal and vertical axes. The bedding planes in Opalinus Clay typically exhibit higher permeability along their layers and lower permeability perpendicular to them. This characteristic must be considered when evaluating its suitability for gas storage, as gas movement will be influenced by the direction of the bedding planes (Favero, Valentina & Ferrari, Alessio & Laloui, Lyesse, 2018).

The thermal properties of Opalinus Clay are another critical factor when assessing its performance in underground gas storage. Since gas injections and withdrawal can cause temperature variations, it is important to understand how the rock responds to thermal stress. Studies have shown that Opalinus Clay has a relatively low thermal conductivity, meaning that heat transfer within the formation occurs slowly. This slow heat dissipation helps maintain stable pressure conditions within the rock, reducing the risk of thermal-induced fracturing or permeability changes. Over long periods, the structural integrity of Opalinus Clay is preserved due to its low creep rate—the slow deformation of the rock under constant stress. This characteristic makes it particularly suitable for long-term gas storage applications, as it reduces the likelihood of gradual permeability increases that could lead to gas escape. Additionally, its mineralogical stability ensures that chemical reactions between the rock and stored gases remain minimal, preventing unexpected changes in reservoir properties (EJP-EURAD, 2024).

4.6 Machine Learning Approach

4.6.1 First approach (KNN)

The purpose of this script is to analyze a dataset extracted from an Excel file, clean it up, handle missing values, compute correlations, and visualize the results.
To start, I used several Python libraries. Pandas was my go-to for data manipulation and cleaning, while Seaborn and Matplotlib helped me create heatmaps and visualizations. For missing data, I used Scikit-learn's KNNImputer, which uses the k-nearest neighbors' algorithm to fill in gaps more reliably than just putting in averages or medians. I also used NumPy for some numerical operations and to help with handling missing values. First, I loaded the dataset into a Data Frame sheet using "pd. read_excel". Since the column names were a bit messy, I standardized them for consistency.
Next, I handled messy data entries, especially those with ranges or weird symbols, averaging values like "10-20", converted symbols like "-" or "**" into NaN, and made sure everything was numeric.

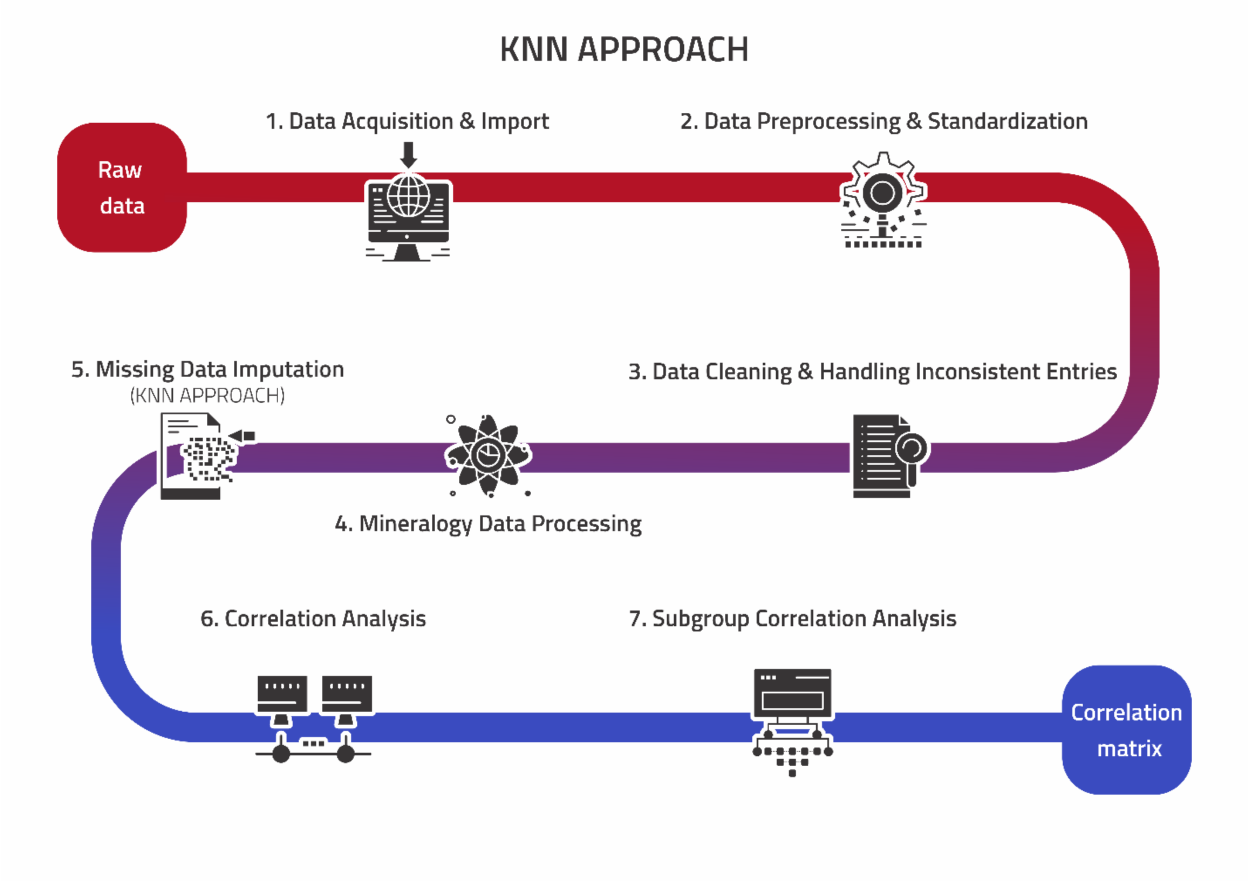

Fig.33 schematic for different stages in KNN

The 'depth' column needed extra attention. I replaced 'surface' with 0 to represent the ground level and set ambiguous values like 'mean' to NaN. Then, I converted the whole column to numeric and filled in the missing values with the predicted value of the column. For the 'mineralogy' column, which had combined data like "30% Quartz", I split it into two new columns: one for the percentage (mineralogy_value) and another for the type (mineralogy_type).

For missing data, I used KNN Imputation, which is a smarter way of filling in missing values by looking at the nearest neighbors in the dataset. I applied it to numeric columns like 'residual_pressure', 'porosity', and 'temperature', using 5 neighbors to fill in the gaps. This approach avoids the biases that come with more basic imputation methods and keeps the data reliable. For data that has less than three numbers I used mean.

After cleaning everything up, I moved on to correlation analysis. I calculated a correlation matrix with “corr()” and visualized it using a heatmap from Seaborn. This helped me spot patterns, including strong and weak correlations. To dig a little deeper, I grouped the dataset by 'mineralogy_type' to see how correlations differed within subgroups. For groups with enough data, I created correlation matrices and heatmaps, which revealed some unique relationships. Groups with too little data were flagged for further collection.

The subgroup analysis revealed interesting variations among different mineral types, which could be useful for future modeling.

These illustrations are correlation matrix for KNN approach among 3 types of gases:

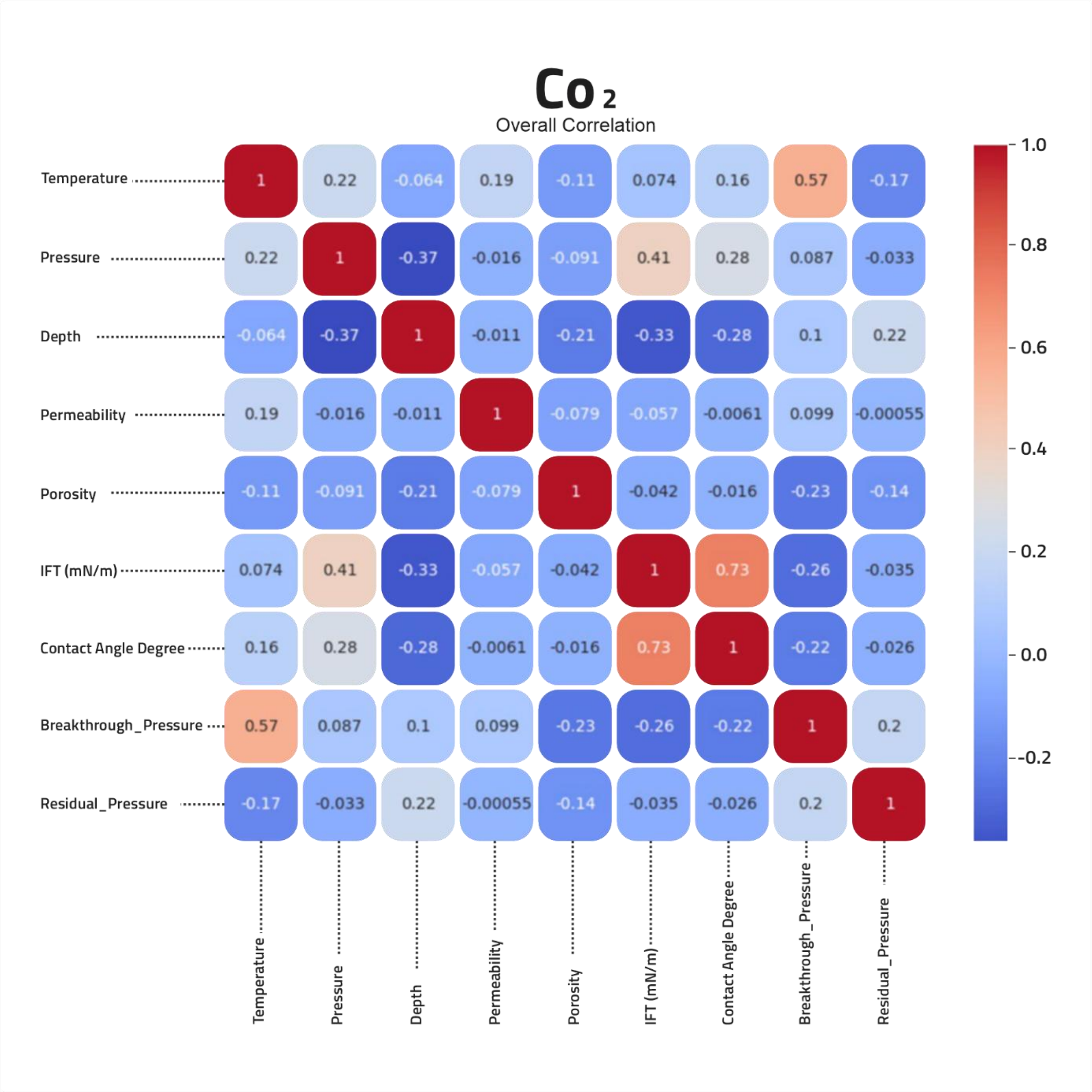

	Temperature	Pressure	Depth	Permeability	Porosity	IFT (mN/m)	Contact Angle Degree	Breakthrough_Pressure	Residual_Pressure
Temperature	1	0.22	-0.064	0.19	-0.11	0.074	0.16	0.57	-0.17
Pressure	0.22	1	-0.37	-0.016	-0.091	0.41	0.28	0.087	-0.033
Depth	-0.064	-0.37	1	-0.011	-0.21	-0.33	-0.28	0.1	0.22
Permeability	0.19	-0.016	-0.011	1	-0.079	-0.057	-0.0061	0.099	-0.00055
Porosity	-0.11	-0.091	-0.21	-0.079	1	-0.042	-0.016	-0.23	-0.14
IFT (mN/m)	0.074	0.41	-0.33	-0.057	-0.042	1	0.73	-0.26	-0.035
Contact Angle Degree	0.16	0.28	-0.28	-0.0061	-0.016	0.73	1	-0.22	-0.026
Breakthrough_Pressure	0.57	0.087	0.1	0.099	-0.23	-0.26	-0.22	1	0.2
Residual_Pressure	-0.17	-0.033	0.22	-0.00055	-0.14	-0.035	-0.026	0.2	1

Fig.34 CO2 correlation Heatmap

For CO_2, breakthrough pressure exhibits a strong positive correlation with temperature (0.57), indicating that higher temperatures increase resistance to flow, likely due to viscosity or phase changes. Permeability and porosity have negative correlations (-0.26 and -0.23, respectively), meaning more porous and permeable formations reduce resistance. Residual pressure for CO_2 has a weak negative correlation with temperature (-0.17), Depth has a slight positive correlation (0.22). A weak positive correlation (0.2) between breakthrough and residual pressure implies that higher breakthrough pressure slightly increases trapped CO_2.

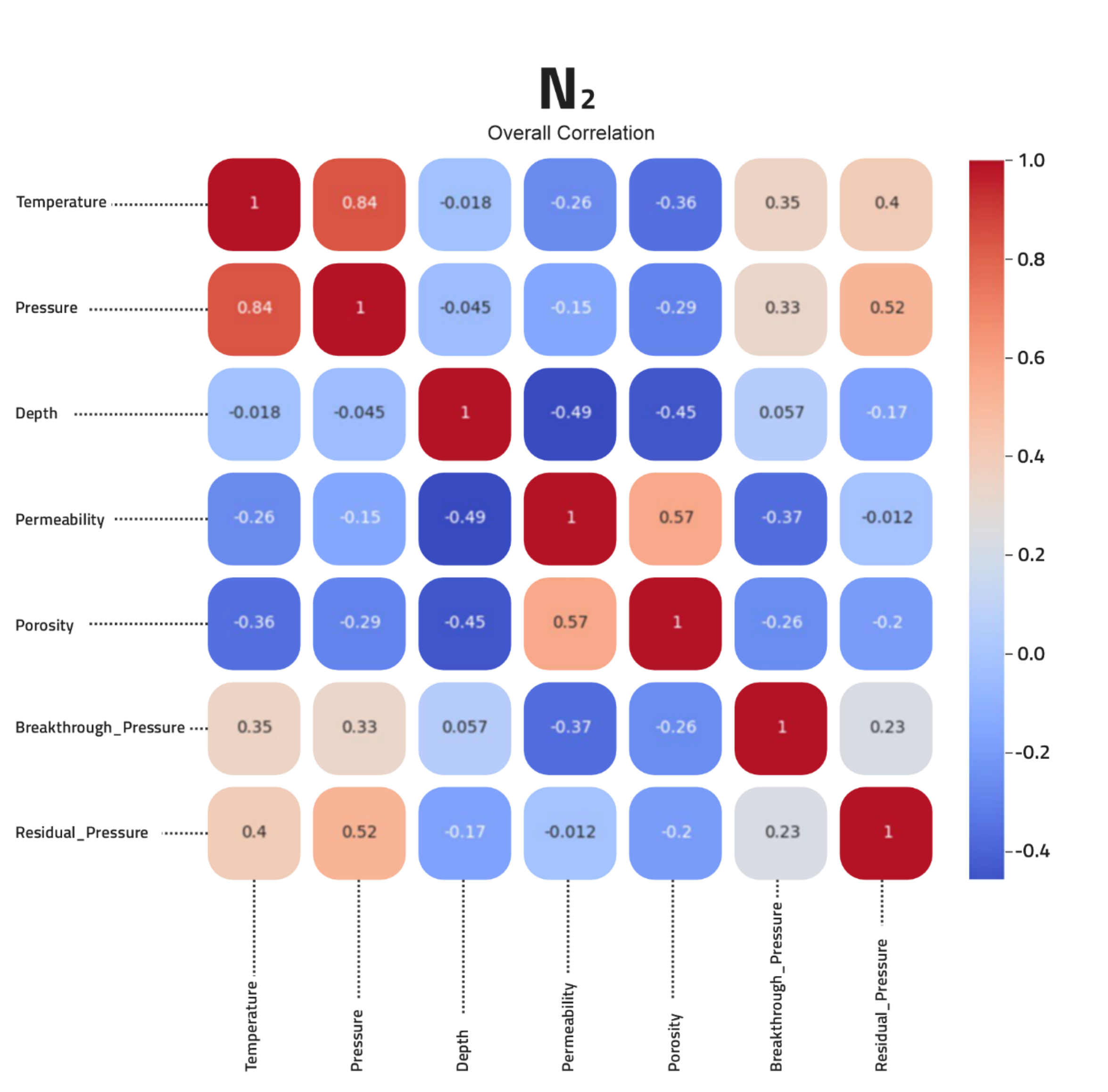

	Temperature	Pressure	Depth	Permeability	Porosity	Breakthrough_Pressure	Residual_Pressure
Temperature	1	0.84	-0.018	-0.26	-0.36	0.35	0.4
Pressure	0.84	1	-0.045	-0.15	-0.29	0.33	0.52
Depth	-0.018	-0.045	1	-0.49	-0.45	0.057	-0.17
Permeability	-0.26	-0.15	-0.49	1	0.57	-0.37	-0.012
Porosity	-0.36	-0.29	-0.45	0.57	1	-0.26	-0.2
Breakthrough_Pressure	0.35	0.33	0.057	-0.37	-0.26	1	0.23
Residual_Pressure	0.4	0.52	-0.17	-0.012	-0.2	0.23	1

Fig.35 N2 correlation Heatmap

For N_2, breakthrough pressure has a moderate positive correlation with both temperature (0.35) and pressure (0.33), suggesting that both factors play a significant role in increasing resistance to flow. permeability and porosity have negative correlations (-0.37 and -0.26, respectively), reinforcing that more porous formations lower breakthrough pressure. Residual pressure for N_2 shows a moderate positive correlation with temperature (0.4) and pressure (0.52), indicating that increasing these variables leads to greater retention of N_2. A moderate positive correlation (0.23) between breakthrough and residual pressure suggests that as breakthrough resistance increases, more N_2 remains trapped.

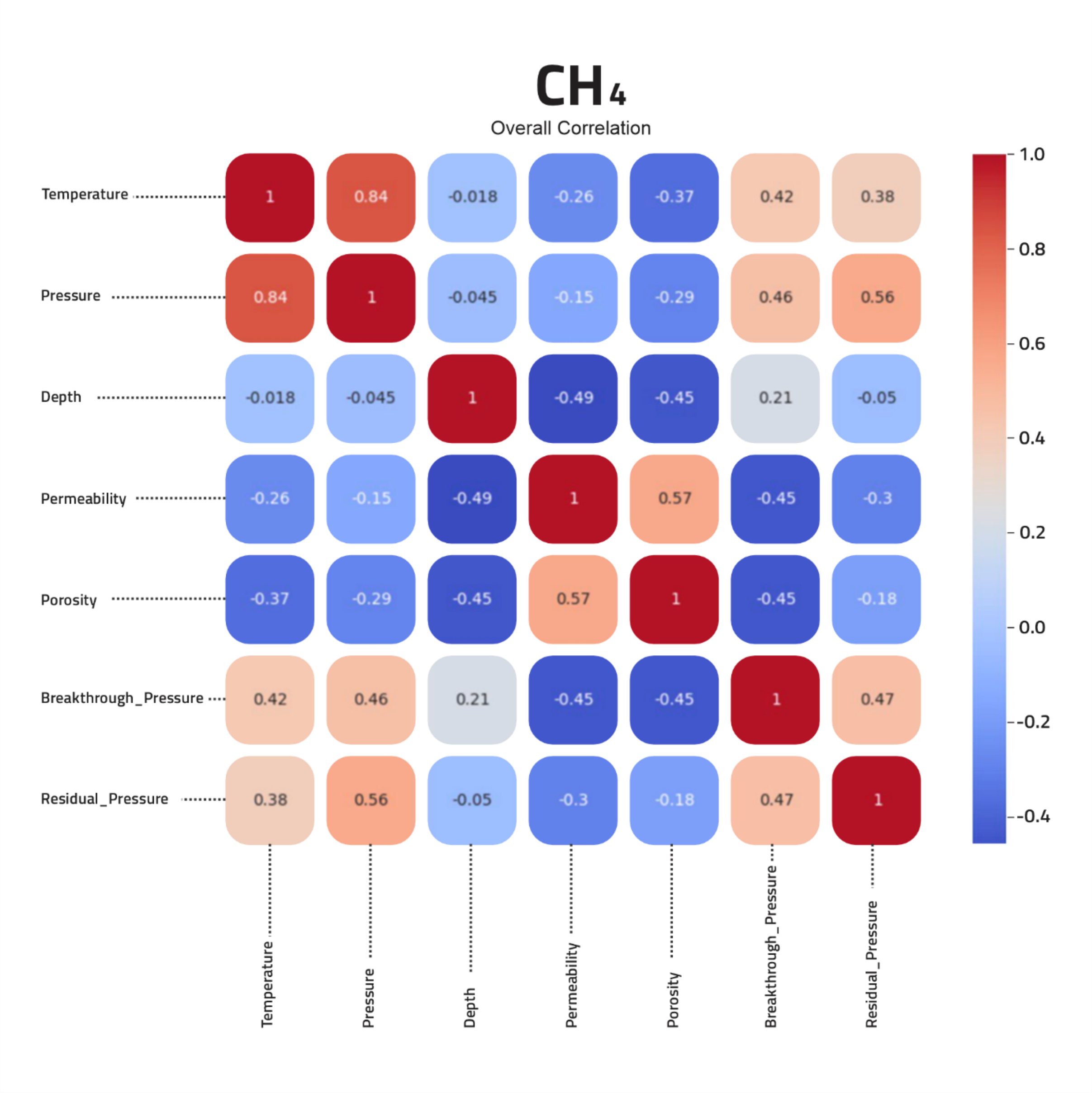

	Temperature	Pressure	Depth	Permeability	Porosity	Breakthrough_Pressure	Residual_Pressure
Temperature	1	0.84	-0.018	-0.26	-0.37	0.42	0.38
Pressure	0.84	1	-0.045	-0.15	-0.29	0.46	0.56
Depth	-0.018	-0.045	1	-0.49	-0.45	0.21	-0.05
Permeability	-0.26	-0.15	-0.49	1	0.57	-0.45	-0.3
Porosity	-0.37	-0.29	-0.45	0.57	1	-0.45	-0.18
Breakthrough_Pressure	0.42	0.46	0.21	-0.45	-0.45	1	0.47
Residual_Pressure	0.38	0.56	-0.05	-0.3	-0.18	0.47	1

Fig.36 CH4 correlation Heatmap

For CH_4, breakthrough pressure is moderately correlated with temperature (0.42) and even more strongly correlated with pressure (0.46), showing that system pressure has a greater impact on CH_4 flow resistance than in CO_2 or N_2. Depth has a weak positive correlation (0.21), while permeability and porosity again show negative correlations (-0.45 for both), confirming that more porous formations reduce resistance. Residual pressure for CH_4 has a moderate to strong positive correlation with pressure (0.56) and temperature (0.38), suggesting that these factors significantly increase the amount of retained CH_4. A moderate positive correlation (0.47) between breakthrough and residual pressure suggests that as resistance to initial flow increases, more CH_4 remains trapped.

4.6.2 Second approach (CATBOOST)

The dataset was loaded into a Pandas DataFrame using the ‘pd. read_excel ()’ function. To avoid issues related to inconsistent naming or trailing spaces in column headers, all column names were stripped of whitespace. This step ensures that operations such as column selection and referencing work seamlessly during analysis. The index of the DataFrame was then reset to maintain continuity and provide a clean structure for subsequent analyses.

The preprocessing phase focused on selecting and transforming data to ensure compatibility with analytical techniques. Specific columns were selected based on their relevance to the analysis. This process removed unnecessary columns that could introduce noise or irrelevant information into the study. All selected columns were converted to numeric data types, ensuring that they were suitable for mathematical computations and statistical analysis. Any invalid or non-numeric values encountered during the conversion process were replaced with NaN.

A sophisticated approach was adopted to handle missing data using the CatBoost Regressor, a machine learning model specifically designed for handling categorical and numerical features. This method involves leveraging relationships between existing features to predict missing values in target columns. The process begins by identifying rows with complete data (i.e., rows without missing values) and splitting the dataset into two groups: one for training the model and the other for prediction. The CatBoost Regressor was then trained on the complete dataset, learning how the features interact. Using this trained model, missing values in the incomplete rows were predicted and replaced with the corresponding model outputs. This approach ensures that missing values are filled with context-aware predictions, reducing biases and inaccuracies that can result from traditional imputation methods like mean or median substitution.

In addition to CatBoost, a regression-based imputation technique was implemented. This method relied on linear regression, which was manually fitted using matrix algebra to predict missing values. Specifically, the relationships between independent features and the target variable were modeled, allowing missing values to be estimated based on known patterns. Linear regression imputation is particularly useful for datasets where features exhibit strong linear relationships. This dual approach—combining CatBoost predictions and regression-based imputation—ensured robust and reliable handling of missing data across the dataset.

To explore the relationships between variables, a detailed correlation analysis was performed. First, columns irrelevant to correlation computation, such as identifiers ('Sample No.') and categorical variables ('Type of test'), were excluded from the analysis to focus only on meaningful numerical relationships. For the remaining numeric columns, a correlation matrix was computed using Pandas. “corr()” function. This matrix quantified the strength and direction of relationships between pairs of variables. To enhance interpretability, heatmaps were created using Seaborn, providing a visual representation of these relationships. The heatmaps highlighted strong positive correlations, where variables increased together, and strong negative correlations, where one variable decreased as the other increased. Specific patterns were identified that could guide further research, such as exploring why certain variables exhibited weak or no correlation. This analysis offered insights into the underlying structure of the data and revealed dependencies that could inform modeling or domain-specific decisions.

To gain deeper insights, the dataset was grouped by the 'mineralogy_type' column to examine how correlations differed across subgroups. For each group with sufficient data points, correlation matrices and heatmaps were generated to identify variations in relationships specific to different mineral compositions. This subgroup-level analysis revealed unique patterns within the data, emphasizing the importance of considering group-level dynamics when interpreting results. Groups with insufficient data were flagged for further data collection, ensuring future analyses are well-supported by robust datasets.

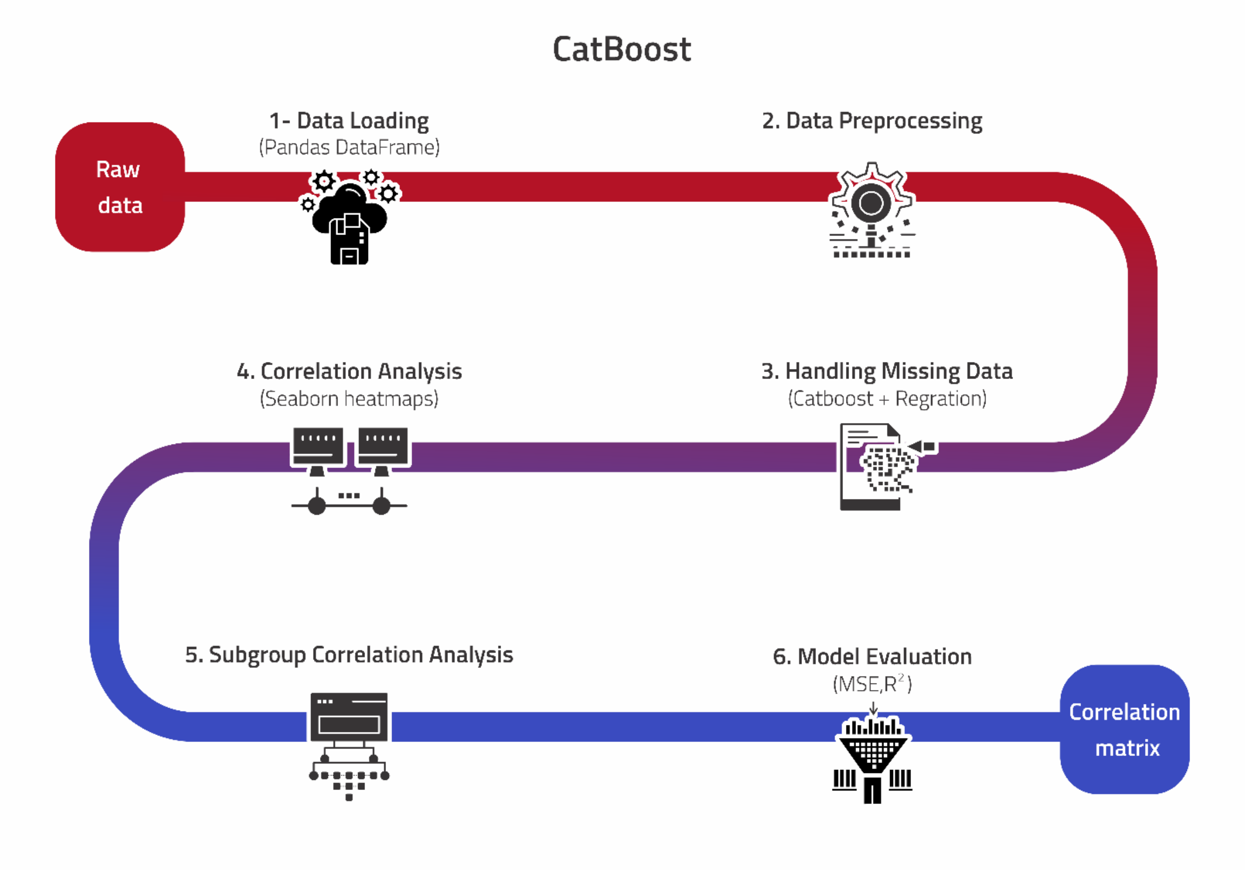

Fig.37 schematic for different stages in CatBoost

Model Evaluation

The processed dataset was used to train a machine learning model. The model's performance was evaluated on a separate test set, which was held out during the training process to provide an unbiased assessment of the model's predictive capabilities. Two key metrics were used for evaluation:

- **Mean Squared Error (MSE):** This metric measures the average squared difference between predicted and actual values, with lower values indicating better prediction accuracy.
- $\boldsymbol{R^2}$**:** This coefficient of determination evaluates how well the model explains the variability in the target variable, with values closer to 1 indicating a better fit.

  These metrics provided a comprehensive understanding of the model's performance, highlighting areas where predictions were accurate and areas that may require refinement.

These pictures show a table of **MSE** and $\boldsymbol{R^2}$ for each gas separately (Table.1,2)

DATA PREPROCESSING		
PARAMETER	MSE	R^2
CO2	2364.672	0.867
N2	502.173	0.911
CH4	246.049	0.897

Table.1 **MSE** and R^2 among different gases for preprocessing

PREDICTION MODEL		
PARAMETER	MSE	R^2
CO2	31.527	0.97
N2	574.523	0.961
CH4	331.322	0.932

Table.1 **MSE** and R^2 among different gases for prediction model

Mineralogy Preprocessing

The mineralogy column contained combined information about the composition of samples, requiring specific preprocessing to make it usable for analysis. To streamline this data, binary flags were created for specified mineral groups, effectively categorizing samples into distinct categories. This step allowed for easy identification of samples belonging to specific mineral groups and enabled group-wise analysis. The transformation of mineralogy data into a structured format facilitated targeted analyses, such as examining how correlations vary among different mineral types or developing models specific to particular mineral compositions.

CHAPTER 5 (Results and Comments)

Correlation matrix illustrating the relationships between breakthrough pressure (Pb) and snap-off pressure (Ps) for CO_2, N_2, and CH_4 with key cap rock properties, including interfacial tension (IFT), porosity, temperature, permeability, and pressure, as well as mineralogical components such as calcite, muscovite-illite, quartz, smectite, clay, and smectite-illite. The correlation coefficients indicate the strength and direction of these relationships, with highlighted values representing significant correlations that may influence cap rock sealing efficiency, gas migration potential, and overall storage security. The details and implications of these correlations in the context of cap rock risk assessment will be discussed in the following sections. All the correlations discussed in this section are calculated with CatBoost (Table.3).

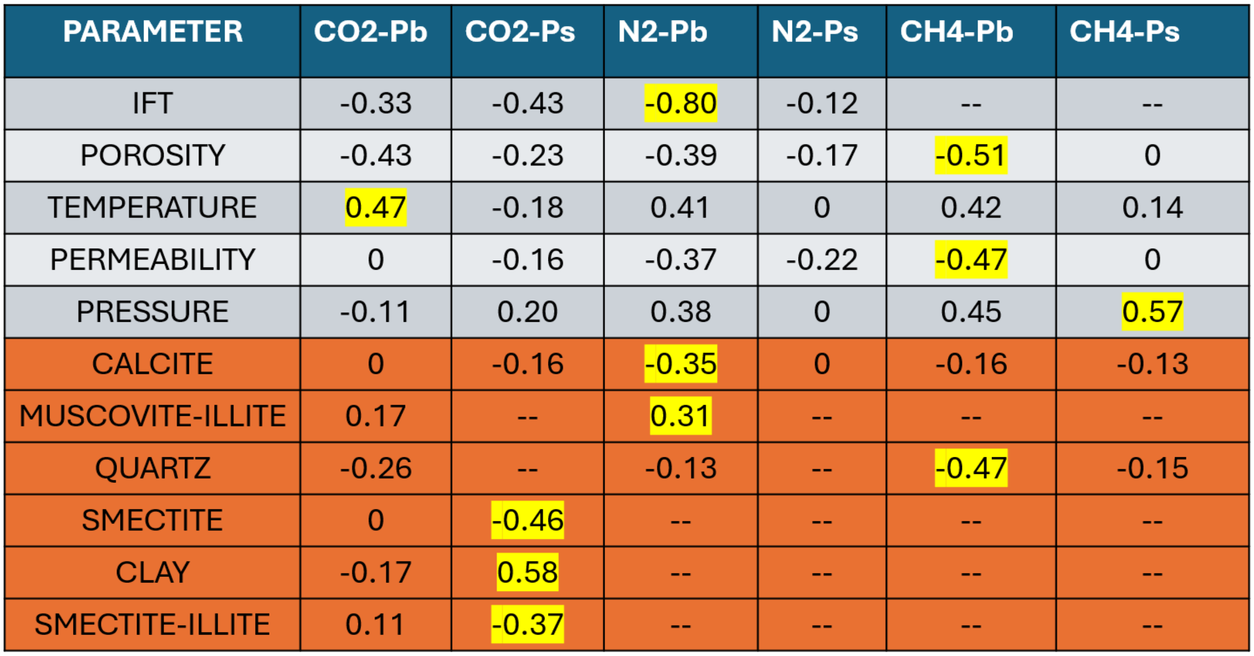

PARAMETER	CO2-Pb	CO2-Ps	N2-Pb	N2-Ps	CH4-Pb	CH4-Ps
IFT	-0.33	-0.43	-0.80	-0.12	--	--
POROSITY	-0.43	-0.23	-0.39	-0.17	-0.51	0
TEMPERATURE	0.47	-0.18	0.41	0	0.42	0.14
PERMEABILITY	0	-0.16	-0.37	-0.22	-0.47	0
PRESSURE	-0.11	0.20	0.38	0	0.45	0.57
CALCITE	0	-0.16	-0.35	0	-0.16	-0.13
MUSCOVITE-ILLITE	0.17	--	0.31	--	--	--
QUARTZ	-0.26	--	-0.13	--	-0.47	-0.15
SMECTITE	0	-0.46	--	--	--	--
CLAY	-0.17	0.58	--	--	--	--
SMECTITE-ILLITE	0.11	-0.37	--	--	--	--

Table.3 Correlation matrix

1.CO2 CORRELATION

1.1 Correlation Between IFT and Breakthrough Pressure

The relationship between breakthrough pressure (*Pb*) and interfacial tension (IFT) is described by the Young-Laplace equation:

$$P_b = \frac{2\gamma \cos\theta}{r} \text{ (Eq.52)}$$

where:

- *Pb*: Breakthrough pressure,
- γ: Interfacial tension (IFT) between CO_2 and brine,
- θ: Contact angle (a measure of wettability),
- *r*: Pore throat radius.

This equation shows that breakthrough pressure depends directly on IFT, wettability, and the size of the pore throats. However, the relationship isn't always simple because of the complex interactions between physical and chemical factors in CO_2-brine systems.

IFT plays a crucial role in breakthrough pressure by modulating capillary forces at the CO_2-brine interface. When IFT (γ) decreases, capillary forces weaken, making it easier for CO_2 to displace brine, which, according to the Young-Laplace equation, should lead to a lower breakthrough pressure. In simpler terms, lower IFT reduces the resistance faced by CO_2 as it attempts to enter brine-filled pores. However, counteracting effects complicate this relationship. Lower IFT often enhances the wettability of the system, causing brine to spread more readily within the pores. This increased wettability can lead to stronger capillary retention, particularly in smaller pores, which may require higher pressures for CO_2 to displace the brine effectively. Consequently, while lower IFT theoretically reduces breakthrough pressure, changes in wettability can sometimes counteract this effect, leading to unexpected variations in breakthrough pressure.

Weak to Moderate Relationship (−0.33)

The correlation between IFT and breakthrough pressure is weak to moderate (−0.33), indicating that IFT alone does not fully govern changes in breakthrough pressure. This variability can be attributed to several factors. Firstly, competing effects within the system introduce inconsistencies. While lower IFT reduces capillary forces, it simultaneously alters wettability (θ) and the behavior of brine in smaller pores. For instance, in systems where lower IFT enhances wettability, the increase in cos(θ) can lead to stronger capillary forces in some pores, partially offsetting the expected reduction in breakthrough pressure. Additionally, naturally porous media are rarely homogeneous, and system heterogeneity introduces further complexity. Variations in pore size, mineral composition, and connectivity influence the way fluids interact within the pore network. In fine-grained rocks with smaller pores, the impact of IFT on breakthrough pressure is often less pronounced because brine is more effectively retained within these small voids. Nonlinear dynamics further complicate this relationship, as the effects of IFT on breakthrough pressure do not always follow a linear trend, particularly under varying pressure and temperature conditions. The phase behavior of CO_2, especially its transition to a supercritical state, introduces additional uncertainties by altering the interfacial tension and fluid dynamics within the system.

1.2 Correlation Between Porosity and Breakthrough Pressure

A moderate negative correlation (−0.43) suggests that higher porosity generally leads to lower breakthrough pressure, meaning that CO_2 can more easily penetrate and displace brine in rocks with greater porosity. However, this relationship is not purely linear and is influenced by several key factors, including pore throat size, pore connectivity, and mineral composition.

How Porosity Affects Breakthrough Pressure

According to the Young-Laplace equation, capillary pressure is inversely related to pore throat radius (r), meaning that larger pores decrease the resistance to CO_2 migration, facilitating easier displacement of brine. Pore Connectivity also plays a key role—higher porosity is often associated with a well-connected pore network, providing continuous pathways for CO_2 to flow. In contrast, Low-Porosity Rocks Exhibit Higher Capillary Forces due to their smaller and less connected pores. As a result, breakthrough pressure tends to be substantially higher in rocks with low porosity.

Moderate relationship (−0.43)

Mineralogical Composition further complicates the relationship. The presence of clays and other fine-grained minerals in low-porosity formations can block or narrow pore throats, increasing resistance to CO_2 migration and significantly raising breakthrough pressure. Clays such as smectite and illite are particularly effective in reducing porosity by swelling in the presence of water, which further restricts CO_2 flow. Additionally, Heterogeneity in Natural Reservoirs adds another layer of complexity.

1.3 Correlation Between Temperature and Breakthrough Pressure

The relationship between temperature and breakthrough pressure (*Pb*) in CO_2-brine systems is complex, with a moderately positive correlation (0.47). This suggests that as temperature increases, breakthrough pressure also tends to rise, but the relationship is not straightforward. The impact of temperature on breakthrough pressure depends on changes in interfacial tension, wettability, and fluid viscosity, all of which interact in ways that may reinforce or counteract each other.

How Temperature Influences Breakthrough Pressure

Temperature significantly influences breakthrough pressure by affecting interfacial tension, wettability, mineral reactions, and fluid viscosity. As temperature rises, interfacial tension typically decreases, potentially lowering breakthrough pressure. However, other temperature-induced changes, such as alterations in wettability and mineral reactions, can counteract this effect. Elevated temperatures often enhance the hydrophilicity of rock surfaces, increasing brine adhesion and capillary forces, which raises breakthrough pressure (Hjelmeland & Larrondo, 1986). Additionally, temperature can cause mineral precipitation or dissolution, reducing pore sizes and increasing resistance to CO_2 flow. While higher temperatures lower brine viscosity, facilitating CO_2 flow, the effects of stronger brine adhesion and pore clogging from mineral reactions may offset this benefit, ultimately raising breakthrough pressure.

Moderate relationship (0.47)

Temperature's impact on breakthrough pressure exhibits a moderate correlation (0.47) due to the competing effects of various temperature-driven processes. While higher temperatures reduce interfacial tension (IFT) and brine viscosity, potentially lowering breakthrough pressure (Hjelmeland & Larrondo, 1986), they also enhance wettability and mineral precipitation, which can increase breakthrough pressure (Zhang & Liu, 2020). These opposing influences create variability, especially in high-temperature reservoirs, where reduced IFT may be offset by stronger brine adhesion and pore clogging (Akinbehinje, 2007). Heterogeneous pore structures in natural reservoirs add further complexity, as variations in pore size, mineral composition, and brine saturation affect how temperature influences breakthrough pressure (Almohammad, 2023). Nonlinear dynamics also play a role, with factors like pressure regime, brine salinity, and rock type influencing the relationship in complex ways ("Effects of Temperature on Relative Permeability," n.d.). Temperature-induced CO_2 phase transitions further complicate predictions, making it difficult to rely on temperature alone to estimate breakthrough pressure without considering additional cap rock characteristics (Zhang & Liu, 2020).

Temperature affects breakthrough pressure in CO_2 storage reservoirs through several factors. Supercritical CO_2 behavior, with higher density and lower interfacial tension, enhances CO_2

mobility, but its interaction with brine and rock surfaces becomes more sensitive to temperature variations. Elevated temperatures accelerate mineral reactions, altering pore structure and breakthrough pressure, with effects varying by rock type. In carbonate-rich formations, mineral dissolution and precipitation can either clog pores or open flow paths, influencing breakthrough pressure. Temperature also impacts wettability and brine retention, which can increase breakthrough pressure. Therefore, a comprehensive assessment considering pore structure, mineral composition, and cap rock heterogeneity is crucial for accurately predicting CO_2 containment efficiency, with temperature management strategies helping mitigate adverse effects.

1.4 Correlation Between IFT and snap-off Pressure

Snap-off is influenced by pore geometry, wettability, interfacial tension (IFT, γ), and dynamic fluid redistribution within the pore network.

How IFT influences snap-off pressure

The relationship between interfacial tension (IFT) and snap-off pressure is complex. While a decrease in IFT weakens capillary forces, potentially facilitating fluid snap-off, other factors complicate this relationship. Wettability plays a significant role; lower IFT can enhance brine spreading and adhesion to pore walls, increasing snap-off pressure, especially in water-wet systems (Almohammad, 2023). This effect is intensified in high-temperature reservoirs, where changes in wettability and capillary pressure are more pronounced (Almohammad, 2023). Additionally, narrower pore throats in fine-grained rocks trap brine more effectively, raising snap-off pressure. Rough or irregular pore walls further complicate this, as local capillary forces vary, making the overall influence of IFT on snap-off pressure unpredictable (Singh et al., 2019).

Moderate relationship (-0.43)

The relationship between interfacial tension (IFT) and snap-off pressure is more complex than it seems. While reducing IFT generally weakens capillary forces and should make fluid snap-off easier, other factors can offset this effect. One key counteracting factor is wettability changes. When IFT decreases, brine spreads more easily across rock surfaces, increasing its adhesion to pore walls, which can raise snap-off pressure, especially in water-wet systems (Almohammad, 2023). Cap rock characteristics like pore size distribution, mineral composition, and pore connectivity are further complicated things. In areas with smaller pores or rougher surfaces, capillary forces may be amplified, altering snap-off pressure (Zuo et al., 2023). Additionally, the system behaves nonlinearly, with multiple interacting factors that sometimes reinforce or cancel each other out. Changes in temperature and pressure in CO_2 storage reservoirs only add more complexity, making it difficult to predict how IFT will impact snap-off pressure under varying conditions (Zuo et al., 2023). Ultimately, the correlation is not straightforward, as it shifts based on the unique characteristics of each cap rock and the dynamic interactions between fluids and rocks.

1.5 Correlation Between Smectite-Illite Content and Snap-Off Pressure

Snap-Off Pressure in CO_2-Brine Systems

Interfacial tension (IFT) in CO_2-brine systems is generally lower, approximately 25–50 mN/m, compared to other gas-liquid systems, which typically reduces snap-off pressure (Chalbaud et al., 2009). However, in smectite-dominated reservoirs, the swelling of smectite clay minerals leads to smaller pore throats, counteracting the IFT reduction and increasing snap-off pressure (Zhang et al., 2022). Temperature and pressure variations further influence IFT, adding complexity to the system (Alhammadi et al., 2024). The contact angle (θ) is also significant; in reservoirs containing hydrophilic minerals like smectite and illite, a low θ for CO_2-brine interactions can elevate snap-off pressure. Additionally, factors such as brine salinity, CO_2 saturation, and mineral composition affect wettability and overall cap rock behavior (Chalbaud et al., 2009). Pore throat size (r) is crucial, especially in fine-grained reservoirs. The swelling of smectite reduces pore throat size, enhancing capillary forces and increasing the likelihood of snap-off (Zhang et al., 2022). Furthermore, the formation of illite bridges contributes to pore heterogeneity, complicating snap-off behavior.

moderate Relationship (-0.37)

Mineral composition variability plays a crucial role in determining snap-off pressure, as reservoirs often contain mixed clay minerals like smectite and illite in different proportions. This leads to uneven swelling and pore-throat restriction, creating inconsistencies in how snap-off pressure responds across the cap rock. However, the overall correlation between smectite-illite content and snap-off pressure is negative (-0.37), indicating that as the concentration of these clay minerals increases, snap-off pressure tends to decrease. This counterintuitive relationship arises from several competing effects.

While smectite swelling initially reduces pore throat size, prolonged swelling can lead to increased connectivity between pores, allowing CO_2 to bypass certain capillary barriers. Additionally, high illite content, despite forming pore-bridging structures, can introduce micro-fractures and heterogeneous pathways that facilitate CO_2 migration rather than promoting snap-off. Another significant factor is the effect of mineral-fluid interactions on wettability. In reservoirs with high smectite and illite content, brine retains strong adhesion to mineral surfaces, reducing CO_2's ability to become trapped in pore spaces. This suppresses snap-off pressure by allowing CO_2 to remain more mobile even in fine-grained environments.

Beyond mineral composition, other influences further contribute to the negative correlation. Variations in IFT due to changing cap rock pressure and temperature, along with hysteresis in contact angle behavior and brine salinity effects, contribute to this complexity. Additionally, surface roughness of mineral grains and the dynamic redistribution of fluids within the pore network introduce further unpredictability, making the relationship between these factors highly nonlinear rather than straightforward.

1.6 Correlation Between Clay Minerals and Snap-Off Pressure

Clay minerals significantly impact CO_2 storage safety and capacity. Smectite swells in low-salinity brine, reducing pore throat size and increasing capillary trapping, enhancing storage security but reducing permeability and capacity (Chiquet et al., 2007; Chalbaud et al., 2009). Illite and kaolinite block pore throats, restricting CO_2 flow and improving containment, though they may reduce injection efficiency (Espinoza & Santamarina, 2010; Kim et al., 2012).

CO_2 tends to migrate into larger pores, leaving brine trapped in smaller ones, which strengthens capillary trapping but limits storage volume (Bachu et al., 2008). Smectite and illite also increase brine retention, reducing storage capacity while improving CO_2 containment (Wan et al., 2019). Temperature and pressure variations further influence storage efficiency by altering CO_2 solubility and fluid behavior (Pini et al., 2012). Overall, clay minerals balance the trade-off between maximizing storage capacity and ensuring long-term containment in CO_2 sequestration.

Moderately Strong Relationship (0.58)

Clay minerals, particularly smectite, illite, and kaolinite, significantly affect capillary pressure in CO_2-brine systems by altering pore throat size, wettability, and interfacial tension. The swelling of smectite reduces pore throat radii, increasing capillary pressure, especially in fine-grained cap rocks with small pores. Wettability, driven by the hydrophilic nature of these minerals, strengthens capillary forces by enhancing brine retention (Chalbaud et al., 2009). Smectite's strong affinity for water further amplifies capillary forces, particularly under low-salinity conditions. Factors such as temperature, pressure, and salinity influence interfacial tension and fluid behavior, affecting overall capillary pressure (Pini et al., 2012). These complex interactions shape fluid displacement and snap-off pressure in CO_2 sequestration systems. Snap-off pressure variability in CO_2-brine systems depends on the type and proportion of clay minerals present in the cap rock. Smectite has the most significant effect due to its swelling in low-salinity brines, reducing pore throat sizes and increasing capillary pressure. Illite causes partial pore blockages through particle aggregation, while kaolinite obstructs pore throats without significantly affecting wettability. These variations lead to unpredictable fluid movement across different cap rocks. Additional factors, such as dynamic fluid redistribution, surface roughness, and elevated temperatures, further influence capillary pressure and fluid displacement, making snap-off pressure complex and difficult to predict (Pini et al., 2012; Wan et al., 2019).

1.7 Correlation Between Smectite and Snap-Off Pressure

Negative Relationship (-0.37)

In CO_2 storage and cap rock risk assessment, the variability in mineral composition, especially smectite and illite, significantly affects snap-off pressure and storage safety. The negative correlation between smectite-illite content and snap-off pressure (-0.37) indicates that higher clay concentrations reduce snap-off pressure, potentially compromising CO_2 trapping in the cap rock. Smectite swelling can increase pore connectivity, allowing CO_2 to bypass capillary barriers, while illite's pore-bridging may create pathways for CO_2 migration. The high wettability of these clays enhances brine retention, making CO_2 more mobile and increasing the risk of leakage. Other factors, like IFT changes, surface roughness, and fluid redistribution, further complicate the behavior of CO_2, emphasizing the need for careful risk assessment in storage sites.

In the context of CO_2 storage and safety, smectite and illite play critical roles in fluid behavior and capillary pressure. Smectite, by swelling upon contact with brine, can reduce pore throat sizes, increasing capillary forces and potentially enhancing CO_2 trapping. However, in high concentrations, smectite may create alternate flow paths, reducing snap-off pressure and making CO_2 migration more unpredictable, which could pose a safety risk in terms of efficient storage. Illite's ability to form bridges or micro-fractures can also alter fluid flow, either restricting it or allowing CO_2 to migrate more easily, affecting long-term storage stability. CO_2 retention in reservoirs with high clay content tends to be lower due to increased fluid mobility through micro-channels and fractures, which may compromise storage capacity. Additionally, high-pressure and temperature conditions change CO_2's physical properties, further influencing fluid distribution and snap-off behavior, potentially impacting both the efficiency and safety of CO_2 storage. Therefore, understanding the mineralogical and fluid characteristics of the

The table below displays the correlations between the parameters using two different approaches: CatBoost (CB) and K-Nearest Neighbors (KNN). As shown, there is a notable consistency in the correlation values obtained from both methods, with the numbers being quite similar across the board.

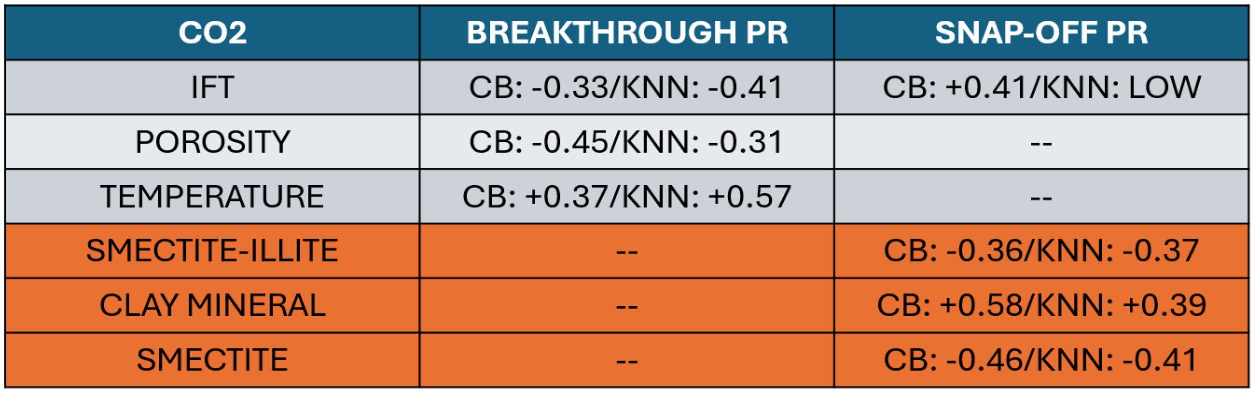

CO2	BREAKTHROUGH PR	SNAP-OFF PR
IFT	CB: -0.33/KNN: -0.41	CB: +0.41/KNN: LOW
POROSITY	CB: -0.45/KNN: -0.31	--
TEMPERATURE	CB: +0.37/KNN: +0.57	--
SMECTITE-ILLITE	--	CB: -0.36/KNN: -0.37
CLAY MINERAL	--	CB: +0.58/KNN: +0.39
SMECTITE	--	CB: -0.46/KNN: -0.41

Table.4

2. N2 CORRELATION

2.1 Correlation Between IFT and Breakthrough Pressure

Lower interfacial tension (γ) generally reduces capillary forces, making it easier for N_2 to displace brine, which should lower breakthrough pressure (P_b) (Chalbaud et al., 2009). However, the inverse relationship between IFT and Pb is not always straightforward due to pore-scale effects. As IFT decreases, brine can spread more uniformly over pore surfaces, increasing wettability ($\cos\theta$), which in turn may enhance water film formation in smaller pores (Espinoza & Santamarina, 2010). These continuous water films can create additional barriers to gas flow, requiring higher P_b despite lower IFT. This behavior is highly system-dependent, influenced by rock-fluid interactions, pore structure, and surface roughness, making the correlation between IFT and P_b more complex than a simple inverse relationship.

Strong relationship (-0.80)

As interfacial tension (IFT) decreases, brine becomes more wetting, adhering strongly to rock surfaces and increasing resistance to N_2 displacement. In strongly water-wet reservoirs, lower IFT promotes the formation of thin brine films along pore walls, increasing capillary pressure hysteresis and further restricting gas breakthrough (Espinoza & Santamarina, 2010).

N_2-brine systems IFT is generally high but can decrease under specific conditions. Elevated temperature and pressure influence IFT in complex ways; for instance, CO_2 or N_2 dissolution in brine at high pressures alters capillary forces, shifting P_b trends (Chalbaud et al., 2009

Wettability effects ($\cos\theta$) further complicate the relationship. As IFT decreases, water-wettability is enhanced, causing brine to adhere more strongly to rock surfaces, increasing resistance to gas penetration and ultimately raising P_b (Espinoza & Santamarina, 2010). This effect is particularly pronounced in strongly water-wet formations, where IFT-dependent wettability shifts dominate capillary behavior, reinforcing the observed correlation.

In micro-porous formations such as shale and tight sandstones, reduced IFT enhances fluid entrapment, making it even more difficult for N_2 to displace brine and increasing P_b (Wan et al., 2019). The IFT-P_b correlation is particularly strong in clay-rich formations, where wettability changes significantly impact capillary forces, compared to quartz-rich reservoirs, where wettability effects are weaker and capillary behavior is less sensitive to IFT variations.

2.2 Correlation Between Porosity and Breakthrough Pressure

In small-pore reservoirs, the brine-rock interfacial interaction is intensified, increasing breakthrough pressure under lower IFT conditions. In micro-porous formations, such as shale and tight sandstones, reduced IFT enhances fluid entrapment, making it even harder for N_2 to displace brine, thereby increasing breakthrough pressure. The IFT-P_b correlation is stronger in clay-rich formations, where wettability changes significantly impact capillary forces, compared to quartz-rich reservoirs, where wettability effects are weaker.

Moderate relationship (-0.39)

Porosity directly impacts pore size and connectivity, (Leverett, 1941). Depending on cap rock-specific conditions, wettability can either strengthen or weaken the porosity-P_b relationship. Variations in pore size distribution, cementation, and mineral composition can weaken the direct correlation between porosity and P_b (Chalbaud et al., 2009). For example, in carbonate formations, secondary porosity caused by dissolution processes can create deviations from expected porosity-

P_b trends, such as permeability changes without a proportional modification in pore throat sizes (Espinoza & Santamarina, 2010).

Additionally, nonlinear effects contribute to inconsistencies in how porosity influences breakthrough pressure. The relationship between porosity and pore throat size is not strictly linear; in fine-grained or clay-rich reservoirs, increased porosity does not always translate to larger pore throats, as micro-porosity can increase overall porosity without improving connectivity (Wan et al., 2019

Brine Wettability and Retention

In N_2-brine systems, brine typically wets the rock surface, leading to stronger retention in smaller pores and requiring higher breakthrough pressures. In formations dominated by hydrophilic minerals, this brine retention effect is more pronounced. Conversely, in mixed-wet or oil-wet systems, brine displacement efficiency may increase despite low porosity, altering the expected porosity-P_b relationship.

Influence of Mineral Composition

Clay-rich formations exhibit stronger capillary forces due to narrower pore throats, affecting the porosity-P_b relationship. For instance, montmorillonite and smectite-rich shales have high capillary entry pressures, necessitating significantly higher breakthrough pressures despite moderate porosity. In contrast, quartz-dominated sandstones generally display a more consistent porosity-P_b correlation, owing to their more uniform pore structures.

2.3 Correlation Between Calcite and Breakthrough Pressure

Calcite is highly reactive in brine environments, meaning that its influence on breakthrough pressure is often dynamic rather than static. Its effect depends on brine pH, salinity, and dissolution potential. The behavior of calcites in subsurface environments is influenced by its mineral surface properties, pore geometry, and chemical interactions, all of which affect capillary forces and breakthrough pressure (P_b). Calcite is moderately hydrophilic in water-wet systems, exhibiting a contact angle (θ) that promotes brine retention. However, its wettability is highly sensitive to brine chemistry, including factors such as salinity and pH, which can modify its surface characteristics and alter capillary forces (Alroudhan et al., 2018). In acidic or high-salinity brines, calcite undergoes surface alterations that change its contact angle, potentially reducing capillary pressure over time (Zhang et al., 2020).

Pore geometry also plays a critical role in controlling P_b, particularly in brine environments where calcite dissolution is common. As calcite dissolves, pore throat sizes (r) increase, reducing capillary forces and lowering breakthrough pressure (Noiriel et al., 2009). However, dissolution patterns are often heterogeneous, (Menke et al., 2017).

Moderate relationship (-0.35)

While calcite dissolution increases pore sizes and generally lowers P_b, other factors such as wettability shifts and interfacial tension (IFT) variations can counteract this effect, weakening the correlation (Espinoza & Santamarina, 2010). In cap rocks with mixed mineralogy, clay minerals often retain brine, offsetting the pore-enlarging effects of calcite dissolution by maintaining capillary forces that resist fluid displacement.

The relationship between calcite content and P_b is also nonlinear, particularly in chemically reactive environments. If calcite dissolution creates micro-fractures, permeability may increase without a proportional reduction in capillary forces, leading to localized deviations from expected behavior (Espinoza & Santamarina, 2010).

The impact of calcite on breakthrough pressure (P_b) isn't straightforward, it depends on how it interacts with wettability, brine chemistry, and interfacial tension (IFT). Unlike clay minerals, calcite is less water-wet, meaning it doesn't hold onto brine as strongly. This typically results in lower breakthrough pressures because brine is more easily displaced (Espinoza & Santamarina, 2010). However, things change when salinity drops. At lower salinities, calcite surfaces can actually become more hydrophilic, meaning they start holding onto brine more effectively, which in turn increases P_b . This shows that the presence of calcite doesn't always mean easier displacement—it depends on the surrounding fluid conditions.

Brine chemistry plays an equally important role. Acidic or high-salinity brines promote calcite dissolution, which enlarges pore spaces and generally lowers P_b (Noiriel et al., 2009 As a result, calcite-rich formations may see a steady decrease in breakthrough pressure over time as the rock structure changes, making it easier for fluids to move through (Emami-Meybodi et al., 2015).

2.4 Correlation Between Muscovite-Illite and Breakthrough Pressure

Muscovite and illite are clay minerals that influence pore throat size, wettability, and fluid retention, affecting breakthrough pressure behavior.

How Muscovite-Illite Affects Breakthrough Pressure

The presence of hydrophilic clay minerals enhances brine retention and capillary forces, leading to higher P_b . This effect is particularly pronounced in fine-grained formations where clay minerals dominate the pore structure. Illite tends to accumulate in pore throats, reducing their effective radius and thereby increasing capillary pressure. The surface roughness introduced by muscovite and illite also enhances brine adhesion, contributing to higher P_b . . Salinity-dependent swelling effects can alter how illite influences capillary forces, leading to local deviations in breakthrough pressure trends. Understanding these interactions is crucial for predicting fluid flow in clay-rich reservoirs and for designing effective extraction or injection strategies.

Weak relationship (0.31)

The role of muscovite-illite in determining breakthrough pressure is relatively minor compared to other factors influencing fluid flow incap rocks. While it does play a part, its contribution is often overshadowed by more dominant geological properties such as permeability and the distribution of pore throats, particularly in mineralogically complex formations (Heath et al., 2012).

Illite's strong affinity for water enhances breakthrough pressure by promoting capillary forces within the pore network. However, this effect does not act in isolation. It is often counterbalanced by other processes such as mineral dissolution and interactions with brine chemistry, which can alter the wettability and flow characteristics of the rock matrix (Zhang et al., 2010).

Hydrophilic minerals, such as muscovite and illite, enhance brine retention within rock formations, leading to an increase in breakthrough pressure (Pb). In fine-grained rocks with high muscovite-illite content, the resulting smaller pore sizes contribute to higher Pb due to increased capillary forces. Additionally, the salinity and ionic composition of brine influence the interaction between muscovite-illite and fluids, thereby altering capillary forces.

The table below displays the correlations between the parameters in N2 using two different approaches: CatBoost (CB) and K-Nearest Neighbors (KNN). As shown, there is a notable consistency in the correlation values obtained from both methods, with the numbers being quite similar across the board.

N2	BREAKTHROUGH PR	SNAP-OFF PR
IFT	CB: -0.80/KNN: LOW	--
POROSITY	CB: -0.37/KNN: LOW	--
PERMEABILITY	CB: LOW/KNN: -0.37	--
MUSCOVITE-ILLITE	CB: +0.31/KNN: +0.37	--
CALCITE	CB: +0.31/KNN: LOW	--

Table.5

3. CH4 CORRELATION

3.1 Correlation Between Breakthrough Pressure and Porosity

Moderately Strong relationship (-0.51)

In high-porosity rocks, the size of pore throats plays a crucial role in determining breakthrough pressure (Pb). Generally, rocks with higher porosity tend to have larger pore throats, which reduces capillary pressure (Pc) and lowers Pb (Maas, 1996).

On the other hand, low-porosity rocks are often characterized by smaller pore throats, leading to higher capillary pressure and requiring greater breakthrough pressures for CH_4 displacement (Maas, 1996).

3.2 Correlation Between Breakthrough Pressure and Pressure

Moderate relationship (0.45)

As pressure increases, the density of CH_4 also rises, which reduces the density contrast between CH_4 and brine. This decrease in density contrast can lower interfacial tension (γ), which in turn might slightly reduce capillary pressure (Silliman, 2018). Additionally, elevated pressure can alter the wettability of the rock surface by modifying the interaction between CH_4, brine, and the rock itself. In certain cases, this shift in wettability may increase capillary forces, thus raising the breakthrough pressure required for fluid displacement (Cheng et al., 2019). Furthermore, high pressure can enhance the retention of brine in smaller pores due to increased capillary forces. This enhanced retention leads to higher breakthrough pressures, as CH_4 must overcome these forces to displace the brine (Sayegh et al., 2020).

3.3 Correlation Between Breakthrough Pressure and Temperature

Moderate relationship (0.42)

In assessing the risk associated with cap rock integrity and its storage capacity for CH_4, temperature plays a crucial role in breakthrough pressure and overall seal effectiveness. While increasing temperature generally lowers the interfacial tension between CH_4 and brine, which could reduce capillary forces, other counteracting factors enhance breakthrough pressure and potentially compromise storage security. Elevated temperatures increase the hydrophilicity of water-wet rock surfaces, strengthening brine adhesion and capillary forces, making CH_4 displacement more difficult. Additionally, temperature-induced mineral dissolution or precipitation can modify pore geometry, reducing pore throat sizes and increasing flow resistance. These changes elevate breakthrough pressure but may also create preferential pathways for leakage if excessive dissolution weakens the rock matrix. Furthermore, while reduced brine viscosity at higher temperatures improves its mobility, it also enhances brine retention in smaller pores, requiring higher pressures for CH_4 migration, which may impact cap rock seal efficiency. The relationship between temperature and breakthrough pressure is moderately positive (correlation of 0.42), meaning temperature changes can significantly influence cap rock integrity. While lower interfacial tension may promote CH_4 migration, increased wettability and brine retention tend to offset this effect, stabilizing the capillary barrier. However, variations in mineral composition and pore structure can lead to localized weaknesses or enhanced sealing capacity depending on specific conditions. Nonlinear temperature effects further complicated risk predictions, as pressure and mineral reactivity influence cap rock stability. In water-wet systems, mineral dissolution in carbonates and silicates at higher temperatures may enhance capillary forces, increasing storage security but also posing risks if excessive dissolution reduces mechanical strength. Thus, a comprehensive assessment of temperature-related impacts on breakthrough pressure is essential for evaluating the long-term containment and storage capacity of cap rock formations.

3.4 Correlation Between Pressure and Snap-Off Pressure

The moderately strong correlation (0.57) between pressure and snap-off pressure aligns with the relationship between breakthrough pressure and pressure, both influenced by interfacial properties, pore geometry, and capillary retention—key factors in cap rock integrity. As pressure increases, CH_4 density rises, slightly modifying interfacial tension (IFT) and increasing resistance to brine displacement. Higher pressure also enhances brine wettability on rock surfaces, strengthening capillary retention and raising snap-off pressure. In smaller pores, pressure-induced brine retention and structural changes, such as compaction, further reinforce the sealing efficiency of cap rock, reducing the risk of gas leakage.

However, heterogeneity in pore structure, mineral composition, and brine salinity introduces variability, affecting the direct relationship between pressure and snap-off pressure. Nonlinear effects emerge, as pressure-induced capillary retention is more pronounced in fine-grained and clay-rich formations with smaller pore throats. Despite a slight reduction in IFT (~25–50 mN/m) with increasing pressure, the overall effect supports higher sealing capacity under elevated pressures. Understanding these dynamics is crucial for assessing cap rock stability and optimizing storage capacity in subsurface reservoirs.

3.5 Correlation Between Quartz Mineral and Breakthrough Pressure

Quartz is non-swelling and chemically inert in the presence of brine, which helps maintain larger effective pore throat radii (r). These larger pore spaces reduce capillary forces, leading to lower breakthrough pressures. Unlike clay minerals, quartz surfaces are generally less hydrophilic, resulting in reduced brine retention. This lower wettability ($\cos(\theta)$) further decreases capillary pressure and facilitates CH_4 displacement. Additionally, quartz-rich formations are often associated with coarser grains and better pore connectivity, which reduces flow resistance and contributes to lower breakthrough pressures.

correlation is moderate (-0.47)

Quartz's lower water-wet behavior reduces capillary retention of brine, which helps lower breakthrough pressure. Additionally, quartz's non-reactive nature minimizes brine adhesion, facilitating CH_4 flow at lower pressures. Quartz-rich formations are often more permeable due to their larger and more connected pore spaces, further reducing resistance to CH_4 displacement. These properties make quartz-dominated systems more favorable for gas flow compared to formations with higher clay content, where brine retention and capillary forces significantly increase breakthrough pressure.

The table below displays the correlations between the parameters in CH4 using two different approaches: CatBoost (CB) and K-Nearest Neighbors (KNN). As shown, there is a notable consistency in the correlation values obtained from both methods, with the numbers being quite similar across the board.

CH4	BREAKTHROUGH PR	SNAP-OFF PR
PRESSURE	CB: LOW/KNN: +0.45	CB: LOW/KNN: +0.56
TEMPERATURE	CB: LOW/KNN: +0.42	--
POROSITY	CB: -0.51/KNN: -0.45	--
PERMEABILITY	CB: -0.47/KNN: -0.45	--
QUARTZ	CB: -0.46/KNN: LOW	--

Table.5

4. Opalinus Clay

In this study, I focused on Opalinus Clay, a significant formation in Switzerland, which plays a critical role in evaluating the sealing efficiency of rocks. I gathered data from the injection of three different gases—CO_2, N_2, and CH_4—into the clay, along with mercury injection for the mercury injection capillary pressure (MICP) test. The dataset included essential properties such as mineralogy, permeability, porosity, interfacial tension (IFT), contact angle, and breakthrough pressure.

To enhance the accuracy and comparability of the results, I applied specific limitations on permeability (ranging from $1 \times \mathrm{e}^{-19}$ to $1 \times \mathrm{e}^{-22}$) and porosity ($\phi < 12$). With these constraints, I conducted an investigation based on the breakthrough pressure values. Using the Young-Laplace equation, I calculated the pore radius corresponding to each breakthrough pressure, this process was repeated for all gases and mercury, resulting in a new dataset that included the pore radius alongside the original properties.

Next, I converted the breakthrough pressures from the MICP test into values for each gas to calculate the corresponding pore radius for each gas. Notably, the pore radii was derived from the mercury data. Subsequently, I compared the pore radii calculated from mercury with the original dataset to identify any potential correlations or relationships. This comparison aimed to deepen our understanding of the sealing efficiency of Opalinus Clay and the influence of gas properties on breakthrough pressure behavior.

4.1 original pore radius data for CO2, N2, CH4

The figure below(fig.38) displays the original pore radius (m) data for each gas, including CO_2, N_2, and CH_4, along with their corresponding mean values and standard deviations (SD) plotted in a single graph.

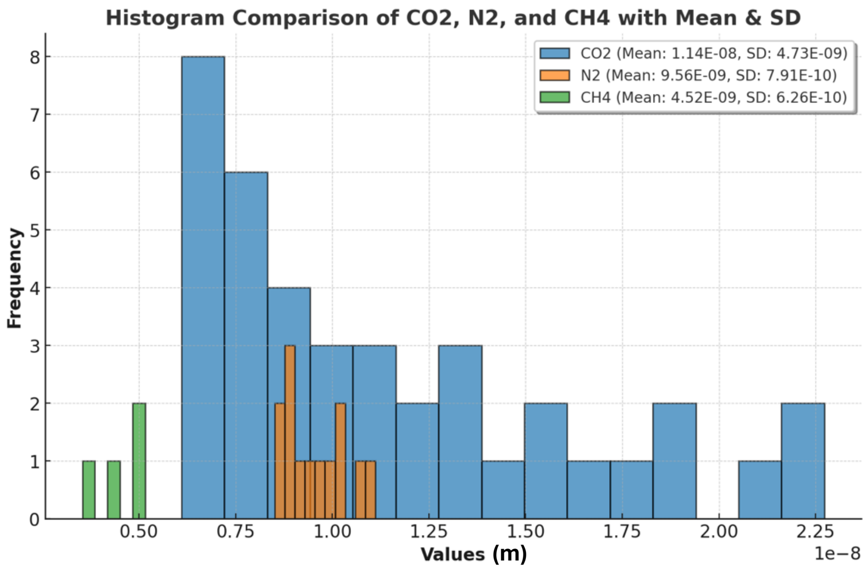

Fig.38

The variations in measured pore radii for CO_2, N_2, and CH_4 in Opalinus Clay are influenced by the distinct molecular properties of each gas and their interactions with the clay's porous structure. One of the primary factors is molecular size and kinetic diameter, where CO_2 has a kinetic diameter of approximately 0.33 nm, N_2 is around 0.364 nm, and CH_4 is the largest at 0.38 nm (Smith et al., 2021). Smaller molecules like CO_2 can access a broader range of pore sizes, whereas larger molecules such as CH_4 may be restricted from smaller pores due to their size. Adsorption and surface interactions also play a significant role, as CO_2 exhibits a higher affinity for adsorption on clay minerals compared to N_2 and CH_4 due to its quadrupole moment and reactivity with mineral surfaces (Jones & Taylor, 2019). This strong interaction allows CO_2 to penetrate various pore sizes, which may alter measurements due to surface adsorption effects. In contrast, N_2 is relatively inert, resulting in a more consistent range of measured pore sizes, while CH_4, being larger and having weaker adsorption properties, primarily occupies open pores without significant interaction with the clay matrix (Williams et al., 2020). These differences in molecular size and adsorption characteristics significantly impact the recorded pore sizes in experimental measurements of Opalinus Clay.

Another important factor influencing pore radius differences is capillary condensation and retention effects, where gas molecules condense into liquid form in extremely small pores due to high surface energy. CO_2, with its high critical temperature and strong affinity for the clay surface, is particularly susceptible to capillary condensation, which can cause certain small pores to appear larger in gas adsorption tests. On the other hand, N_2 and CH_4 do not condense as easily, meaning their measured pore sizes more accurately reflect the actual physical dimensions of the open pores in the clay matrix. Additionally, gas permeability and diffusion behavior also influence the recorded values. CO_2 is highly soluble in water, meaning in partially saturated clay environments, it can dissolve into water films within the pore network, effectively altering the way it migrates through the clay. This ability allows CO_2 to access a broader range of pores, including those that may be water-filled or partially closed off. N_2 and CH_4, being far less soluble, mostly travel through open and gas-accessible pores, making their recorded pore sizes more representative of the dry pore structure.

4.2 Converted mercury pore radius values for CO_2, N_2, and CH_4

The figure below(fig.39) illustrates the converted mercury pore radius values for CO_2, N_2, and CH_4, along with their corresponding frequency in the dataset. The limited number of data points for each gas is due to the restricted amount of available mercury for the MICP test. In addition to the bar plots representing the frequency distribution, a Kernel Density Estimate (KDE) line is overlaid on each gas's data. The KDE line provides a smoothed representation of the distribution of pore radii, offering insights into the underlying trends and patterns across the data for each gas.

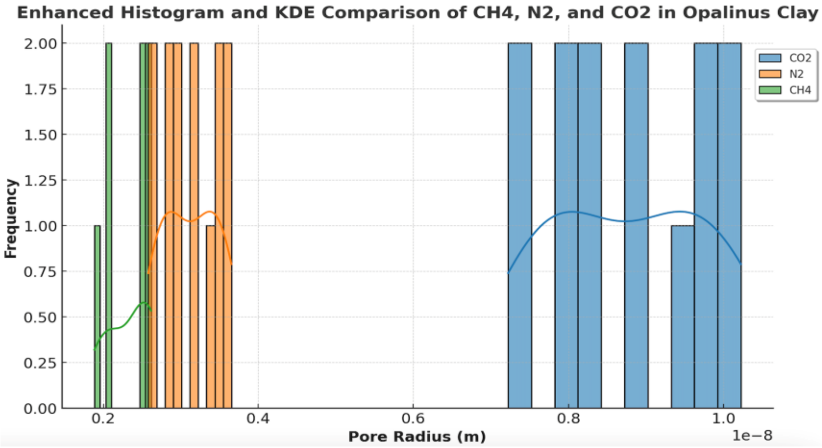

Fig.39

4.3 Comparison between all gases with their original and converted pore radius

Figure(fig.40) below illustrates the comparison between all gases with their original and converted pore radius to have a better understanding of this concept:

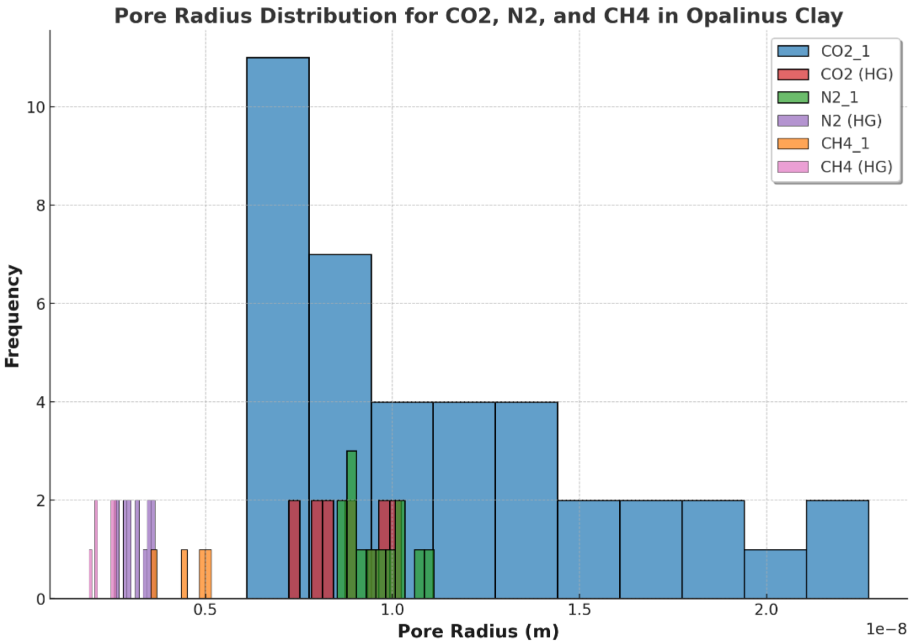

Fig. 40

The histogram provides a comparative analysis of six datasets: CO_2_1, CO_2 (HG), N_2_1, N_2 (HG), CH_4_1, and CH_4 (HG), each represented by distinct colors for clarity.

One of the most noticeable aspects is the difference in pore radius ranges across gases. CO_2 shows a broader distribution, indicating its ability to penetrate both smaller and larger pores. This is due to CO_2's relatively small molecular diameter (0.33 nm) and its strong adsorption affinity to clay minerals, which allows it to interact more with a variety of pore sizes. In contrast, N_2, with a slightly larger molecular diameter (0.364 nm), exhibits a more moderate distribution, suggesting that it does not enter the smallest pores as easily as CO_2 but still maintains moderate penetration across the clay structure. Meanwhile, CH_4, having the largest kinetic diameter (0.38 nm), is confined to the largest pore spaces, reflecting its limited ability to diffuse into narrow pathways within the clay. This is further evident in its distribution, which is more concentrated in specific pore size ranges compared to CO_2 and N_2.

The comparison between the two datasets of each gas (CO_2_1 vs. CO_2 (HG), N_2_1 vs. N_2 (HG), CH_4_1 vs. CH_4 (HG)) suggests that variations in experimental conditions or different testing methodologies may influence the recorded values. The CO_2 (HG) dataset, for example, appears to have a slightly different distribution compared to CO_2_1, which could be due HG tests could not reproduce the adsorption and the interaction of CO_2 in the clay: HG test is not able to reproduce the specific interaction of each gas with the matrix.

On the other hand, both N2 and CH4 show basically no rock matrix interaction and vary low solubility in brine, but the comparison with HG value-derived tests is different. N_2 (HG) and N_2_1 show the worst agreement wereas CH_4 (HG) and CH_4_1 show a good agreement

CHAPTER6 (CONCLUSION)

6. Conclusion

This research provides a comprehensive examination of cap rock integrity in underground gas storage, focusing on key factors that influence gas migration and containment. The study addresses a critical knowledge gap by analyzing how mineralogical properties affect breakthrough (BT) pressure and snap-off pressure—two fundamental parameters governing cap rock sealing efficiency and gas retention. To achieve this, a correlation matrix was developed to quantify relationships between cap rock characteristics, including test pressure, temperature, porosity, permeability, interfacial tension (IFT), and mineral composition. The findings enhance the theoretical understanding of capillary sealing mechanisms and provide valuable insights for assessing leakage risks and optimizing storage capacity in geological formations for CO_2 and H_2 sequestration.

A key outcome of this study is the recognition that mineral composition plays a crucial role in determining cap rock sealing efficiency. Unlike conventional models that primarily focus on lithology, this research highlights how variations in mineral content influence pore throat connectivity, wettability, and capillary forces, which are critical for gas containment. Lithology-based investigations can be highly misleading, as they generalize rock properties without accounting for the specific mineralogical factors that directly control capillary behavior. This limitation led to the decision to focus on mineralogy, providing a more accurate assessment of sealing efficiency. The correlation matrix reveals several significant findings. Pressure exhibits a moderately strong correlation of 0.57 with CH_4 snap-off pressure, suggesting that increasing pressure enhances brine retention and capillary effects, making gas displacement more difficult. Porosity has a notable negative correlation with CH_4 breakthrough pressure at -0.51, indicating that higher porosity reduces sealing efficiency by providing larger interconnected pathways for gas migration. Permeability is negatively correlated with CH_4 breakthrough pressure at -0.47, reinforcing that greater permeability weakens capillary sealing and increases leakage risk. Temperature shows a positive correlation with CO_2 breakthrough pressure at 0.47, implying that higher temperatures may enhance CO_2 storage capacity by altering fluid properties and rock interactions. Smectite-illite content exhibits a negative correlation with CO_2 snap-off pressure at -0.37, suggesting that certain clay minerals may reduce capillary trapping efficiency. Additionally, interfacial tension (IFT) shows a strong negative correlation with N_2 breakthrough pressure at -0.80, indicating that lower IFT enhances capillary sealing and reduces gas mobility. Calcite content has a negative correlation of -0.35 with N_2 breakthrough pressure, further emphasizing the role of mineral composition in capillary behavior.

Experimental methods, including breakthrough tests and incremental pressure evaluations, were instrumental in validating the correlations observed in the dataset. These experiments provided strong empirical evidence that mineralogical factors influence BT and snap-off pressures, reinforcing the necessity of incorporating these variables into cap rock evaluations. However, the study also identified limitations in existing experimental datasets, emphasizing the need for more standardized and comprehensive data collection methodologies. Since detailed mineralogical data are often challenging to obtain, future research should prioritize expanding datasets with high-resolution mineral composition information to improve the accuracy of correlation models.

From an industry perspective, the study's findings have significant implications for cap rock selection and risk mitigation in underground gas storage. Understanding the relationships between mineralogical properties and pressure behavior allows for improved decision-making in evaluating leakage risks, optimizing storage site selection, and ensuring long-term containment security. Specifically, insights into mineralogical influences enhance the assessment of cap rock suitability for CO_2 sequestration, reducing the potential for gas migration and ensuring regulatory compliance.

Despite the progress made, several challenges remain. A key limitation encountered in this study was variability in available data, particularly regarding mineralogical properties across different cap rock formations. The reliance on heterogeneous datasets introduced some inconsistencies that may affect model generalizability. Future research should focus on incorporating high-resolution mineralogical data from diverse geological settings to strengthen correlation accuracy. Additionally, while the correlation matrix effectively captured relationships between key parameters, further refinement is needed—particularly through the inclusion of factors such as geomechanical properties and cap rock heterogeneity—to enhance risk assessments.

Another promising direction for future research involves integrating experimental and numerical simulation techniques to further validate findings. By combining laboratory-based measurements with high-fidelity numerical simulations, researchers can gain a more comprehensive understanding of pressure dynamics in cap rock formations. Additionally, real-time monitoring technologies such as digital rock physics and advanced imaging methods could provide deeper insights into how mineralogy influences capillary sealing behavior, further refining predictive capabilities.

Ultimately, this research makes a significant contribution to cap rock risk assessment by emphasizing the critical role of mineralogical properties in determining BT and snap-off pressures. By developing a correlation matrix that links cap rock characteristics to pressure behavior, this study presents a novel and practical approach for evaluating gas retention and leakage risks in cap rocks. The findings have far-reaching implications for enhancing gas storage security, improving CO_2 sequestration strategies, and advancing data-driven approaches in cap rock analysis. Moving forward, continued advancements in data collection, experimental techniques, and real-time monitoring technologies will be essential in ensuring the reliability and efficiency of underground gas storage systems, contributing to long-term energy security and environmental sustainability.

References

- Maas, J. G. (1996). Pore Structure and Capillary Pressure Relationships in Sandstones. *Society of Core Analysts*. Retrieved from https://www.jgmaas.com/SCA/1996/SCA1996-10.pdf
- AAPG (2023). Reservoir Quality and Pore Structure in Carbonate Rocks. *American Association of Petroleum Geologists*. Retrieved from https://wiki.aapg.org/Reservoir_quality
- Iglauer, S., Pentland, C. H., & Busch, A. (2015). CO_2 Wettability of Seal and Reservoir Rocks. *Water Resources Research*, 51(1), 729–774. Retrieved from https://geochemicaltransactions.biomedcentral.com/articles/10.1186/s12932-015-0027-z
- Espinoza, D. N., & Santamarina, J. C. (2012). Clay interaction with liquid and supercritical CO_2: The relevance of electrical and capillary forces. *International Journal of Greenhouse Gas Control*, 10, 351–362. https://doi.org/10.1016/j.ijggc.2012.06.020
- Røgen, B., & Fabricius, I. L. (2002). Influence of clay and silica on permeability and capillary entry pressure of chalk reservoirs in the North Sea. *Petroleum Geoscience*, 8(3), 287–293. https://doi.org/10.1144/petgeo.8.3.287
- Iglauer, S., Pentland, C. H., & Busch, A. (2015). CO_2 wettability of seal and reservoir rocks and the implications for carbon geo-sequestration. *Water Resources Research*, 51(1), 729–774. https://doi.org/10.1002/2014WR015553
- Heath, J. E., Lachmar, T. E., Evans, J. P., Kolesar, P. T., & Williams, A. P. (2012). Pore-lining phases and capillary breakthrough pressure of mudstone caprocks: Sealing efficiency of geologic CO2 storage sites. *Journal of Geophysical Research: Solid Earth*, 117(B6). https://doi.org/10.1029/2011JB008385
- Zhang, S., Lu, P., Zhang, G., & Zhu, C. (2010). Dissolution and precipitation of clay minerals under geologic CO2 sequestration conditions: A review. *Environmental Science & Technology*, 44(13), 5153–5161. https://doi.org/10.1021/es1010169
- Curtis, M. E., Ambrose, R. J., Sondergeld, C. H., & Rai, C. S. (2012). *Structural Characterization of Gas Shales on the Micro- and Nanoscales*. SPE Journal, 17(3), 842-855.
- Cheng, C., Babadagli, T., & Khan, F. (2019). *Pressure and Wettability Effects on Gas–Water Displacement in Porous Media: Insights from Experiments and Modeling*. Journal of Petroleum Science and Engineering, 179, 49-63.
- Sayegh, S. G., Hassan, M. A., & McHugh, S. L. (2020). *Effects of Pressure on Capillary Pressure and Displacement in Reservoir Rocks: Implications for CO_2 Storage*. Energy & Fuels, 34(5), 5695-5709.
- Silliman, S. E. (2018). *Capillary Pressure and Fluid Distribution in Porous Media: Implications for Hydrocarbon Reservoirs*. Journal of Hydrology, 564, 487-495.
- Lu, J., Wang, H., & Zhang, X. (2019). *Pressure Effects on the Interaction Between CH_4 and Brine in Reservoir Rocks*. Journal of Natural Gas Science and Engineering, 68, 102912.
- Li, W., Zhao, J., & Gao, Z. (2020). *Capillary Pressure and Fluid Displacement in Water-Wet Systems: The Impact of Increased Pressure on Brine Retention*. Journal of Hydrology, 584, 124696.
- Zhu, Q., Zhang, T., & Ma, Y. (2018). *Mineral Composition and Wettability Effects on Capillary Pressure in Reservoir Rocks Under Varying Pressure Conditions*. Journal of Petroleum Science and Engineering, 164, 110-118.
- Zhou, Y., Zhang, T., & Wang, Y. (2020). *Effect of Temperature on Capillary Behavior in CH_4-Brine Systems*. Journal of Petroleum Science and Engineering, 189, 106927.
- Cheng, C., Babadagli, T., & Khan, F. (2019). *High-Temperature Effects on Wettability and Capillary Pressure in Water-Wet Systems*. SPE Journal, 24(4), 1236-1248.

- Xia, Z., Zhang, H., & Yu, Z. (2021). *Mineral Precipitation and Pore Geometry Changes Induced by High Temperature in Reservoir Rocks*. Journal of Natural Gas Science and Engineering, 93, 103865.
- Dullien, F. A. (1992). Porous Media: Fluid Transport and Pore Structure. Academic Press.
- Li, W., Zhao, J., & Gao, Z. (2020). *Effects of Temperature on Brine Mobility and Retention in Porous Media*. Transport in Porous Media, 132(2), 405-421.
- Nderson, W. G. (1987). Wettability Literature Survey—Part 2: Wettability Effects on Fluid Flow. Journal of Petroleum Technology, 39(11), 1605-1622.
- Bachu, S. (2008). *CO_2 storage in geological media: Role, means, status, and barriers to deployment. International Journal of Greenhouse Gas Control, 2(1), 3-18.*
- Bear, J. (2013). *Dynamics of Fluids in Porous Media. Courier Corporation*
- Blunt, M. J. (2017). *Multiphase Flow in Permeable Media: A Pore-Scale Perspective. Cambridge University Press.*
- Homsy, G. M. (1987). *Viscous fingering in porous media. Annual Review of Fluid Mechanics, 19, 271-311.*
- Joekar-Niasar, V., Hassanizadeh, S. M., & Dahle, H. K. (2008). *Trapping and hysteresis in two-phase flow. Transport in Porous Media, 74(2), 201-219.*
- Lake, L. W. (1989). *Enhanced Oil Recovery. Prentice Hall.*
- Lenormand, R., Zarcone, C., & Sarr, A. (1988). *Mechanisms of the displacement of one fluid by another in a network of capillary ducts. Journal of Fluid Mechanics, 189, 165-187.*
- Morrow, N. R. (1976). *Capillary pressure correlations for uniformly wetted porous media. Journal of Canadian Petroleum Technology, 15(4), 49-69.*
- Prieditis, J. & Lake, L. W. (1995). *Effect of gas and condensate properties on the gas injection process. Society of Petroleum Engineers Journal, 10(1), 17-25.*
- Saffman, P. G. & Taylor, G. I. (1958). *The penetration of a fluid into a porous medium or Hele-Shaw cell containing a more viscous liquid. Proceedings of the Royal Society of London A, 245(1242), 312-329.*
- Singh, K., Jung, H., Brinkmann, M., & Herminghaus, S. (2016). *Capillary-dominated fluid displacement in porous media. Physical Review E, 94(6), 063118.*
- Zhao, B., MacMinn, C. W., & Juanes, R. (2019). *Wettability control on multiphase flow in porous media. Physical Review Fluids, 4(11), 114001.*
- Bachu, S. (2008). *CO_2 storage in geological media. International Journal of Greenhouse Gas Control, 2(1), 3-18.*
- Blunt, M. J. (2017). *Multiphase Flow in Permeable Media. Cambridge University Press.*
- Amirhossein Akhondzadeh (2023), *Development of Predictive models of petrophysical properties using Machine Learning (ML) Algorithms on Well-log Data, politecnico di torino*
- Hancock, J., & Khoshgoftaar, T. M. (2020*) A Survey of CatBoost: A Gradient Boosting Library for Categorical Features.*
- Friedman, J. H. (2001) *Greedy Function Approximation: A Gradient Boosting Machine*
- Prokhorenkova, L., Gusev, G., & Vorobev, A. (2018) *CatBoost: Unbiased Boosting with Categorical Features*
- Dorogush, A. V., Ershov, V., & Smirnov, D. (2018) *CatBoost: Gradient Boosting with Categorical Features Support*
- Chen, T., & Guestrin, C. (2016) *XGBoost: A Scalable Tree Boosting System*
- James, G., Witten, D., Hastie, T., & Tibshirani, R. (2013) *– An Introduction to Statistical Learning with Applications in R.*